1-1-2008

Dispersion Coefficient Determination In Vapex Process

Muhammad Imran
Ryerson University

DISPERSION COEFFICIENT DETERMINATION IN VAPEX PROCESS

by

Muhammad Imran

Bachelor of Chemical Engineering, Pakistan, 1996

A thesis
presented to Ryerson University
in partial fulfillment of the
requirements for the Degree of
Master of Applied Science
in the Program of
Chemical Engineering

Toronto, Ontario, Canada, 2008

Author's Declaration

I hereby declare that I am the sole writer of this thesis.

I authorize Ryerson University to lend this thesis to other institutions or individuals for the purpose of scholarly research.

I further authorize Ryerson University to produce this thesis by photocopying or by other means, in total or part, at the request of other institutions or individuals for the purpose of scholarly research.

Abstract

Dispersion Coefficient Determination in Vapex Process

Muhammad Imran
Master of Applied Science, 2008
Department of Chemical Engineering,
Ryerson University

In this work, the dispersion of butane in heavy oil and bitumen is experimentally determined during the Vapex process with varying drainage heights. The experiments are performed at constant temperature using butane as solvent at the dew point pressure. Cylindrical models with different heights packed with uniform mixture of bitumen and glass beads are used. From the experimental data, the production rate dependency towards the drainage height is evaluated along with determination of butane gas solubility, live oil density and viscosity.

A mathematical model is developed to simulate live oil production rates. A variable metric method in multi dimensions is used to optimally determine concentration dependent dispersion coefficient as well as solvent mass fraction at liquid gas interface by matching up experimental and predicted live oil production rates. A computational algorithm is developed to solve a set of models simultaneously to evaluate effect of drainage height on dispersion of solvent gas.

Acknowledgements

I would like to extend my deepest gratitude to my supervisors, Dr. Ali Lohi and Dr. Simant R. Upreti, for providing me the opportunity to work on this project. I highly appreciate the continuous support, encouragement and guidance throughout this work. Their unconditional availability and desire to share scientific knowledge and experience were exceptional elements for nourishing the passion to carry out this research.

The financial support of Natural Sciences and Engineering Research Council of Canada (NSERC) is gratefully acknowledged.

Finally, I would like to thank my family, friends and fellow graduate students for their moral support and understanding during my studies.

Instruction for Borrowers

Ryerson University requires the signatures of all persons using or photocopying this thesis.

Please sign below, and give address and date.

Name	Signature	Address	Date

Table of Contents

List of Tables

List of Figures

List of Figures (Continued)

Nomenclature

c	concentration of diffusing species, kg/m^3
D	dispersion coefficient of butane in the medium, m^2/s
D_0	D when $\omega = 1$, m^2/s
D_{AB}	diffusion coefficient of diffusing species A in material B, m^2/sec
E	root-mean-square error
$\overline{G}$	gradient for error
g	gravitational acceleration, m/s^2
J	dispersive flux of butane in the medium along the radial direction, $kg/m^2 \cdot s$
K	permeability of the medium, Darcy
K_r	relative permeability of the medium
m_{cal}	calculated mass of the produced live oil, kg
m_{exp}	experimental mass of the produced live oil, kg
N	number of experimental data points
N_I	number of grid points along the radial direction
N_J	number of grid points along the axial direction
N_s	dimensionless Number
Q	live Oil Production Rate, m^3/hr m
r	distance along the radial direction, m
R	radius of cylindrical medium, m
T	temperature ^oC, or absolute temperature ^oK
t	time, s
v	Darcy velocity, m/s

Nomenclature (Continued)

Z	bitumen height in the medium at a given r and t, m
z	distance along the axial, vertical direction, m
Z_0	initial Z, m

Greek Symbols

μ_B	viscosity of liquid B, mPa.s
α	coefficient for the viscosity dependent diffusivity (Hayduk and Cheng, 1971)
β	exponential coefficient for the viscosity dependent diffusivity (Hayduk and Cheng, 1971)
ϕ	porosity of the medium
μ	viscosity of the live oil, mPa.s
μ_0	viscosity coefficient of the live oil, mPa.s
ρ	density of the live oil, kg/m^3
ω	mass fraction of butane in bitumen
ω_{sat}	the saturation ω under equilibrium
ΔA	area transverse to v, m^2
Δr	intergrid distance along the radial direction, m
ΔS	area transverse to J, m^2
ΔV	volume of a finite element in the medium, m^3
$\Delta\varsigma_i$	dimensionless intergrid distance along the vertical direction
ζ	dimensionless bitumen height in the medium at a given r and t

1 Introduction

1.1 Heavy Oil and Bitumen Classification

Heavy oil and bitumen is a form of crude oil that occurs naturally and are mixtures of petroleum hydrocarbons and other complex organic compounds. The worth or greatest commercial interest of the crude oil is based on the API (American Petroleum Institute) gravity classification. Table (1.1) shows grading of the crude oil based on API gravity.

Table 1.1: Crude Oil Classification
(http://en.wikipedia.org/wiki/API)

Crude Oil Classification	API Gravity
Light Crude Oil	Higher then 31.1
Medium Crude Oil	Between 22.3 and 31.1
Heavy Crude Oil	Below 22.3

Further classification of crude oil is based on viscosity, under reservoir temperature and pressure conditions and is turned to heavy oil and bitumen. Table (1.2) shows heavy crude oil classification.

Table 1.2: Heavy Crude Oil Classification
(Das, 1995)

Oil Type	API Gravity	Viscosity
Heavy Oil	Lower than 22.3	Less than 10,000 mPa.s
Extra Heavy Oil or Bitumen	Lower than 10.0	Higher than 10,000 mPa.s

Based on the same approach the world oil reserves are classified as conventional and unconventional reserves. The conventional oil reserves are typically the highest quality, lightest oil and easily recoverable with API gravity higher than 21°. Unconventional oil reserves are very hard to extract due to their higher viscosities and having API gravity lower than 21°. Some examples are tar, oil shale, bitumen, heavy oil, extra heavy oil and deep sea oils.

1.2 Importance of Unconventional Oil reserves

As the conventional crude oil production declines, the importance of unconventional oil reserves (heavy oil and bitumen) has increased due to their much higher in place volumes. An estimate for conventional oil reserves in the world is to be 159 billion m^3 as compared with 950 billion m^3 in place amount of heavy oil and bitumen. Bitumen is located in several parts of the world. The countries with the highest amount of bitumen in place are Canada, Venezuela, and Russia (Friedrich, 2005), (Figure 1.1).

Figure 1.1: World In Place Bitumen (Friedrich, 2005)

1.3 Canadian Oil Reserves

Canada has huge heavy oil and bitumen resources. Estimated original oil in place (OOIP) is more than 400 billion m^3 (2.5 trillion barrels) approximately twice that of the total conventional oil reserves in the Middle East (ERCB, 1989). The hydrocarbon reserves exist in the unconsolidated sand and carbonate sedimentary formations of the Athabasca, Cold Lake, Peace River and Wabasca regions in Alberta, Saskatchewan and British Columbia (PCF, 2000). Due to depletion of conventional crude oil reserves in the world, heavy oil and bitumen resources in Canada have great potential to meet the future demands for petroleum products. Table (1.3) shows the statistics of Alberta oil industry for bitumen, conventional light medium oil and conventional heavy oil (PTAC, 2006).

Table 1.3: Alberta Oil Resources Volume in Place and Reserves (PTAC, 2006)

	Initial Volume In Place (Billion m^3)	Remaining Established Reserves (Billion m^3)	Currently Not Recoverable with Commercial Technologies (Billion m^3)	Percent Not Recoverable (Billion m^3)	Reserve Index (Years)
Bitumen	269.95	27.66	241.55	89.5%	436
Conventional Light Medium Oil	7.86	0.18	5.57	70.9%	8
Conventional Heavy Oil	2.14	0.07	1.76	82.3%	6

1.4 Oil Production in Canada

Western provinces of Canada are very rich in natural energy resources (Table 1.3). According to Alberta Energy and Utility Board (AEUB, 2005) Alberta oil sands contain approximately 269 billion m^3 of crude bitumen with 241.55 billion m^3 not recoverable by

current anticipated technology and economic conditions, (Figure 1.2). Canada's domestic production mainly comes from conventional oil resources but has been steadily declining since 1983. According to the report, if same trends prevail, by 2010 Alberta's light oil production is predicted to be one third of what it was in 1986, while over the same period of time the production from heavy oil, bitumen and tar sands will increase dramatically (CIM Directory, 1993). The Canadian Associate of Petroleum Producers (CAPP) has forecast the total oil production (conventional and bitumen) to rise from 2.7 million barrel per day in 2003 to 3.4 million barrels per day by 2010.

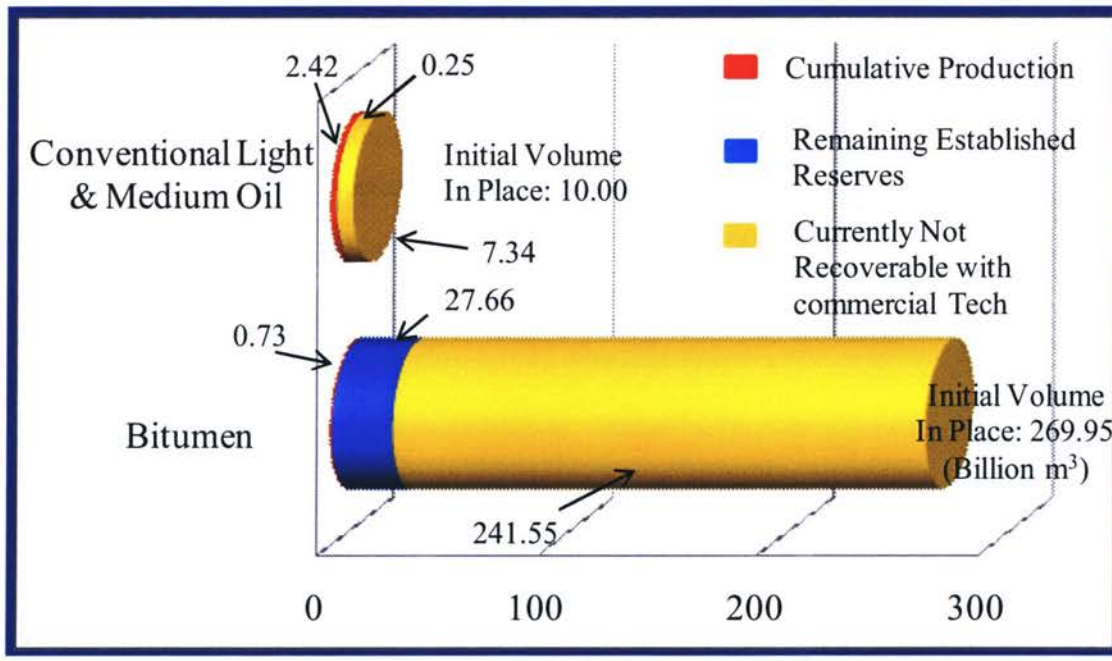

Figure 1.2: Canada (Alberta) Conventional and Unconventional Resources (AEUB, 2005)

Note: "Remaining established reserves are not clear in conventional light, medium and heavy oil bar. Due to very little number (0.25) as compared with x axis scale.

Properties of bitumen present in Canada vary from area to area. Bitumen viscosity at reservoir temperature and pressure conditions may vary from 10,000 mPa.s to 1,000,000 mPa.s. Table (1.4) shows area with huge amounts of bitumen reserves along with their properties.

Table 1.4: Properties of Canadian Heavy Oil
(Speight, 1991)

Location	Specific Gravity	API Gravity	Asphaltenes	Physical Asphaltenes	Composition Resins
Cold Lake	0.999	10.1	15.7	15.7	28.7
Lloydminster	0.966	15.0	12.9	38.4	48.7
Athabasca	1.030	5.9	16.9	34.1	49.0

1.5 Difficulties with Bitumen Production

Heavy oil and bitumen due to the high viscosities under reservoir conditions are partially or completely immobile, therefore use of conventional recovery processes for bitumen extraction are ineffective or almost impossible. One of the reasons for higher viscosity of heavy oil or bitumen is the presence of asphaltenes, which ranges between 15 to 20%. Asphaltenes have high boiling point, and are components of heavy metals like (nickel, vanadium, sulphur and iron). Moreover presence of high molecular weight hydrocarbons in heavy oil or bitumen also adds difficulties toward extraction processes.

One of the major barriers in the bitumen recovery is the cost. But due to the delineation of the yearly production by conventional means, the bitumen production seems to be the next economic alternative to meet increasing demands.

1.6 Bitumen Recovery Techniques

The recovery of heavy oil and bitumen is difficult, as 90% of these reserves lie deep inside the earth crust and are not easily recoverable owing to their high viscosity and immobility. The objective of recovery process is to reduce the viscosity, or equivalently to increase the mobility of heavy oil and bitumen. This objective is achieved by providing

additional energy to heavy oil and bitumen reserves (Upreti et al., 2007). Generally heavy oil and bitumen recovery techniques are characterized as:

1. Surface Mining
2. In Situ or In Place Production Techniques.

1.6.1 Surface Mining

Surface mining or open pit mining is the oldest technique and history of this process starts from 1967 when Suncor opened the first commercial mine. The process involves digging up the oil sand and then transporting the oil sand mixture to treatment facility where it is washed with hot water and bitumen is separated from the sand. Surface mining is very effective in terms of oil recovery, which is usually more than 90%, but is limited to some extent. Only those shallow reservoirs with overburden formation of less than 75 meters can be exploited economically by surface mining (Jiang, 1997). Two tons of sand must be mined to produce one barrel of oil, leaving a huge volume of sand to be disposed of. Requirement of extensive land reclamation projects is also one of the drawbacks for this recovery technique.

1.6.2 In Situ Processes

In situ or in place processes are those that use different techniques to improve the properties of oil within the reservoir, resulting in recovery of the targeted oil. The techniques implemented to improve the properties of buried oil are known as EOR, Enhanced Oil Recovery techniques. The use of EOR techniques can bring oil recovery to over 60% of OOIP (Friedrich, 2005). In situ EOR are further classified as thermal, non thermal and chemical recovery processes.

Thermal methods increase the production flow rate by increasing the reservoir temperature with addition of heat, thereby reducing heavy oil viscosity. Most commonly used thermal recovery methods for EOR are Steam Assisted Gravity Drainage (SAGD),

Cyclic Steam Simulation (CSS), Steam Flooding and In Situ Combustion. SAGD is one of the most commonly used thermal processes in Canada (only this process would be discussed in detail). Non thermal methods are normally applied to conventional oil reserves for example Cold Heavy Oil Production with Sand (CHOPS). Chemical recovery processes such as Vapex, uses chemicals like pure or mixed solvent gases to reduce the viscosity of heavy oil and bitumen upon gas absorption.

Table (1.5) shows currently used recovery techniques for different oil fields in Alberta.

1.6.2.1 SAGD (Steam Assisted Gravity Drainage Process)

SAGD is thermal oil recovery process, in which steam is used to increase the reservoir temperature and drastically reduce heavy oil and bitumen viscosity. In this process, two horizontal wells are drilled near the bottom of the reservoir, (Figure 1.3). The two horizontal wells are closely placed (generally 3 to 7 meter apart). The top well is usually to inject steam and the bottom well is to produce oil. The steam injected from the top well rises into the formation, forming a steam chamber above the injection well. The rising steam condenses near the boundary of the steam chamber, heating the oil and allowing it to drain to bottom production well by gravity. SAGD process can achieve an oil recovery of more than 50% OOIP with steam to oil ratio of 2.5 to 4.0 (Jiang et al., 2000).

Despite SAGD's effective role in heavy oil and bitumen recovery, large heat requirements can make it uneconomical specifically in some reservoirs with thin pay zone, low thermal conductivity, high water saturation or bottom water aquifers (Jiang, 1997; Yazdani and Maini, 2004). Moreover steam generation facilities account for about 30% of the capital cost in SAGD (Das, 1998). Steam production also requires a large source of water and a significant amount of surface equipment is required to produce steam and separate the produced oil water mixture. Also several environmental issues, such as greenhouse gas emissions and effluent water disposal are associated with SAGD process.

Table 1.5: Alberta Bitumen Deposits- In Place Volumes Billion m^3 (AEUB, 2005)

Deposit Type	Athabasca	Cold Lake	Peace River	Total	Percent
Thermal Processes	66.8	7.5	8.6	82.9	30.7
Surface Mining	9.4	0.0	0.0	9.4	3.5
Cold Production	2.0	21.0	0.06	23.1	8.6
Total Accessible deposits	**78.2**	**28.5**	**8.7**	**115.4**	**42.8**
Deposits with no recovery factors					
Bitumen in Carbonate formation	60.8	0.0	10.3	71.1	26.4
Too thin for thermal recovery Processes	60.4	3.4	1.3	65.1	24.1
Deposits with clay barriers	5.8	0.0	0.0	5.8	2.1
Too deep for surface mining but too shallow for SAGD	4.4	0.0	0.0	4.4	1.6
Deposits with Tar	2.2	0.0	0.0	2.2	0.8
Others	5.7	0.0	0.2	5.9	2.2
Total deposits with no recovery Factors	**139.3**	**3.4**	**11.8**	**154.5**	**57.2**
Total All Deposits	**217.5**	**31.9**	**20.5**	**269.9**	**100.0**

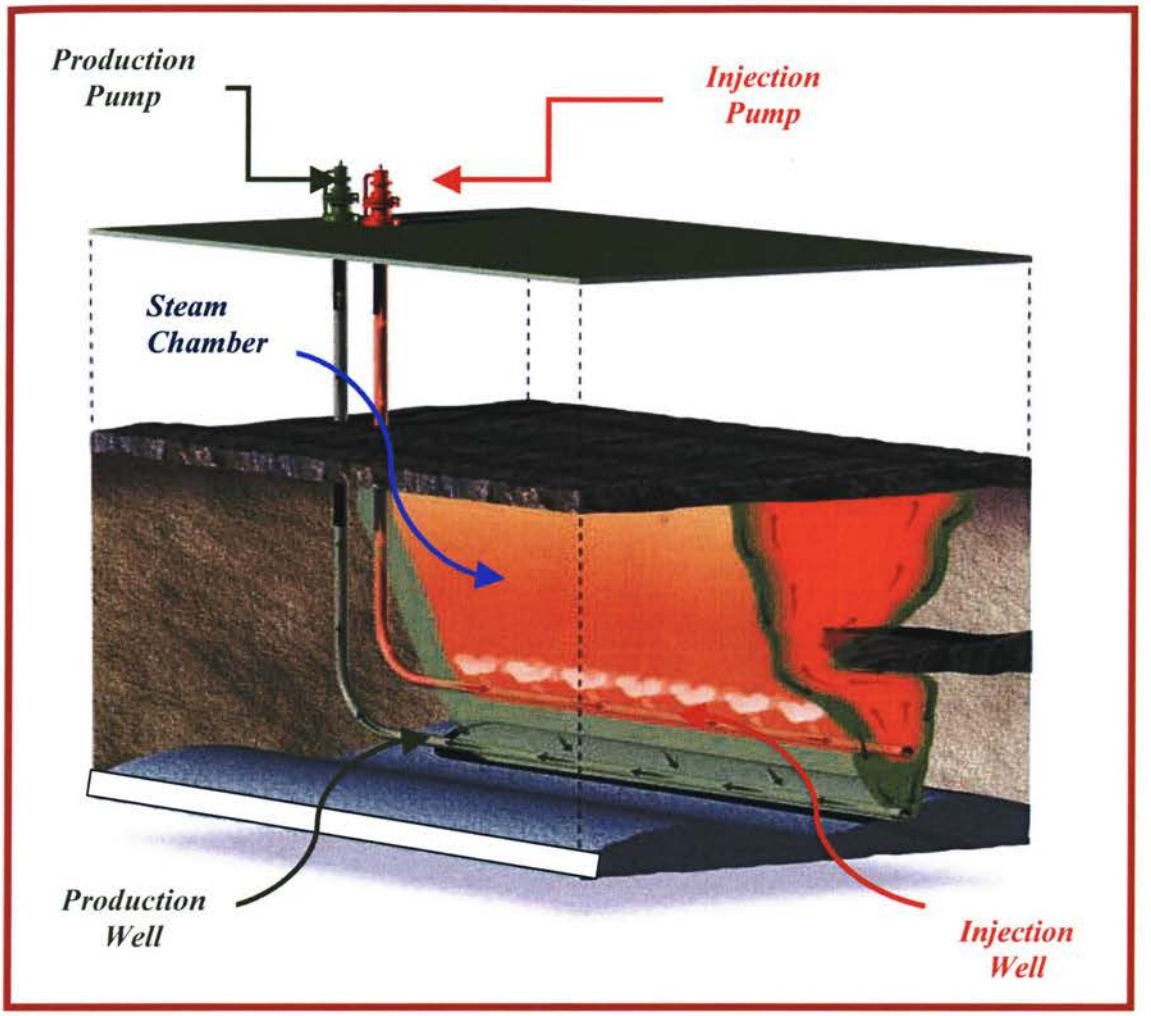

Figure 1.3: Schematic of SAGD Process

1.6.2.2 Chemical Recovery Processes

These processes use chemicals such as pure or mixed solvent gases to reduce viscosity of heavy oil and bitumen upon gas absorption. Before Vapex invention many chemical recovery processes were proposed in the 1970s. These processes were based on solvent gas absorption in a vertical well or groups of vertical wells inside heavy oil reserve (Allen, 1973). The limitation of the early chemical recovery processes were addressed by Butler, who proposed the use of horizontal wells with injection of vaporized hydrocarbon

solvents to promote deasphalting and promote recovery rates by viscosity reduction (Butler and Mokrys, 1991). This process involving vapour extraction was named Vapex.

1.7 Vapex (Vapor Extraction Process)

Vapex or Vapor Extraction is a non thermal alternative for heavy oil and bitumen production that was first proposed by Dr. Roger Butler in 1991. He investigated the recovery of Tangleflags North oil from a laboratory scale reservoir model using hot water and propane gas (Butler and Mokrys, 1991). The experimental results showed that oil recovery was higher than that with hot water alone. In a subsequent development of Vapex oil recovery was found even higher with the use of propane gas alone close to its dew point under reservoir temperature and pressure conditions (Butler and Mokrys, 1993). The results reveal suitability of Vapex for effective heavy oil and bitumen production from reservoirs, where conventional recovery processes like SAGD are ineffective. Examples of these types of reservoirs are reservoirs with bottom water, thin pay zones, fractures, gas caps and low conductivity of rock formation.

Vapex uses a pair of parallel horizontal wells, and vaporized solvents to mobilize heavy oil and bitumen in reservoirs, (Figure 1.4). Examples of vaporized solvents are carbon dioxide, methane, ethane, propane, butane or their mixtures. The concept of injecting low molecular weight hydrocarbon vapors is to reduce energy losses or energy requirements and to mobilize heavy oil and bitumen in the reservoir without changing reservoir temperature and pressure conditions.

Light hydrocarbons are insoluble in formation water and most hydrocarbons can be recovered. These hydrocarbon vapors form a solvent chamber rather than a steam chamber, and are dissolved to oil near the chamber boundary resulting huge reduction in oil viscosity (diluted oil). When a critical concentration of solvent has diluted the oil, oil begins to flow. Diluted oil drains along the solvent vapour oil interface under the force of gravity to the production well.

Figure 1.4: Schematic of the Vapex Process

Vapex has a number of advantages over other heavy oil and bitumen recovery processes. It has low capital cost as no surface facilities are required for injection of vaporized solvents. Vapex is relatively very economical as compared to thermal recovery processes as solvent injection does not involve the energy loss. For the same production rate Vapex consumes only 3% of the energy compared with SAGD (Singhal et al., 1997). In Vapex the green house gas emission is cut down to 80% as there is no steam generation with fuel burning (Luhning et al., 2003). Compared to liquid solvents, vaporized solvents provide higher driving force for gravity drainage of heavy oil and are easily recoverable. Vapex has positive bearing on quality and cost effectiveness of recovered heavy oil and bitumen. Solvent vapors injected close to their dew points can cause asphaltenes to precipitate and deposit onto reservoir sand surface. Thus produced oil is already in-situ

upgraded resulting in significant reduction in capital and operational cost of pipeline transportation and oil refining.

In general, oil production rates in Vapex are much lower than that in SAGD process, because of process mechanism. Slow mixing of the solvent with heavy oil and bitumen reserves result in long start-up times and low initial rates of heavy oil and bitumen recovery. The production rate of Vapex is governed by two processes: mass transfer of solvent vapor (molecular diffusion) into heavy oil and bitumen and gravity drainage. Experiments have shown that rate of mass transfer is much higher as compared with diffusion alone, that highlights the importance of another phenomenon that is molecular dispersion in Vapex (Das and Butler, 1998).

2 Literature Review

Vapex or vapour extraction is a process to recover heavy oil from oil tar sands in reservoirs that are not suitable for the oil recovery by conventional processes such as those using heat or mechanical displacement. Vapex was first introduced by Butler and Mokry (1991) to recover heavy oil from highly viscous reserves deep inside the earth crust. In this process a light hydrocarbon solvent or mixture of hydrocarbon solvents is injected close to the dew point via a horizontal well inside a reservoir. The solvent absorption in the heavy oil reduces its viscosity, and causes it to drain into an underlying horizontal production well. The produced oil from horizontal well is then easily pumped out to the surface.

The use of solvents in Vapex reduces the energy requirements and environmental effects compared with thermal energy processes. The oil production in Vapex is directly related to mass transfer of solvent into the heavy oil and bitumen. Reduced viscosity of heavy oil results from solvent concentration, that augments as solvent penetrates and mixes with the heavy oil. Lower production rates as compared with SAGD are due to primary mode of solvent transfer that is molecular diffusion, which is slower than thermal diffusion. (Gupta et al., 2003).

2.1 Experimental Methods

Experimental techniques to visualize the performance of Vapex can be divided into two classes. **1.** Experiments performed in Hele-Shaw Cell. **2.** Experiments performed in sand pack models. The Hele-Shaw cell has been used to study the rate of interface advancement in Vapex for a two dimension system, as well as to understand the growth of vapour chamber. The Hele-Shaw cell consists of two parallel glass plates separated by

a uniform gap. The gap between the plates is used to set the permeability of the cell. The cell cavity is formed by sealing three edges of the two parallel glass plates. The cell cavity is then placed in a pressure vessel. The gap between the plates is filled with heavy oil or bitumen, and the solvent gas is injected to the cell. Gas comes into contact with the oil from the unsealed portion of the cell.

Butler and Mokrys (1989), Butler and Mokrys (1991), Mokrys and Butler (1993), Das and Butler (1994) all performed set of experiments in vertical Hele-Shaw cell using heavy oil and different solvents to investigate different aspects of Vapex process. It was found that experiments performed in Hele-Shaw cell do not represent a real system to investigate the pore scale phenomenon.

The sand packed models has been used to simulate actual porous media. Different geometries of cylindrical and rectangular models filled with porous media have been under investigation. Glass beads with different sizes, or sand with different permeability is used to simulate the permeability of the media. It is observed that in porous media the process occurs approximately ten times faster than predicted on Hele-Shaw cell results. Butler and Mokrys (1993), Jiang and Butler (1996), Jiang (1997), Butler and Mokrys (1998), Jin (1999), Butler and Jiang (2000), Oduntan et al., (2001), Karmaker and Maini (2003), Yazdani and Maini (2004) and El-Haj (2007) all performed such experiments.

Table (2.1) (Upreti et al., 2007) lists some of the characteristics of the experimental studies carried out for Vapex.

2.1 Potential Strategies to Enhance Oil Recovery

The potential strategies to enhance oil recovery through Vapex addressed by Imran et al., (2008) have been published in book "***Petroleum Science Research Progress***" published by Nova Publishers (2008). The paper is attached in Appendix A.

2.2 Effect of Drainage Height and Permeability on Vapex

Interest in Vapex for heavy oil and bitumen recovery has grown considerably as a viable and environmental friendly alternative to the currently used thermal processes. However the predicted low production rates from Vapex for its field application remain serious barriers towards its commercial application. Most of the scale up methods used to translate the laboratory results to field application were based primarily on the reservoir transmissibility. An analytical model developed by Butler and Morky (1989) showed that the oil rate should be proportional to square root of reservoir transmissibility. The effect of convective dispersion between the solvent and heavy oil was ignored in this model development.

Oduntan et al., (2001) developed a scale up method for Vapex process using physical model experiment carried out in model of different sizes with Cold Lake bitumen and butane as solvent. To determine the effect of pay zone thickness the production rate of live oil was correlated with the pay zone length of the models. Different model heights from 21 cm to 247 cm were employed, and the height of retention by capillarity observed experimentally was subtracted from the length of the models. Production rate of live oil through Vapex was not found to be a linear function of drainage height instead was a power function for a particular permeability and dip angle. Following production rate to drainage height dependency correlation was obtained:

$Q=1.4\times10^{-3}L^{0.55}$ (Valid for 136 Darcy permeability and 45° dip angle). (2.1)

where Q is the volumetric flow rate, and L is the effective drainage height.

Production rates were found to be directly proportional to square root of the permeability.

For scale up of laboratory scaled models to field scale following correlation was suggested (Oduntan et al., 2001):

$$\frac{Q_f}{Q_M} = \sqrt{\frac{k_f h_f}{K_M h_M}} \tag{2.2}$$

Where Q_f is volumetric production rate of live oil for field, Q_M is volumetric production rate of live oil from model, k_f and k_m are field and model permeability and h_f and h_m are model and field drainage heights.

Yazdani and Maini (2005) performed a series of experiments using butane as solvent and two different types of oil (Dina oil and Elk Point oil). They used a sliced type physical model that places the sand pack in the annulus formed by two cylindrical pipes. Their aim was to understand the effect of drainage height on production rates in Vapex for transmissibility based scale up methods. It was concluded that stabilized oil rates in Vapex process is a function of drainage height to the power range of 1.1 to 1.3. Following relationship was suggested for scaling up the experimental rates to field

$$\frac{Q_f}{Q_M} = \left(\frac{h_f}{h_M}\right)^n \frac{\left(\sqrt{k\phi^m}\right)_f}{\left(\sqrt{k\phi^m}\right)_M} \tag{2.3}$$

where n is in the range of 1.1 to 1.30, h is the drainage height and ϕ is porosity of the medium.

Table 2.1: Characteristics of the Experimental Studies Carried out for Vapex (Upreti et al., 2007).

Reservoir Model	Solvent	Heavy oil and Bitumen	Temp °C	Pressure MPa	Permeability Darcy
Scaled and Packed with 1mm glass beads	Hot water and propane mixture, ethane and propane	Tangleflags oil	20-70	0.89-1.55	1150
Scaled and packed with 1mm glass beads	Propane, propane and steam mixtures	Tangleflags North heavy oil	20-26 with propane, 185 with mixture	0.708-0.984 with propane, 1.1 with mixture	830
Scaled and packed with 1mm glass beads	Butane	Piece River Bitumen, Lloydminste oil	21–22	0.23	20–30,30–50, 50–70 mesh Ottawa sand
Two dimensional multi layer	Butane	Tangleflags Northfield Lloydminste	21–23	0.21–0.23	43.5–217
Packed with silica sand	Ethane	Cold Lake Bitumen	20–33	0.83–4	80–110
Scaled and packed with 1mm glass beads	Propane	Tangleflags Heavy oil, Peace River Bitumen	20–23	0.8–1	20–30 30–50,50–70 mesh Ottawa sand

Table 2.1: (continued)

Reservoir Model	Solvent	Heavy oil and Bitumen	Temp °C	Pressure MPa	Permeability Darcy
Packed with 20-30 mesh Ottawa sand	Propane, butane and their mixture with non condensable gas	Atlee Buffalo Oil	21–27	0.31–2.2	220
Angled rectangle micro models	Butane	Peace River	19–22	0.21–0.23	55–192
Packed with 20-30 mesh Ottawa sand	Propane, butane and their mixture with non condensable gas	Atlee Buffalo Oil	21–27	0.31–2.2	220
Hele-Shaw cell	Propane	Dover and Penny Bitumen	10–23	Below dew point	
Angled rectangle micro models	Butane	Peace River	19–22	0.21–0.23	55–192
Annular Model packed with glass beads	CO2 propane, methane propane	Oil viscosity 3.3 pa,s at 24°C	23–24.9	1.82-4.23	648
Rectangular and packed model	n-butane	Oil viscosity 18.5 pa,s at 15°C	15	0.17	223–648
Rectangular sand packed model	Methane propane	Oil viscosity of 40 pa.s at 10°C	10,19	1.2	2-8

2.3 Diffusion Coefficients

The primary molecular phenomenon responsible for reduced viscosities during Vapor extraction that occurs due to gas absorption and mixing of solvent gas with heavy oil and bitumen is diffusion of the solvent gas to heavy oil. Diffusion plays a vital role in Vapex. For Vapex process actual diffusion data for solvent gas and bitumen systems are necessary to determine, 1) The amount and flow rate of gas required for its injection into reservoir, 2) the extent of heavy oil and bitumen reserves that would undergo viscosity reduction, 3) The time required for reservoirs to become less viscous and more mobile as desired, and 4) The rate of live oil production from the reservoir (Upreti et al., 2007).

Diffusion coefficient is a transport property required to calculate the rate of mass transfer of a species in a medium through molecular transport. Molecular diffusion may be visualized as the random movement of the molecules from higher concentration region to lower concentration zone. Therefore diffusion can be defined as a molecular flux due to concentration difference between two fluids (Bird et al., 2002).The mass flux of a species can be shown by Fick's first law as:

$$j = -D\nabla c \tag{2.4}$$

In above equation j is mass flux of diffusing species, c is concentration of diffusing species (kg/m^3) and D is diffusivity of the diffusing species in the medium (m^2/s).The negative sign is because the molecular diffusion always occurs in the direction of higher concentration to the lower one.

Equations to predict the diffusion coefficients are based on four general theoretical approaches. 1) Hydrodynamic Theory, 2) Kinetic Theory, 3) Absolute Rate Theory and 4) Semi Empirical expressions. Hydrodynamic theory considers diffusing molecules as rigid particles moving through a continuum. Kinetic theory considers binary collision between the molecules of diffusing species and medium. Absolute Rate theory relates diffusivity with the change in the activation energy due to molecular motion from one

equilibrium position to another. Semi empirical expressions are based on hydrodynamic and kinetic theory.

By considering the particles of a diffusing species as rigid sphere moving through a liquid continuum, Stokes Einstein equation relates the diffusion coefficients with the diffusing particles radius, liquid viscosity, and the absolute temperature as follows: (Wilke and Chang, 1955).

$$D_{AB}=\frac{kT}{6\pi r_A \mu_B} \tag{2.5}$$

Where D_{AB} is the diffusion coefficient of diffusing species A in liquid B; k is the Boltzman constant; T is the absolute temperature; μ_B is the viscosity of liquid B; and r_A is the particle radius of diffusing species A. According to this equation diffusion coefficient is inversely proportional to the particle radius of the diffusing species and the liquid viscosity. The Stokes Einstein equation is generally applicable to binary liquid-liquid systems with relative large diffusing molecules. Therefore, the successes in predicting the diffusion coefficient of gas-liquid system is limited.

Hayduk and Cheng (1971) tested the hypothesis that diffusivity of a particular dilute species in any solvent depends only on the solvent viscosity. But with the condition that state of molecular aggregation of both the solute and solvent remains unaltered on mixing. The following relationship between the diffusivity and viscosity was proposed:

$$D = \alpha \mu^{-\beta} \tag{2.6}$$

Where α and β are constant for each diffusive substance.

Hiss and Cussler (1973) studied the diffusion of small solute molecules in dilute solutions. They measured the diffusivity of n-hexane and naphthalene in 2,2,4 tri methyl

pentane and a series of hydrocarbon oil mixtures with viscosity ranging from 0.5 to 5,000 mPa.s. Following relationship was suggested:

$$D = \alpha \mu^{-\frac{2}{3}} \tag{2.7}$$

Hayduk and Minhas (1982) presented a correlation for estimation of molecular diffusion of paraffin solute/solvent pairs as a function of temperature, molar volume of solvent propane and viscosity of the medium within which the diffusion is occurring. The relationship is shown below:

$$D = 13.3 \times 10^{-8} T^{1.47} V_a^{0.71} \mu^{(10.2/V_a - 0.791)} \tag{2.8}$$

Where T is Temperature and V_a is molar volume of the solvent and μ is viscosity of the medium where diffusion occurs.

The application of the theoretical or semi empirical equations is valid only at the atmospheric pressure (Yang, 2005). But heavy oil and bitumen recoveries are mostly under higher than atmospheric pressures, so mostly experimental methods are developed to calculate the diffusion of solvent gases in heavy oil and bitumen.

The different experimental methods for determination of diffusivity of gases in bitumen can be classified into direct or conventional and indirect or unconventional methods. Direct methods are based on determination of composition of the diffusing species along the length of the bitumen sample with time and require compositional analysis. The indirect methods measure the change in one of the system parameters that varies because of the diffusion, without determining the composition. Such parameters are pressure, interface velocity, magnetic field strength, or the volume of the diffusing solute.

Das and Butler (1996) calculated the diffusion coefficients of propane and butane in Piece River bitumen. The experiments were carried out in Hele-Shaw cell along a vertical

edge with solvent vapor at a constant temperature and pressure. The production rates were predicted by applying the model of Butler and Mokrys (1991). The diffusivity of the hydrocarbon molecules was expressed by the general form of Hayduk and Cheng (1971). The unknown in the equation for diffusivity were calculated by assuming the value of β between 0 to 1, and the model equation was solved for α for experimental points. The corresponding value of α was found to be 1.306×10^{-9} at the minimum deviation with $\beta = 0.46$. The relationship between the diffusivity and viscosity by using propane as a solvent was suggested:

$$D = 1.306\times10^{-9}\mu^{-0.46} \qquad \text{(propane as solvent)} \qquad (2.9)$$

The above expression is almost the same as shown by Hayduk et al., (1973), but is about ten times higher than that for the same viscosity. The reason could be that the liquid through which the molecules are diffusing is much less viscous than the overall fluid comprising the macromolecules.

Due to similarity of the diffusivity vs viscosity relation between methane, ethane and propane in identical solvents, the diffusivity of the butane was expressed by changing the coefficients in Equation [2.6]. The following relationship for the butane diffusivity was obtained (Das and Butler, 1996):

$$D = 4.13\times10^{-10}\mu^{-0.46} \qquad \text{(butane as solvent)} \qquad (2.10)$$

The above relation shows that butane diffuses at a slower rate than propane.

Upreti and Mehrotra (2000,2002) used indirect non-intrusive pressure decay experimental method to find the diffusivity of CO_2, CH_4, C_2H_6 and N_2 gases in Athabasca bitumen. They observed that diffusivity is a function of gas concentration in bitumen. At a given gas concentration and pressure, the diffusivity increases with temperature. Their results indicate that gas diffusivity generally increases with pressure at a given temperature and

gas concentration. They estimated the diffusivity of these gases in Athabasca bitumen, in the temperature range of 25–90°C at pressure 4 and 8 MPa. Based on the experimental results, they developed a correlation for average gas diffusivities as follows:

$$\ln D = d_0 + d_1(T + 273.15) \tag{2.11}$$

where D is diffusivity of gas, d_0 and d_1 are coefficient of equation and T is Temperature. Experimental procedures were developed by James et al., (2003) for investigating the transient behaviour of butane solubility in heavy oil for direct contact with butane vapour. Experiments were performed at 25°C in a tube (for diffusion purposes). The decrease in butane height due to uptake of butane in heavy oil was measured. The change in height of the butane and change in height of bitumen was modeled based on fundamental equation of continuity adapted from Grogan and Pinczewski (1987). Solvent concentration and mixture density profiles were determined based on input diffusion functions. The following diffusivity functions dependent on the solvent mass fraction were used:

$$D = 1\times10^{-6} \tag{2.12}$$

$$\ln D = a\omega^5 + b\omega^4 + c\omega^3 + d\omega^2 + e\omega + f \tag{2.13}$$

$$D = 2\times10^{-6}\omega + 2\times10^{-8} \tag{2.14}$$

$$D = 1\times10^{-6}\omega + 1\times10^{-6} \tag{2.15}$$

$$D = 8\times10^{-6}\omega^2 + 2\times10^{-7} \tag{2.16}$$

ω is solvent mass fraction and D is diffusivity. In Equation [2.13] a, b, c, d, e and f are the coefficients of polynomial expression and their values can be found elsewhere (James et al., 2003). None of the above mentioned linear as well as polynomial functions gave a perfect match with experimental results. It was concluded that model developed

successfully determines the change in butane and bitumen height, and instead of using diffusivity function an optimization program should be used to optimally determine the diffusivity.

The experimental diffusivities of solvent gases in heavy oil and bitumen are on the order of 10^{-9} to 10^{-11} m^2/sec. (Upreti et al., 2007). Table (2.2) lists some of the available diffusivity data (Upreti and Mehrota, 2002; El-Haj, 2007).

Table 2.2: Available Diffusivity Data of Gases in Bitumen (Upreti and Mehrota, 2002).

Bitumen	Gas	Pressure (MPa)	Temperature (°C)	Diffusivity $\times 10^9$ (m²/s)
Athabasca bitumen	CO_2	5	20	0.28
			50	0.50
			75	0.71
			100	0.92
			125	1.15
			150	1.41
			175	1.55
			200	1.75
Maljamar Crude Oil	CO_2	5.2	25	2.1
Stock Tank Oil	CO_2	15	66	3
			75	8.5–9.2
			80	4.6
Heavy Oil	CO_2	2.84	21	4.76
Aberfeldy Oil	CO_2	1	23	6
Athabasca bitumen	CH_4	5	50	0.4–0.75
Athabasca bitumen	C_2H_6	5	20	0.175
			50	0.174
			75	0.337
Athabasca bitumen	CO_2	4	25	0.1335
			50	0.2338
			75	0.3739
			90	0.4280
Athabasca bitumen	CO_2	8	50	0.3980
			75	0.7436
			90	0.9319
Athabasca bitumen	CH_4	4	25	0.0810
			75	0.2932
			90	0.4315
Athabasca bitumen	CH_4	8	25	0.0582
			50	0.1518
			75	0.2029
Athabasca Bitumen	N_2	4	50	0.0513
			75	0.2335
			90	0.4960

2.4 Dispersion Coefficient

In Vapex, mixing of fluids due to combined effect of diffusion and convective motion cannot be ignored. This mixing phenomenon can be referred as dispersion or effective diffusion. As from definition, dispersion is directly applicable to a dynamic process such as Vapex where gravity induces the convective motion in fluids. Dispersion is the combined effect of molecular diffusion, convective motion, surface renewal, viscosity reduction and gravity drainage in Vapex, and prevails in the direction perpendicular to the fluid flow under gravity.

The dispersive mass transfer in Vapex is comprised of two components: the longitudinal dispersion and transverse dispersion. Longitudinal dispersion develops along the direction of the bulk flow in systems where solute and solvent are flowing in the same direction. Downward movement of diluted oil along the interface will cause longitudinal dispersion in the same direction. While transverse dispersion is perpendicular to the direction of the bulk flow and into the bitumen bulk. The process of the transverse and longitudinal dispersion is schematically illustrated in Figure (2.1).

Several aspects of the Vapex process have been under investigation for the past twenty years. Butler and Mokrys (1989) developed the first analytical model for Vapex based on thin-film flow theory, as direct analogue of the SAGD process. The model was primarily developed by combining Ficks law of diffusion and Darcy equation of flow into mass and momentum balance of their model. They assumed that mass transfer of solvent into the bitumen bulk is under steady state condition, also solute solvent interface moves at a constant speed. They developed the following equation to estimate the recovery rates from Vapex:

$$Q = \sqrt{2K\,g\phi\Delta S_0\,N_s\,h} \qquad (2.17)$$

Where Q is the volumetric recovery rate of live oil, K is the permeability of media, ϕ is the porosity of the medium, ΔS_0 is the change in oil saturation, g is the gravitational acceleration, h is the height of the medium or cell height and N_s is a dimensionless number as

$$N_s = \int_{c_m}^{c_i} \frac{\Delta\rho D(1-c_s)}{\mu c_s} \qquad (2.18)$$

In the above expression c_m is the minimum solvent concentration, c_i is the maximum solvent concentration, c_s is the concentration of solvent in bitumen, $\Delta\rho$ is the difference between density of pure bitumen and density of pure solvent, μ is the viscosity of the diluted oil and D is the diffusivity of the solvent gas.

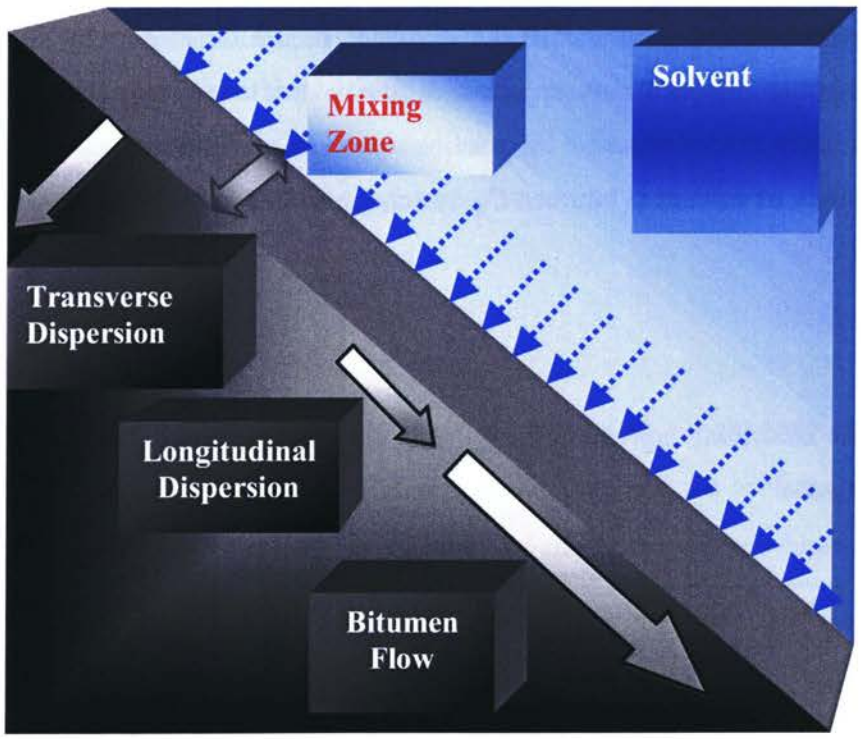

Figure 2.1: Schematic of Dispersion at Heavy Oil and Bitumen Interface

Butler and Mokrys (1991) performed their experiments in Hele-Shaw cell using toluene as a solvent with Suncor and Athabasca bitumen. Discrepancy between the actual recovery rates and obtained from Equation [2.17] was very little. Dun et al., (1989) developed a similar mathematical model for injection of solvent gases in porous media. They did not consider the strong dependency of diffusion on solvent concentration. In order to history match the modeled results with experimental results obtained from performing the experiments with Athabasca bitumen and ethane and CO_2 solvents, they had to employ diffusion coefficients much higher than published in the literature. The authors pointed out the possibility of increased recovery due to dispersion.

Lim et al., (1996) used an effective diffusivity; two to three orders of magnitude higher than the molecular diffusivity to history match their experimental results in sand pack models. They could not explain the reason for enhanced recovery rates in porous media, but they pointed out "physical dispersion" to be the most effective reason for higher recovery rates.

Das and Butler (1998) modified the earlier model developed by Butler and Mokrys (1989), by introducing an apparent diffusion coefficient in porous media. Following relationship was presented by relating apparent diffusion coefficient D_p to intrinsic diffusivity of solvent in bitumen D_0, system porosity ϕ, and cementation factor Ω as:

$$D_p = D_0 \phi^{\Omega} \tag{2.19}$$

and the analytical expression for oil recovery rates [Equation 2.17] in porous media was modified as

$$Q = \sqrt{2 k g \phi^{\Omega} \Delta S_0 N_s h} \tag{2.20}$$

They performed a number of experiments in sand pack model with Peace River and Athabasca heavy oil and concluded that an effective diffusion coefficient is required to

history match the experimental results. They also observed that extent of gas liquid interface becomes more dispersed in finer sands. Diluted residual oil drainage phenomenon was explained as, the solvent bitumen interface moves away the oil left behind in still in contact with solvent chamber, therefore after a long residence time solvent concentration increases, the surface tension decreases and hence the gravity forces exceeds the capillary forces thus draining the diluted oil.

Das and Butler performed a number of experiments to understand the prime factors involved in enhanced mass transfer in porous media (Das and Butler, 1995; Das and Butler, 1998). Proposed mechanism for enhanced recovery rates through porous media are physical dispersion, improved interfacial contact, enhanced surface renewal, development of transient mass transfer across the interface, increased solubility due to solvent vapour condensation in fine capillaries and enhancement during the rising of the solvent chamber.

The relationship between the effective diffusivity of gas and the viscosity μ of its mixture with heavy oil and bitumen in Vapex experiment was experimentally determined by Das and Butler (1996) on the basis of following correlation proposed by Hayduk and Chang (1971) by performing the experiments in Hele-Shaw cell with Peace River bitumen and propane and butane as solvents.

$$D = \alpha \mu^{-\beta} \, (\mathrm{m}^2/\mathrm{s}) \qquad (2.21)$$

They found optimum value for α and β. They concluded for propane value of α is higher than of butane while value of β is constant for both the solvents, and that gas diffusivity increases with decrease in viscosity of the heavy oil and bitumen in a non linear fashion.

Nghiem et al., (2001) developed a compositional model for prediction of asphaltene dropout and down hole upgrading capability of bitumen by Vapex. They incorporated molecular diffusion and convective dispersion into the material balance. They concluded

that mixing mechanism is effectively controlled through a total dispersion coefficient, and also showed that larger dispersion coefficient results in higher mixing.

Boustani and Maini (2001) examined Vapex in Hele-Shaw cell with Penny bitumen and propane as the solvent. They compared diffusivity of solvent as a function of concentration on the basis of three different correlations. They incorporated dispersive effects in mass transfer models of the Vapex process and found reduced discrepancy between the experimental and analytical models. They concluded that correlation developed by Das and Butler (1996) tends to overestimate the molecular diffusion coefficient and under estimate over all mass transfer in porous media. By incorporating Taylors dispersion accounting for a likely wall effect in Hele-Shaw cell they found better agreements between the predicted results and experimental values using Hayduk et al., (1971) correlation.

Das (2005) indicated the concentration dependent solvent gas dispersion in Vapex, by using different values of dispersion coefficient. He found that a bulk constant value of dispersion coefficient cannot model Vapex process because the phenomenon such as diffusion and viscosity that are embodied in dispersion are strong function of solvent viscosity.

Kapadia et al., (2006) developed mathematical model to describe the experimental vapour extraction of the bitumen held in a rectangular porous block. Following assumptions were adopted: The process is carried out at constant temperature and pressure, the porosity and permeability of the porous medium is constant, the mass fraction of the solvent at the interface is saturation mass fraction under equilibrium, the dispersion of the gas takes place along x axis and along y axis the transfer of the gas is governed by the y component of the Darcy's velocity in porous medium, the dispersion of gas causes molecular diffusion, the effect of surface renewal and any convective component along $x-$ direction, there is no mass transfer at the end of the vertical face and no variation of state variables along the thickness of the block.

Following partial differential equation resulted from pseudo-unsteady state mass balance of constant density block was to solve:

$$\phi\frac{\partial\omega}{\partial t}=\frac{\partial}{\partial x}\left(D\frac{\partial\omega}{\partial x}\right)-v\frac{\partial\omega}{\partial y} \tag{2.22}$$

Where

$$v=\frac{K_r K\rho g\cos\theta}{\mu} \tag{2.23}$$

Relation between mass fraction and dispersion was achieved by using the following correlations:

$$\mu=\mu_0\omega^{-2} \tag{a}$$

and

$$D\ \alpha\ \omega \tag{b}$$

The cumulative volume of live oil produced at any time was given by:

$$V_{cal}=\alpha V\text{, where } V=\phi^{2/3}Z\int_0^X(Y_0-Y)\mathrm{d}x. \tag{2.24}$$

An objective function that is fractional error between the simulated and experimental values of live oil production was calculated. Optimum dispersion of butane along with its solubility was determined by minimizing the objective function. The saturation mass fraction of solvent was found to be 0.87 and Dispersion coefficient achieved was 0.556 cm^2/s. The optimal value of D_0 was in four orders of magnitude higher than corresponding coefficient reported for the molecular diffusion of butane on Peace River bitumen.

El-Haj (2007) experimentally determined butane dispersion in Vapor extraction of heavy oil and bitumen. The experiments were carried out at room temperature ranging from 19 to 24°C, using butane as a solvent at the dew point pressure. Cylindrical geometries were used packed with porous media of different permeability. A mathematical model based on theory was developed to describe the process of butane absorption and subsequent live oil drainage in the experiments. The dispersive flux that embodies the effect of molecular diffusion, viscosity reduction of heavy oil, surface renewal of bitumen upon its drainage and capillary forces in porous medium was assumed to be insignificant in vertical direction compared with the gravity generated flux. Assuming constant temperature, constant pressure, and constant live oil density the following mass transfer model equation was obtained:

$$\frac{\partial \omega}{\partial t} = -\frac{v}{\varphi}\left(\frac{\partial \omega}{\partial z}\right) + \frac{D}{\varphi}\left(\frac{1}{r}\frac{\partial \omega}{\partial r}\right) + \frac{D}{\varphi}\left(\frac{\partial^2 \omega}{\partial r^2}\right) + \frac{1}{\varphi}\left(\frac{\partial D}{\partial \omega}\right)\left(\frac{\partial \omega}{\partial r}\right)^2 \qquad (2.25)$$

following with Darcy's velocity responsible for live oil flow in porous medium assumption.

Following concentration dependent live oil viscosity expression was employed

$$\mu = \mu_0 \omega^{-2} \qquad (c)$$

For the dispersion of gas in heavy oil and bitumen, the following correlation was used

$$D = D_0 \omega \qquad (d)$$

The cumulative mass of produced oil at any time was calculated as:

$$m_{cal} = 2\pi\rho \int_0^R (Z_0 - Z) r dr \qquad (2.26)$$

Dispersion coefficient was considered a linear function of butane concentration in the medium.

Root mean square errors were obtained by solving the model equation with various values of maximum solvent concentration and dispersion coefficient. The optimal dispersion coefficients were 9.8×10^{-8}, 9.5×10^{-8} and 9.4×10^{-8} m^2/s for 110,157 and 180 Darcy. Dispersion coefficient for a lower permeability medium was observed to be slightly higher and this behaviour was explained as an increase in interstitial area with decrease in glass beads size (irregular shapes) promotes dispersion in the porous medium.

3 Research Objectives

It is obvious from literature survey that to accurately predict the heavy oil and bitumen recovery through Vapex process for its commercial application it is very important to evaluate dispersion of various solvents used in this process for various heavy oil and bitumen (different viscosity). Furthermore as one of the key fundamentals for solvent dispersion is surface renewal that has huge dependency on production rate, determination of solvent dispersion for the factors that may enhance production rate like drainage height becomes more essential. Literature survey indicates lack of much needed dispersion data especially its dependence towards drainage height. Motivated by the same necessity, during this study concentration-dependent dispersion of butane in porous medium exhibiting constant permeability for different drainage heights at constant temperature with corresponding solvent dew point pressure was experimentally determined. In order to achieve the goal research had the following objectives:

- Experimentally determining required input parameters for calculating dispersion coefficient of solvent gas in bitumen.

- Develop a theoretical mathematical model and solve it with experimentally determined parameters to calculate gas dispersion.

- Observe Effect of drainage height on production rates through Vapex.

- Correlate dispersion coefficient of solvent gas to drainage height in Vapex.

3.1 Methodology

This research is combination of experimental and simulation studies. Experiments are performed to generate production data along with determination of input parameters required to simulate the production rates through Vapex process. The input parameters are solvent gas solubility, live oil viscosity and live oil density. The mathematical model developed to simulate dilute oil production rates is solved for two unknowns. Optimal values of unknowns which are dispersion coefficient of solvent and its maximum mass fraction at interface are obtained by history matching experimental and simulation results. Figure (3.1) shows schematic of methodology.

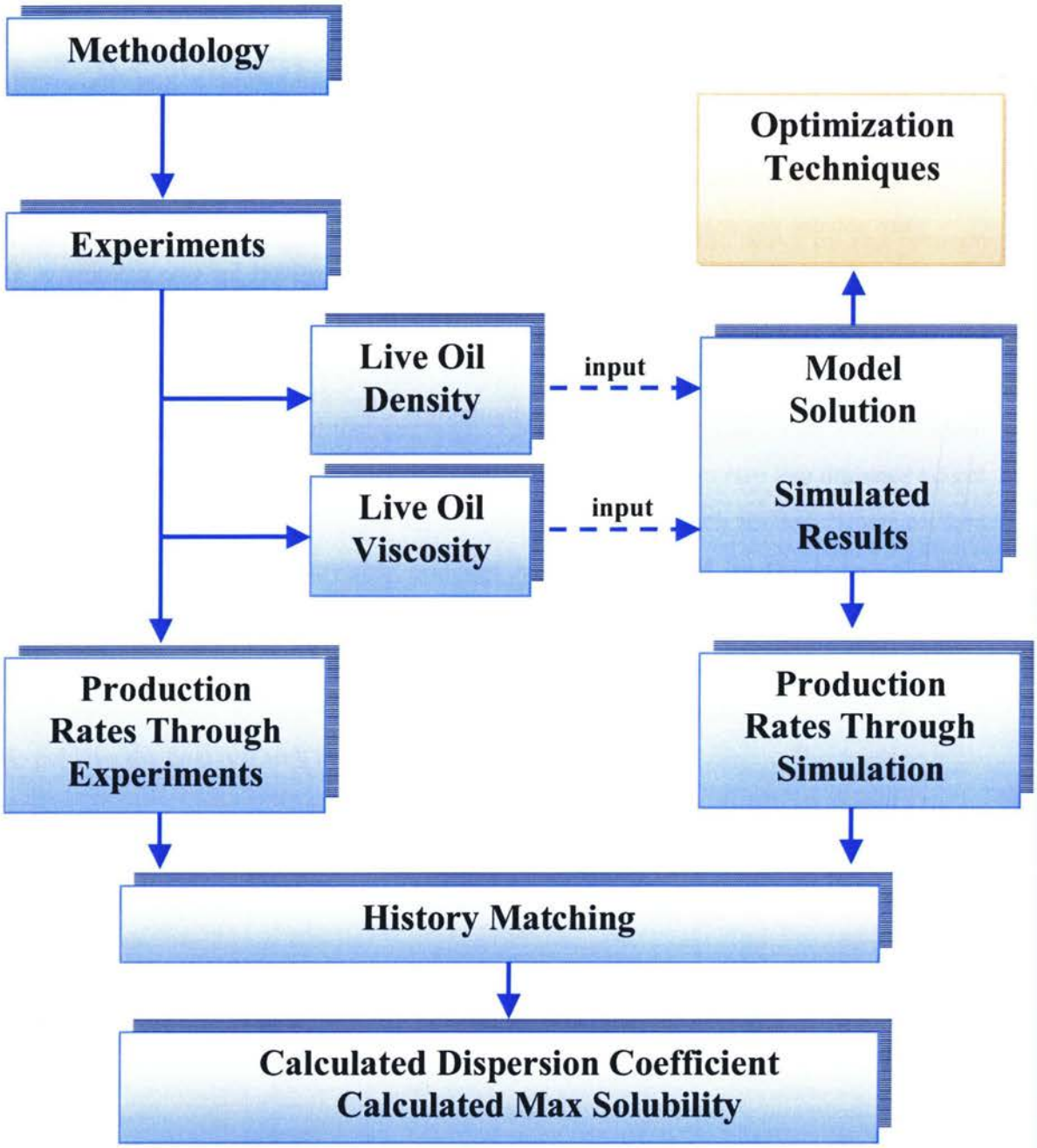

Figure 3.1: Methodology Schematic

4 Experimental Setup & Procedure

In this chapter the details of experimental setup and procedures are described to perform the vapor extraction of heavy oil in transport phenomenon lab of Chemical Engineering Department, Ryerson University. Required data to calculate the dispersion coefficient of butane as solvent gas was generated from the experiments.

4.1 Viscosity of Crude Oil (Heavy Oil)

The viscosity of heavy oil (supplied by The Imperial Oil Inc Canada) was determined by using Bohlin Viscometer. A small amount of oil (10 grams) was placed in the cone and plate arrangement of the viscometer. The viscosity of the heavy oil was determined at different temperatures starting from 20°C to 40°C. The viscosity of the oil at the experimental temperature was found to be 350,000 mPa.s. Figure (4.1) shows viscosity of heavy oil vs temperature trend. The heavy oil had 9.8° API gravity, and 1.0015 specific gravity.

4.1 Experimental Setup

The experimental setup mainly consist of a Chlorinated Poly Vinyl Chloride cylindrical pressure vessel (dimensions: 55 cm height, 15 cm internal diameter) placed inside a water bath with the arrangement of load cell and monitoring instruments like temperature of the vessel, pressure inside the vessel, temperature of the sample and temperature of water bath. The maximum operating pressure of the vessel was 50 psig. The schematic of the experimental setup is shown in Figure (4.2). Figure (4.3) shows the picture of the experimental setup. Four different cylindrical models with inside radius of 3 cm and lengths of 15, 25, 35 and 45 cm were used to study the effect of drainage height on

production rates as well as dispersion coefficient of butane in heavy oil and bitumen, (Figure 4.4).

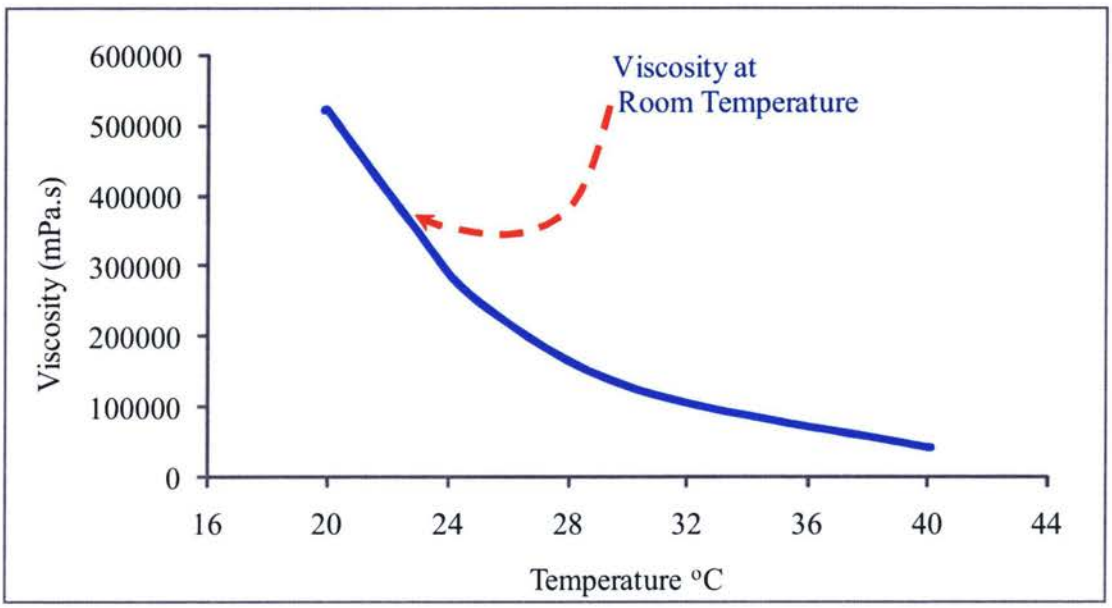

Figure 4.1: Viscosity of Heavy Oil vs Temperature

Oil saturated porous medium with glass beads of known size was packed in one of the cylindrical models and attached with the load cell hook, fitted on the top flange of the pressure vessel. The load cell was used to record the weight change in the sample model resulted from dispersive action of the solvent gas that dilute the heavy oil. A small funnel was fitted at the bottom of pressure vessel to collect diluted drain oil and direct it towards the collection tube.

The directed oil from the funnel was collected in a collection tube calibrated to 25 cm^3. The collection tube was connected to a stainless steel capillary tube with an inside diameter of 0.1016 cm. The length of the capillary tubes was 50 cm, and it was used to measure the viscosity of live oil. A differential pressure transducer was in place with intake from both sides of the capillary tube.

Through capillary tube oil was directed to a stainless steel flash tank with holding capacity of 300 cm^3. Temperature of the flash tank was controlled by wrapping a flexible electrical heating tape (HTWC 101, heat tape with controller) around it. In case of higher temperature difference between the surrounding and live oil, a provision of wrapping the capillary tube with electrical heating tape was also available. Flash separation tank was used to flash the dissolved butane in the live oil. Separated solvent gas from flash tank was then routed to set of two water columns connected to each other, used to measure the amount of dissolved butane in live oil. The cylinders were made of acrylic with a total capacity of 2,600 and 2,900 cm^3 respectively. First cylinder was totally filled with water and second cylinder was scaled and used to collect the water displaced from the first cylinder when butane was flashed out.

A vacuum pump was used to evacuate air from the whole setup at the start of each experiment. Temperature of the water bath was controlled with a heat exchanger that takes supply from a water pump placed at the bottom of water tank. A needle thermocouple and three resistance temperature detectors were used to measure the temperature of physical sample, butane gas, flash tank and water bath. The butane gas pressure and pressure across the capillary tube were transmitted by pressure transducer and industrial differential pressure transducer respectively. Flow of butane gas to the pressure vessel was monitored by a flow meter (Model No: FMA-1605, Type: mass and volume flow meter, STP: 25 °C and 14.696 psia, Operating Temperature: -10 to +50 °C, Maximum Pressure 125 psia) placed on the supply line of butane. Table (4.1) shows the specifications for the instrument used during this study.

Table 4.1: Instrument Specifications used During Vapex Study

Name of Instrument	Used in	Range	Accuracy (Error %)
Needle Thermocouple	Physical Model	0–200°C	0.1%
Resistance Temperature Detectors	Butane Gas, and Flash Separation Tank	0–200°C	0.1%
Pressure Transducer	Pressure Vessel	0–185 (psig)	0.5%
Differential Pressure Transducer	Viscosity Measurement	0–25 (psig) Max Operating Pressure of 200 (psig)	0.5%
Flow Meter	Butane Supply Rate	10–50°C 110 psig(max)	0.1%
Load Cell	Physical Model weight measurement	0–3500 (g)	0.25% (of full load)

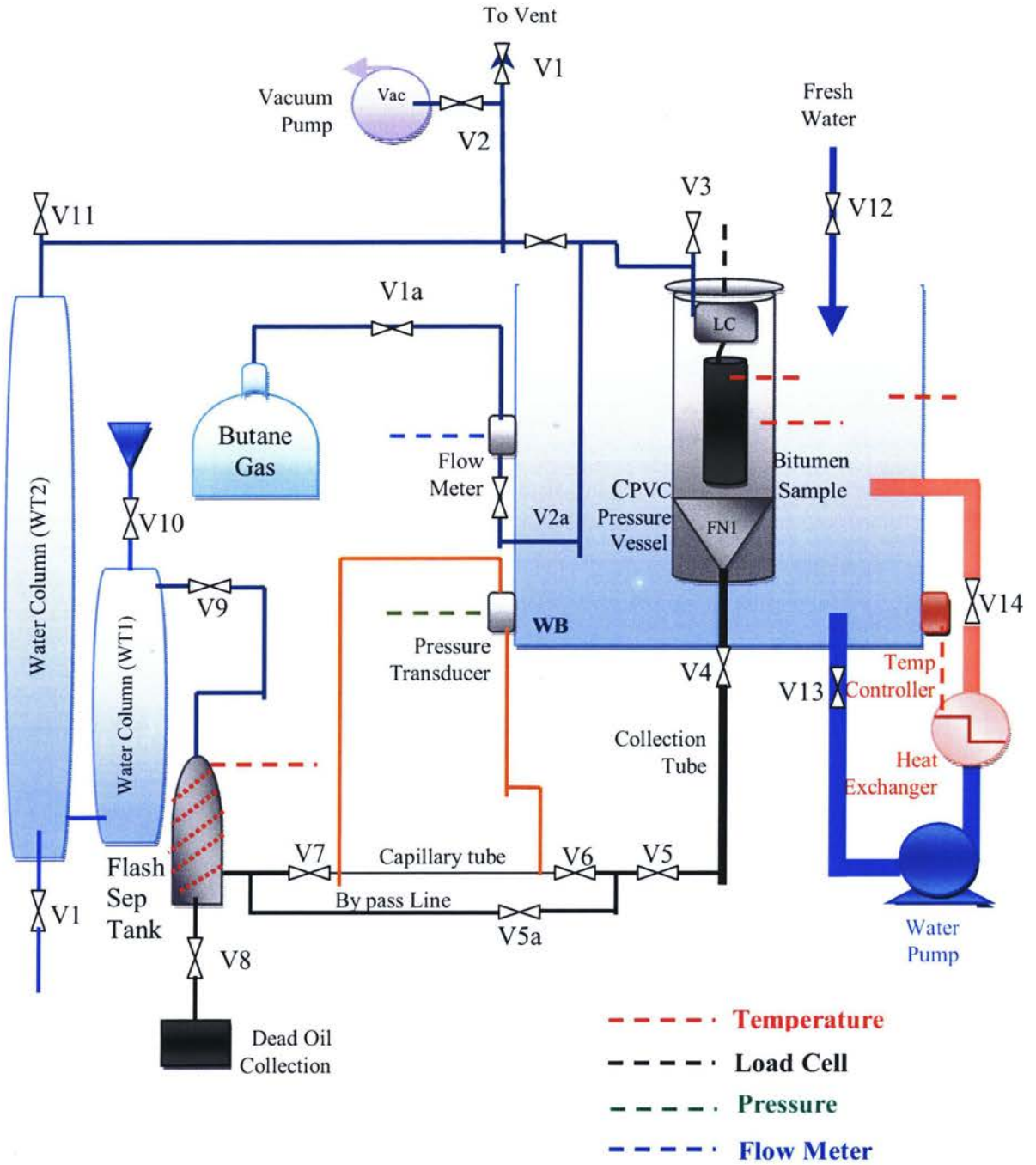

Figure 4.2: Schematic for Vapex Experiment

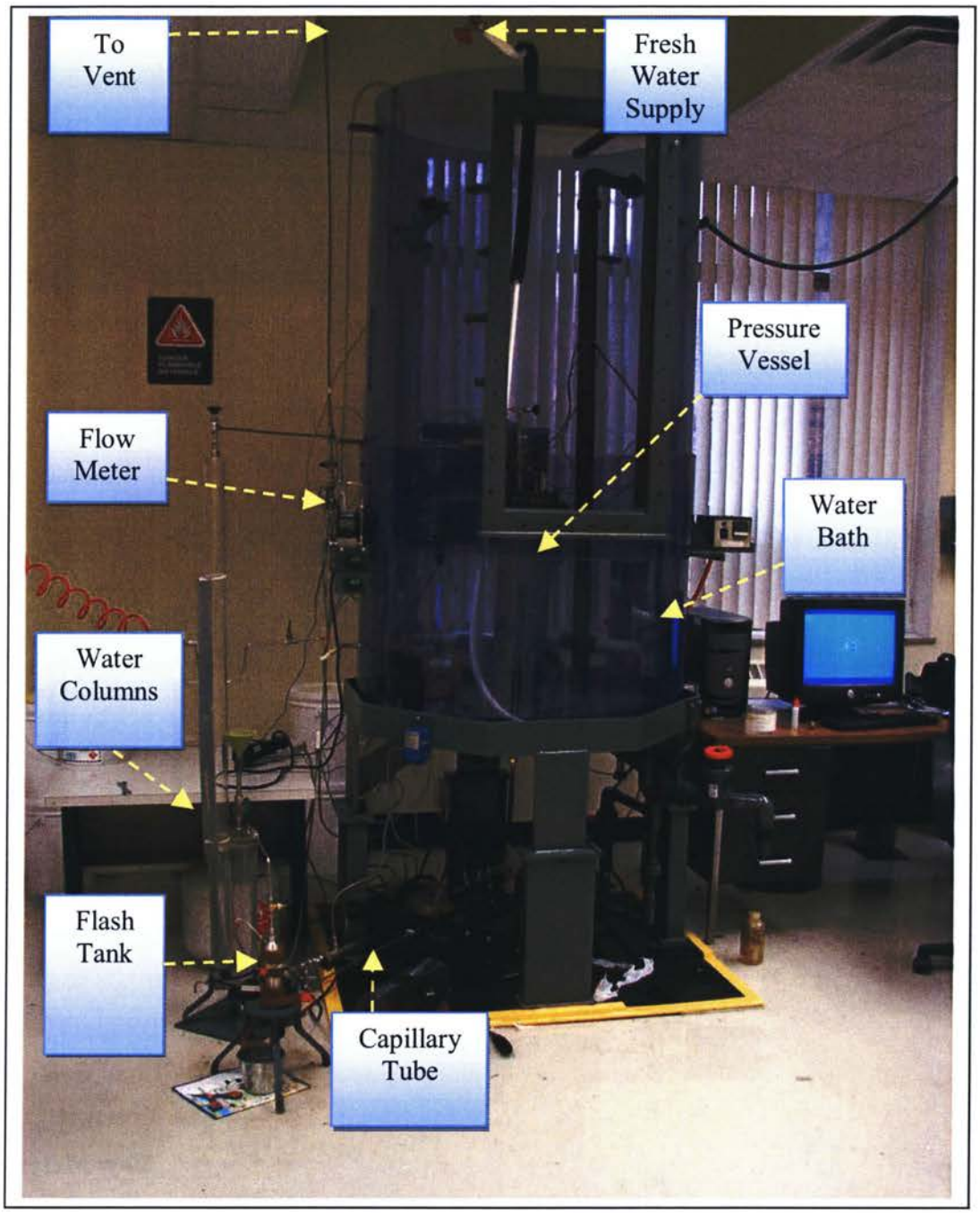

Figure 4.3: Picture of Vapex Experimental Setup

Figure 4.4: Different Model Heights for Experiments

Online monitoring of the process conditions was carried out by attaching the experimental setup with Ethernet Data Acquisition System – EDAS (16 bit resolution), which was connected to the computer. For Graphical user interface the Labview 7 software was used and the following parameters were recorded:

- Temperature of the physical model
- Temperature of the pressure vessel
- Pressure of the pressure vessel
- Inlet gas flow of the solvent gas
- Inlet gas temperature of the solvent gas
- Weight of the physical model
- Temperature of the water bath
- Pressure difference across the capillary tube
- Temperature of flash tank

The sampling time of the acquisition system was set to 5 seconds to precisely measure the pressure difference across the capillary tube for viscosity measurement.

Butane used was of Research grade 99.99% supplied by MEGS specialty gases Inc., Montreal, Quebec.

Knowing the density of the glass beads and density of the heavy oil the porosity of the physical model was calculated to be 0.38. Porosity was measured by taking a known volume of glass beads and heavy oil saturated mixture and placing it in water filled graduated cylinder. Taking the volume of the water displaced, porosity was calculated as:

$$\phi = \frac{\text{Volume of oil}}{\text{Total Volume (Volume of displaced water)}} \tag{4.1}$$

4.2 Sample Preparation

Oil saturated porous media of known permeability was used to perform the experiments for the determination of the dispersion coefficient of the butane gas in heavy oil and bitumen. The sample preparation was conducted in very careful manners to avoid any air trapping within mixture of heavy oil and glass beads. A known amount of heavy oil was collected in a pan which was placed in a temperature controlled heater. The heavy oil was heated for at least 30 minutes at 70°C, for sufficient reduction in oil viscosity to promote glass beads mixing. To study the effect of lower permeable porous media the glass beads of smaller size 360 μm (industrial name BT 5) were used. After heating the oil up to a certain mark the glass beads were carefully added to the oil in the form of thin layers. After allowing the beads to settle down by gravity another layer was added to the oil surface. The same procedure was repeated until there was no more room for the beads to settle down. Knowing the weight of the beads and weight of the heavy oil a basis was set to prepare the samples for any model height. Almost 5 hours was the sample preparation time. Figure (4.5) shows the picture of setup used to prepare the sample for experiments.

After the heavy oil was purely saturated with the glass beads, the oil beads mixture was transferred to the physical model. Physical model was wrapped with foil paper to stop any oozing of the heavy oil out of sample. After filling the model with the porous media, the top of the model was firmly pressed to fill any air gaps within the physical model. The model was then left in an air bath for 24 hours to balance up the sample temperature with the room temperature (approximately 22°C).

Figure 4.5: Picture for Sample Preparation Setup

4.3 Sample Permeability

Permeability of the heavy oil and glass beads mixture was taken from El-Haj (2007). The procedure that was adapted by El-Haj to measure sample permeability is as follows:

To measure the permeability of the porous media consisting of heavy oil and glass beads (BT-5) mixture, a gray PVC cylinder having a cavity size of (21 cm × 6 cm) was used. The cylinder had two ports one for air inlet and one for discharge air with a screen placed at the bottom to avoid any glass beads passage. The uniform packing of the glass beads and heavy oil was prepared within the physical model. Figure (4.6) shows the schematic of apparatus used for permeability measurement.

The inlet and outlet air lines were connected through a differential pressure transducer to measure the pressure drop across the media when air is passed through. Air was injected from the top of the cylinder and inlet flow of the air was measured using a flow meter, while it was discharged from the bottom port of the cylinder. Darcy's law was used to calculate the permeability of the glass beads packing as follows:

$$Q = \frac{kA}{\mu}\frac{\Delta p}{\Delta L} \tag{4.2}$$

where k is the permeability, Q is the air flow rate, A is the cross section area of the glass bead packing, μ is the viscosity of the air, Δp is the pressure drop and ΔL is the length of glass beads packing. Table 4.2 shows calculation of sample permeability with 360 μm by rearranging Equation [4.2].

$$k = \frac{Q\mu\Delta L}{A\Delta p} \tag{4.3}$$

Table 4.2: Calculated Permeability
(El-Haj, 2007)

Glass Beads Average Size (μm)	360
Air Flow Rate "Q" (cm^3/s)	33.33
Cross section area of the glass beads Packing "A" (cm^2)	28.26
Viscosity of air "μ" ($N.s/cm^2$) at (T=20°C)	1.84×10^{-9}
Pressure drop "Δp" (N/cm^2)	4.2×10^{-2}
Length of glass beads packing "ΔL" (cm)	21
Permeability "k" (cm^2)	1.085×10^{-6}
Permeability "k" (Darcy)	1.100×10^{2}

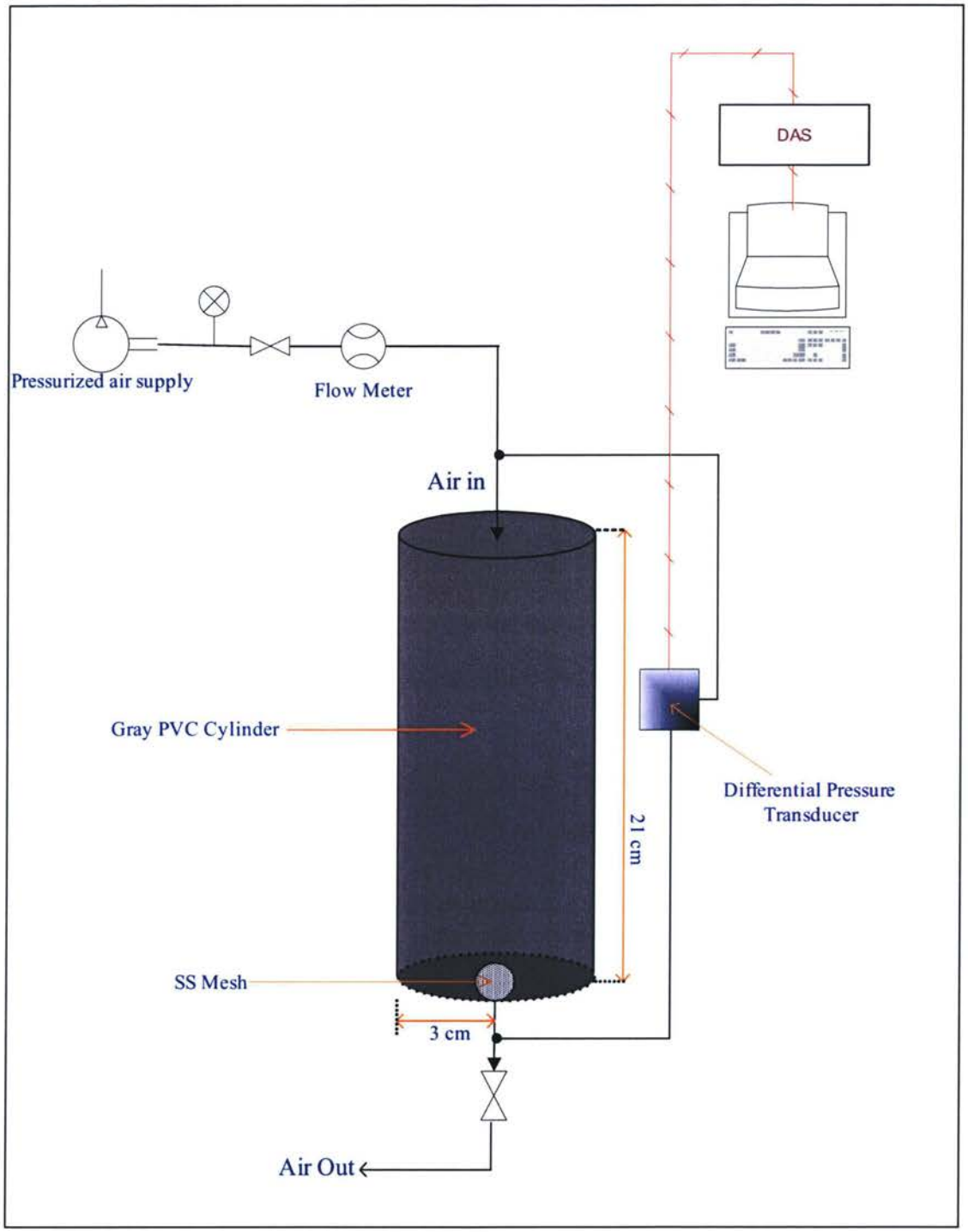

Figure 4.6: Schematic for Permeability Calculation Apparatus (El-Haj, 2007)

4.4 Experimental Procedures

Arrangement of the experimental setup is shown in Figure (4.2). Before starting each experiment the pressure vessel was tested against any leakage. The leak test was conducted by pressurizing the cylindrical pressure vessel with air to a pressure of 40 psig (almost two times higher than experimental pressure), and leaving it for 24 hours. After confirming no pressure drop, the top flange of the pressure vessel was opened and cylindrical model with saturated heavy oil and 360 μm glass beads mixture was attached to the load cell. After sealing the vessel again the leakage test was performed for a short period of time to ensure proper sealing of the vessel.

Before injecting the butane gas whole system was flushed. Vacuum pump Vac1 (shown in Figure 4.2) was started by opening the valve V2, V3, V4, V5, V6 and V7, while the rest of the valves in the system were closed. The initial running of the vacuum pump was found critical for experiment performance. The pump was run up to the mark to ensure -15 mm hg pressure within the process route.

After whole setup was vacuumed, butane gas was injected into the vessel from the top port by opening the valve V1a, V2a (passage through a mass flow meter) and V3 while all the valves after bottom of the pressure vessel were closed as well as the vent valve V1. To replace all the dead air within the vessel, the system was filled with butane gas (took almost six minutes to fill), and then vacuumed again by repeating the same steps as mentioned above. To ensure complete replacement of air with butane the same procedure was repeated for two times.

Before starting the extraction process with continuous injection of butane gas, the supply pressure of butane was adjusted at vapor pressure almost 1°C below the saturated vapor pressure of butane. This was done with a regulator valve placed on the gas supply line. A table showing the vapor pressure of butane gas at different temperature is listed in the Appendix B. At start of each experiment the flow rate of butane injected to pressure vessel was observed 2.5 L/min, and when the pressure vessel was totally filled with the

gas the flow started to reduce and was stable within a range of 0.13 – 0.14 L/min for all model lengths. It took almost 6 minutes for the cylindrical vessel to fill with butane gas.

As the gas came in contact to the exposed surface of heavy oil it started to diffuse, resulting in reduction of the bitumen viscosity. Concentration of butane gas at the interface where bitumen and gas are in contact is less than concentration of butane in rest of the vessel, and that concentration at interface is considered to be maximum concentration of butane at oil medium.

When the oil viscosity was reduced to a certain point, diluted oil now stated as live oil started to drain out of physical model by gravity and accumulated in the funnel (FN1) placed at the bottom of the pressure vessel. The accumulation of the live oil was due to exposure of the new pores filled with oil to the solvent gas resulted from boundary layer drainage and the process continued due to gravity drainage. Valve V4 was opened to direct the diluted oil towards the calibrated collection tube. The process of oil extraction remained in place until interface renewal continued and was slowed down when almost 80–85% of the original oil in place was extracted. Further extraction or oil dilution was observed to be very slow although last 5 to 6 cm of the model was still saturated with oil due to the capillary forces.

Online monitoring of the live oil production was recorded every 5 seconds with data acquisition system from load cell LC, that exhibit reduction in the weight of the model. Before starting each experiment the load cell was calibrated to the desired mark, and its behaviour was closely observed during the leak test as well as gas filling process.

After a certain amount of live oil had been collected in the collection tube (almost 17 cm^3), the live oil was then directed towards the capillary tube and then to flash tank for determining the required parameters for dispersion coefficient calculation. This was accomplished by opening the valves V5, V6, V7, V9 and V11 while V8, V10 and V5a were confirmed close. Provision of bypass line to empty the collection tube in case of capillary tube clogging was in place. The route of live oil in case of capillary tube

chocking was diverted towards flash tank by opening valve V5a. Valve V4 remained open throughout the viscosity determination experiment to supply a constant pressure for live oil viscosity calculations.

The flash separation tank was heated to a temperature of 70°C before starting the experiment. This was conducted by wrapping a flexible heated tape around the tank. The temperature of the flash tank was recorded every 5 seconds. To ensure the proper flashing of the butane gas from the live oil the V9 was fully opened. The two water columns WT1 and WT2 were filled with water up to desired mark before starting the experiment. As the butane gas from the flash tank moved towards WT1 the water level in WT2 started to rise. WT2 was scaled to calculate exact amount of water displaced from the separated gas. Proper operation of water displacement was assured by opening the valve V11 at the top of the WT2.

After satisfying the sufficient separation of butane gas from the live oil from constant water level in WT2 for a long time (1 hour), the valve at the top of WT1, V10 was opened to release the dissolved butane to the fume hood. To calculate the amount of dead oil, after releasing the butane from WT1, the valve under the flash tank V8 was opened, and dead oil was collected in a pan. The oil was weighed and recorded to calculate solubility of butane gas. The process was continued until the production was very slow or ceased and the above procedures were repeated timely during the experiment to calculate live oil viscosity and butane solubility.

4.4.1 Constant Temperature

Constant temperature during the experiment was maintained through the big vessel (Dimensions: 200 cm height, 150 cm diameter) made of PVC, used as water tub (WB), (Figure 4.2). Once leak test for pressure vessel was done (with air), WB was filled with fresh water by opening V12. After filling the water tank up to the height of the vessel, heating procedures were carried out for almost uniform water temperature to surroundings. This was done by making a circulation from water pump underneath the

tank through heat exchanger. Due to higher volume of the water tank it took 3–4 hours to bring water bath at surrounding temperature. Once uniform temperature was attained, the physical model was attached inside the pressure vessel and oil extraction process was started.

For minimum temperature variation during the experiment water bath temperature was set a little higher than surrounding temperature. Figure (4.7) shows temperature trends for 25, 35 and 45 cm model heights.

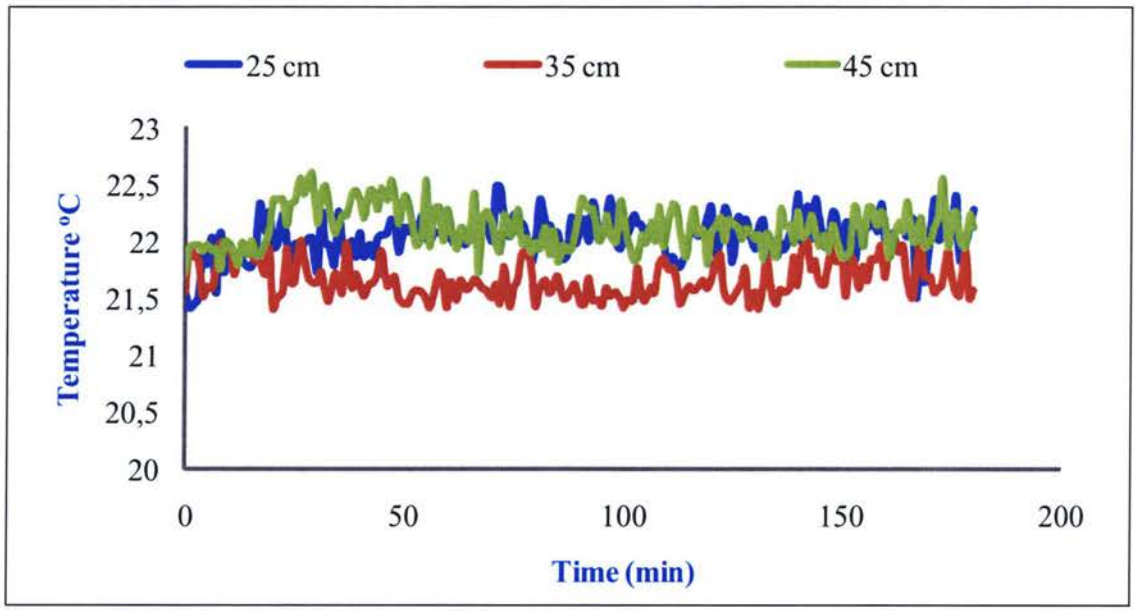

Figure 4.7: Surrounding Temperature for Different Model Heights

4.5 Live Oil Viscosity

Experimental determination for online live oil viscosity was performed as follows:

After collection of sufficient amount of oil (more than 15 cm^3) in the collection tube, adjustment of the valves required to perform viscosity test was done. Viscosity was determined by passing the live oil through a capillary tube of known diameter (0.1016 cm) and of known length (50 cm). A pressure transducer was connected at both sides of tube to measure pressure drop across the tube. Diameter of the capillary tube was finalized by trying different diameter tubes and one with least chance of flow hindrance was selected, while length was marked after confirming the smooth flow across the tube. Figure (4.8) shows picture of the experimental setup used for live oil viscosity determination.

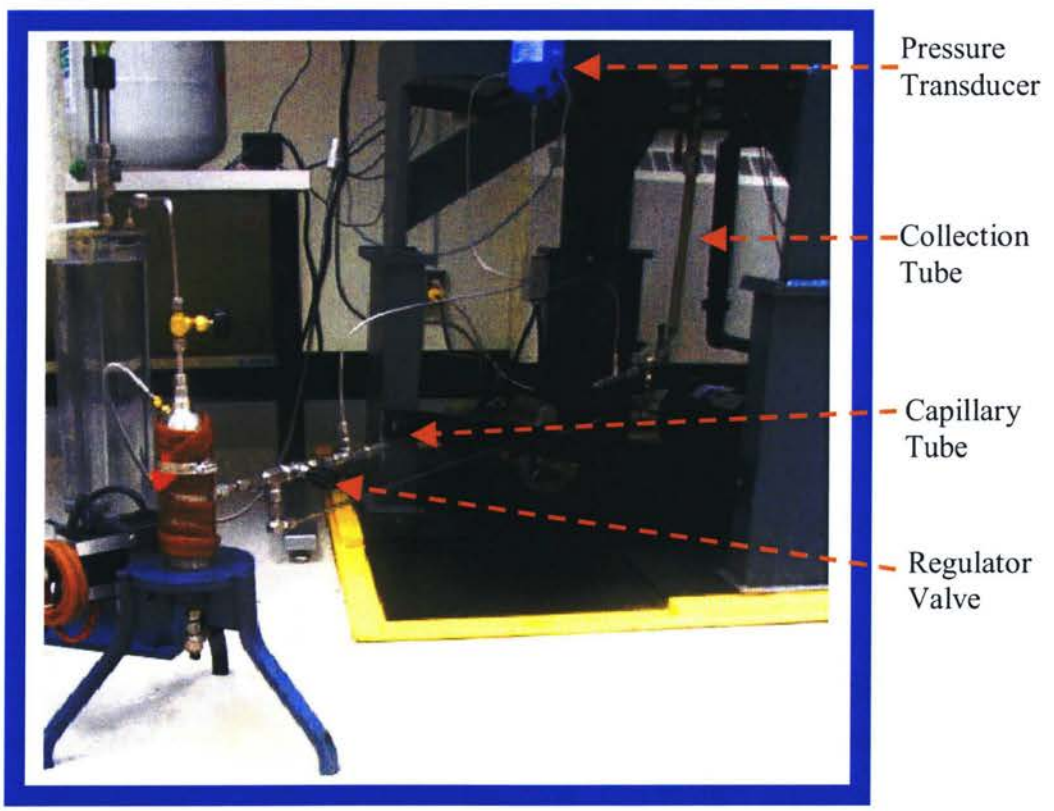

Figure 4.8: Experimental Setup For Live Oil Viscosity Determination

Before passing the live oil through capillary tube Valve V6 was fully opened while Valve V7 at the end of the capillary tube was cracked to take the readings at low values of differential pressure. Valve V9, V11 and V4 were confirmed open while valve V8 and V5a was confirmed close. It was also assured to empty the flash tank before opening valve V5 (passage of live oil to capillary tube). V5 was opened and after differential pressure across the tube was constant at certain value the flow of the live oil from collection tube was calculated using stopwatch for a specific amount of live oil.

The viscosity of the live oil was calculated using Hagen – Poiseuille equation:

$$Q = \frac{\pi d^4 \Delta P}{128 \mu L} \tag{4.4}$$

Knowing the diameter of the capillary tube, ΔP across the tube, length of the capillary tube and flow of live oil across the tube viscosity of the live oil was calculated. A sample calculation is shown in Appendix C.

4.6 Butane gas solubility and Live oil Density

To determine the amount of butane gas dissolved in the heavy oil during extraction process, as well as density of the live oil following experimental procedures were adopted.

Valve V7 was cracked by fully opening the valve V6, V9, and V11. After ensuring V4 in open state, V5 was opened by recording the level of live oil in the collection tube. A known amount of live oil was transferred to flash tank through capillary tube by controlling the amount of oil with V5. Temperature of flash tank was maintained at 70°C to ensure proper flashing of the butane gas. As the gas was separated from the oil due to flashing action it diverted to WC1 and started to compress the water in the column. The water was displaced resulting in rise of the water level in WC2. After one batch had been through, valve V6 was closed while V7 remained open. When sufficient time had been

given for flashing of butane and differential pressure reading approached zero with no more rise in WC2, valve V10 was opened to vent the butane gas, and net amount of dead oil was collected by opening V8.

Knowing the amount of gas absorbed from water displacement as well as weight of the dead oil the solubility of butane gas and density of live oil was calculated as:

$$C_4H_{10} \text{ Dissolved weight fraction} = \frac{\text{weight of librated } C_4H_{10}}{\text{weight of dead oil} + \text{weight of librated } C_4H_{10}} \quad (4.5)$$

$$\text{Live Oil Density} = \frac{\text{weight of librated } C_4H_{10} + \text{weight of dead oil}}{\text{volume of Live Oil}} \quad (4.6)$$

A sample calculation is shown in Appendix D. The same procedure was repeated again to have the readings at different times of the experiment, as well as the same procedure was adopted every time when live oil viscosity experimental steps were performed.

5 Experimental Result & Discussion

5.1 Live Oil Production

To determine the effect of drainage height on production rates, oil recovery was carried out using four different heights of the cylindrical model with same diameter. The lengths of the model used were 15, 25, 35 and 45 cm. The physical model filled with saturated heavy oil and glass beads mixture (glass beads with average size of $360\,\mu$m) was attached to a load cell installed at the top flange of the pressure vessel for each experimental run. The load cell exhibited the change in the weight of the physical model resulted from dilution of heavy oil by diffusion of butane gas into the oil. This weight change was recorded through data acquisition system. Cumulative live oil production was calculated from the load cell data generated. Calculated data for first 400 minutes for all models employed are shown in Appendix E.

Figures (5.1–5.4) shows actual change in the weight of load cell for first 650 minutes of experimental time. Figure (5.5) shows cumulative live oil production for each model length vs experimental time. It was observed that for all model length at start of each experiment weight of load cell increase up to a certain time instance. This time varied between 40 to 55 minutes for different models. This behaviour is due to the fact that as solvent gas comes in contact with the bitumen it starts to diffuse, and load cell shows increase in weight. Weight of the cell keep on increasing until viscosity of the oil reaches the threshold limit for gravity forces to overcome capillary forces and diluted oil starts to drain under gravity. The concentration of the solvent gas at the time when load cell indicates maximum weight is considered as maximum concentration of the solvent gas at the interface.

To plot the cumulative oil production for all model lengths, zero point for the production was taken from maximum load cell value, and was ended when there was no significant change in the load cell decrease rate. The experimental time for smooth production rates of model heights was between 15 to 16 hours. For history matching the simulated results to experimental results, the data (cumulative live oil production) plotted in Figure (5.5) was used. In order to validate the experimental live oil production data each experiment (one model height) was performed at least two times and the percentage error between two experiments was found to be an average of 1.29%.

At the end of each experiment the whole system was flushed with air and procedure to vacuum the system was repeated again to evolve any gas or air trapped between the pores of the sample. The physical model was weighed before and after the end of each experiment, to determine recovery of original oil in place. It was found that for all the model lengths the OOIP (original oil in place) recovery remained between 80 to 85%.

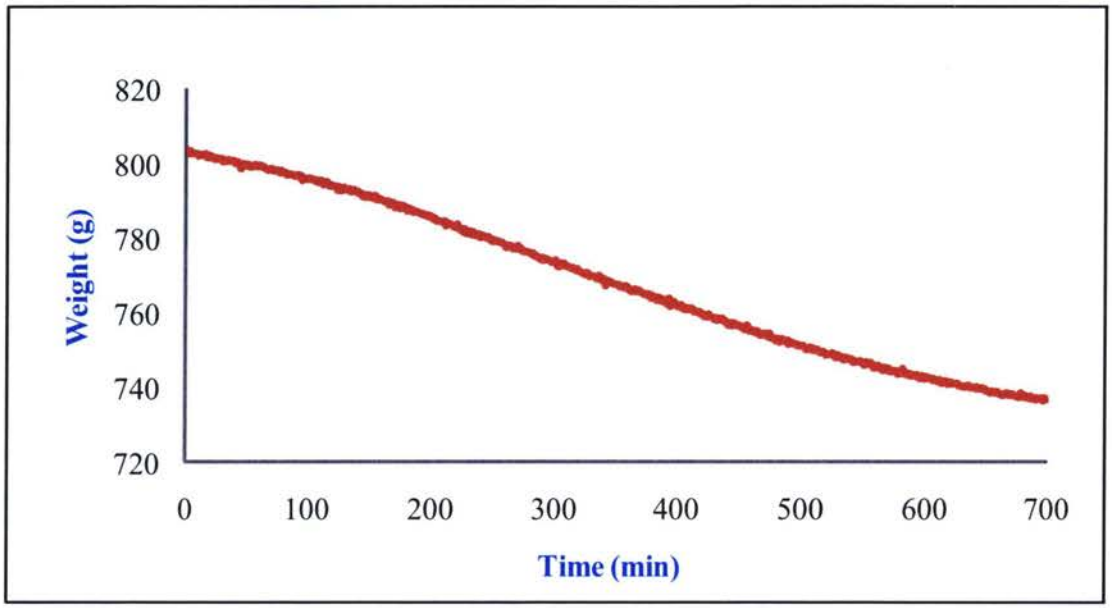

Figure 5.1: Load Cell Weight vs Time (15 cm Model)

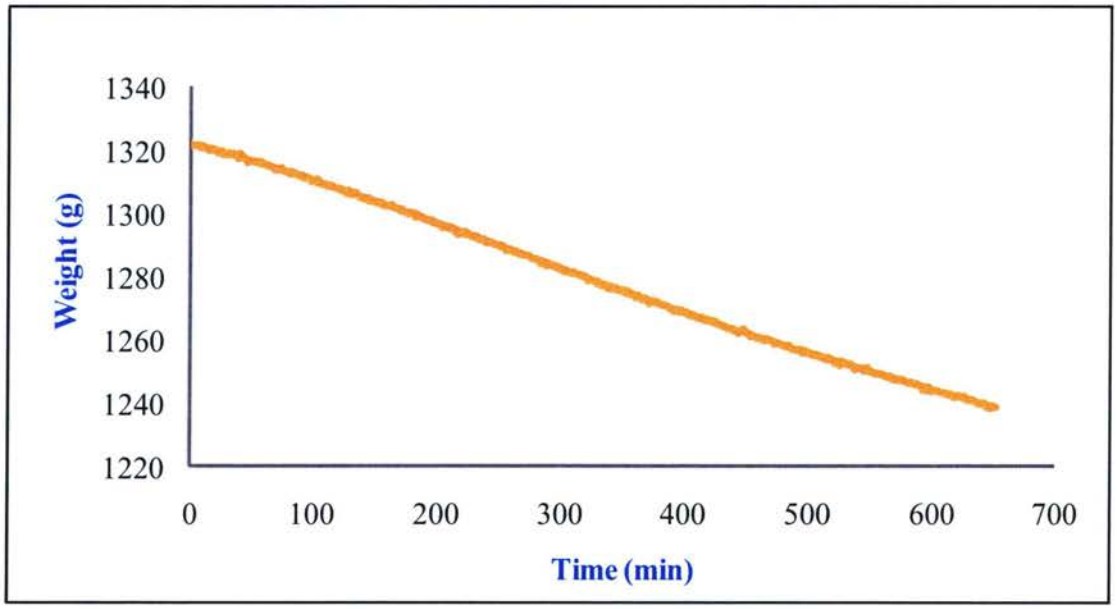

Figure 5.2: Load Cell Weight vs Time (25 cm Model)

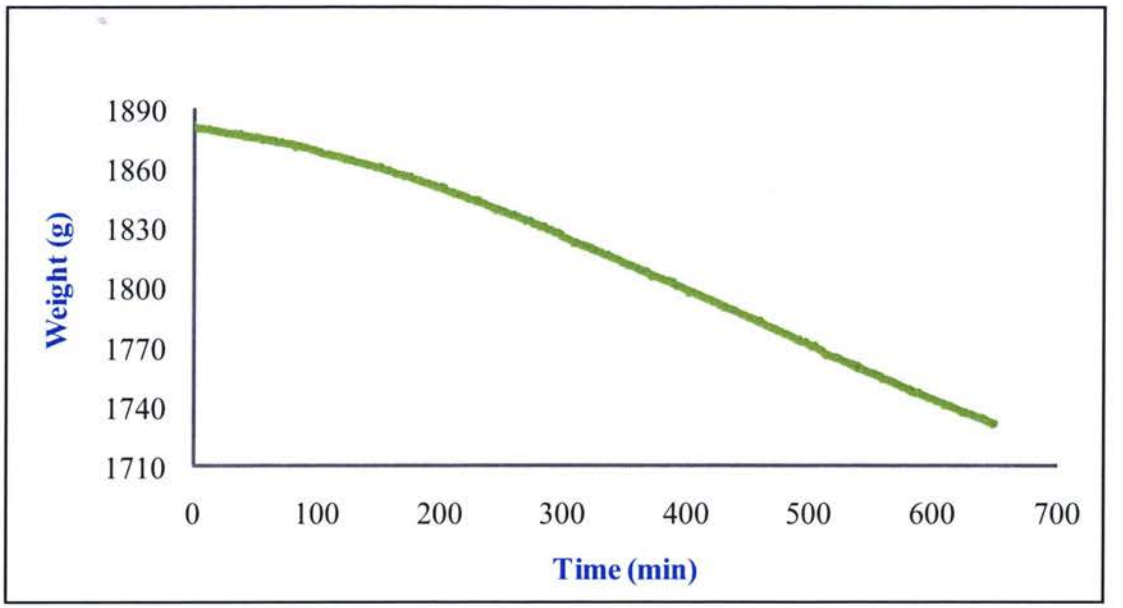

Figure 5.3: Load Cell Weight vs Time (35 cm Model)

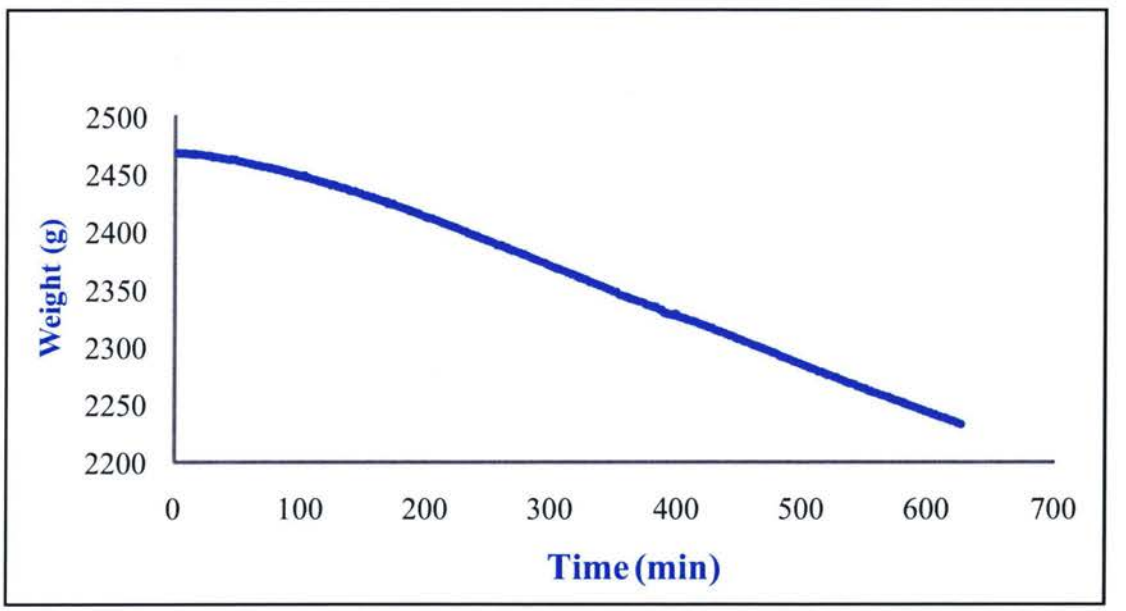

Figure 5.4: Load Cell Weight vs Time (45 cm Model)

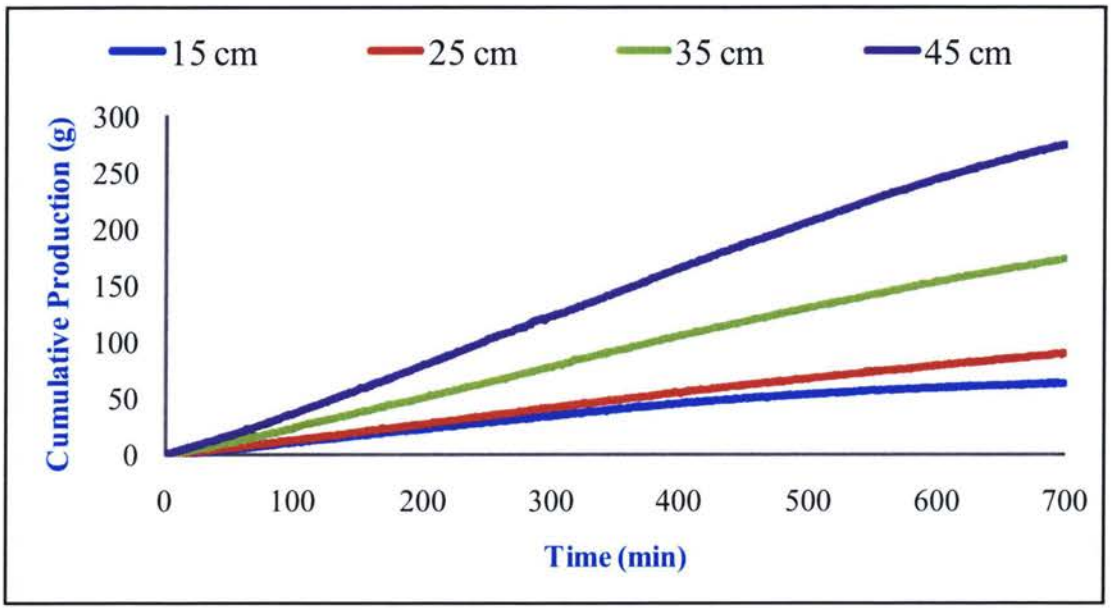

Figure 5.5: Cumulative Live Oil Production vs Experimental Time

5.2 Effect of Drainage Height on Live Oil Production

To investigate effect of drainage height (model height) on production rates through Vapex process the linear portion of cumulative production curves (Figure 5.5) was considered. For effective drainage height the part from where oil was not drained (approximately 5 cm for each model height) was subtracted from total height. An estimate of no production zone was done by dividing the model in different parts and observing the colour difference as shown in Figure (5.6). The average production rates were calculated based on smooth cumulative live oil production divided by time for that particular part. Figure (5.7) shows a comparison of the average production rates for different model heights.

It was observed that production rate for 25 cm model height was 24% higher than 15 cm model while for 35 cm to 25 cm model height the production rate was increased by 71%. Almost the same percentage increase was observed for 45 to 35 cm model. This percent increase indicates that live oil production from Vapex is strongly dependent to drainage

height. In order to correlate effective drainage height to production rate 15 cm model was excluded while developing the relationship to consider smooth percent increase. The following power law relationship is obtained:

$$\dot{m} = 2.1\times10^{-2}\, L^{1.496} \qquad (5.1)$$

where L in Equation [5.1] shows the effective drainage height (cm) per unit diameter of the cylindrical model (cm), and $\dot{m}$ indicates average live oil production rate. Figure (5.8) shows power law dependency of live oil production rate to effective drainage height with r^2 value of 0.993. For linear relationship r^2 was 0.985 therefore power relationship was considered. More over in literature the live oil production through Vapex is correlated in terms of a power function that's why power relationship was considered.

During the early developments of Vapex, it was considered that production rate is directly proportional to square root of drainage height as mathematical model developed by (Das and Butler 1998), but this concept was modified by Yazdani and Maini (2005). They determined the effect of drainage height on production rates in the Vapex process (experimentally). They concluded that drainage rate is not directly proportional to square root of drainage height. Instead stabilized oil rate in the Vapex process is a function of drainage height to the power range of 1.1 to 1.3 (based on three model heights). In the current study the power law dependency of oil production to drainage height is evaluated even higher based on experimental data obtained from three model heights.

(15 cm Model Height)

(25 cm Model Height)

(35 cm Model Height)

(45 cm Model Height)

Figure 5.6: Pictures of Physical Models (After Experiment)

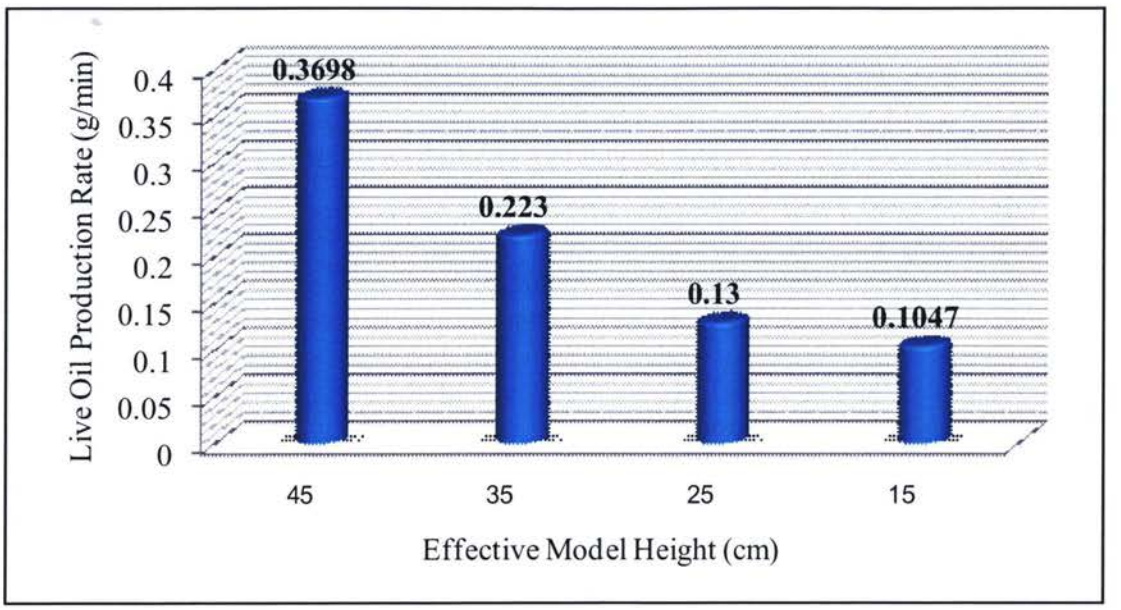

Figure 5.7: Live Oil Average Production Rate (g/min) Vs Model Length

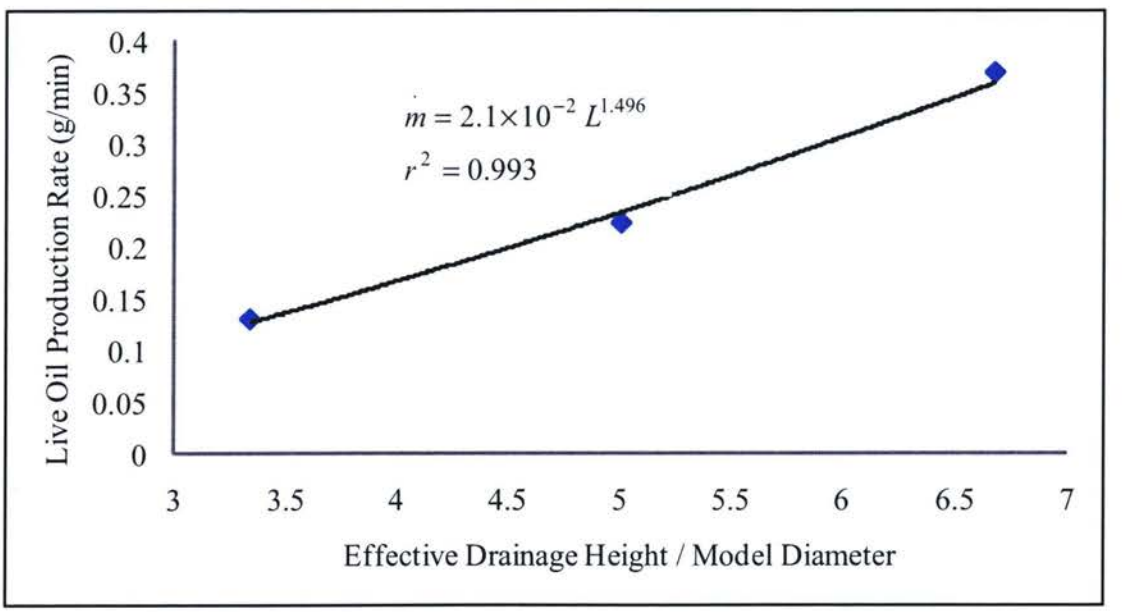

Figure 5.8: Power Law Relationship

5.3 Live Oil Properties

It was observed that model heights did not have any influence on the live oil viscosity, live oil density and butane gas solubility subject to same experimental conditions. Table (5.1) shows live oil viscosity and density calculated from the data obtained from different model heights with almost the same temperature and pressure conditions.

Table 5.1: Live Oil Properties

Run (#)	Model Height (cm)	Solvent Solubility (fraction)	Live Oil Viscosity (mPa.s)	Live oil Density (g/cm^3)
1	15	0.365	9.88	0.8165
2	15	0.3664	9.82	0.8138
1	25	0.3635	9.97	0.815
2	25	0.365	9.89	0.815
1	35	0.368	9.68	0.813
2	35	0.368	9.71	0.815
1	45	0.367	9.54	0.798
2	45	0.3604	10.04	0.817

5.4 Effect of Pressure Variation

Although Vapex process is very crucial to dew point pressure of the solvent gas, but it has been observed in some of the experiments that by solvent pressure variation the recovery rates could increase by 3 to 4 times. As shown in Figure (5.9) that represents cumulative production and pressure for one of the model heights vs time. As in this particular case during the start time production rate was very slow, but as a pressure disturbance was generated by releasing the solvent gas at once to vent and injecting the gas again, there was a significant increase in the production rate.

Slow recovery rates at start of some of the experiments were observed due to sample preparation and not sufficient flushing of the system. As during sample preparation there are chances for air to trap inside the packing of heavy oil and glass beads, and if system is not vacuumed properly this air limits the contact of solvent gas with heavy oil thus slowing the diffusion process and over all recovery rates. But in these particular cases performing the procedures described above, production rates were improved by 3 to 4 times.

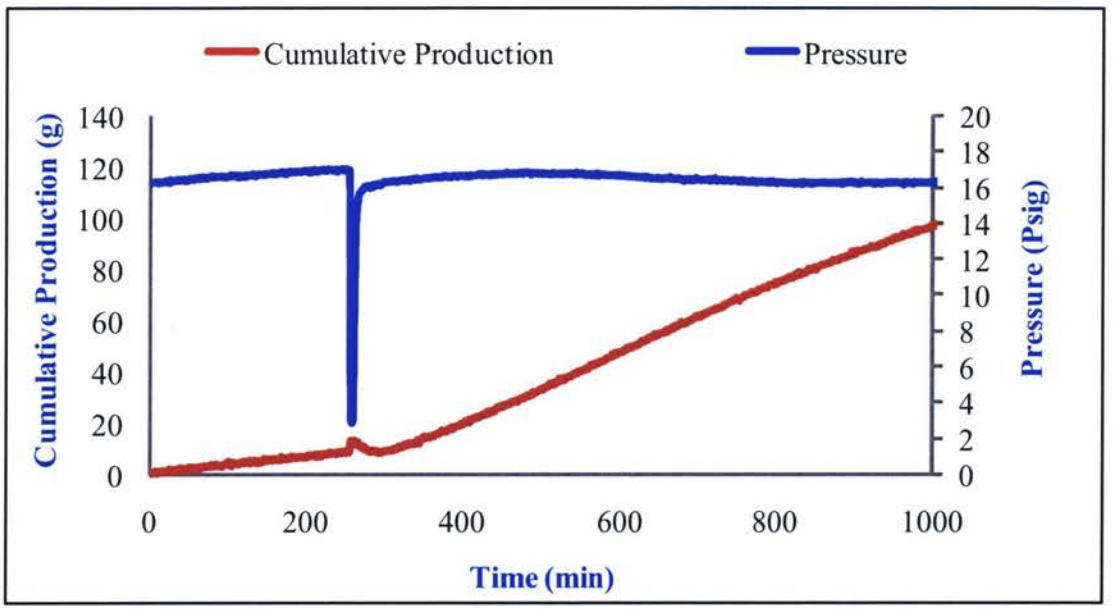

Figure 5.9: Pressure Variation Effect on Live Oil Production

5.5 Asphaltene Precipitation

Deposits of asphaltenes toward the discharge point of the physical model along with frequent blockage of recovery line was observed from the experiments in which oil recovery rates were slow (visual observations). There could be many reasons involved in slow recovery of oil. For example air trapped inside the packing, long duration for pressure chamber to pressurize, slow injection rates of solvent gas at start of the experiments as well as if system is not vacuumed properly. But in any of these cases

injection time for solvent is increased that promotes asphaltene precipitation. Figure (5.10) shows picture of section of packing taken from a low recovery model, with long duration of solvent injection.

It was observed that asphaltene deposits were only near to the production port of the models. The reason could be that oil present within last 5 to 7 cm of the models was not recovered due to lower gravitational forces as compared with capillary forces, but was in contact with the solvent gas throughout the process, and as surrounding pressure of the model tends to reach equal to vapour pressure at that temperature in 24 hours of the experimental time, asphaltenes are precipitated and deposits within that regime.

Figure 5.10: Asphaltene Precipitation

5.6 Experimental Sensitivity

The accuracy of this study was based on data collected from load cell weight change during the experiments. Therefore it was very important to calibrate the load cell at the start of each experiment and compare its readings with scalar at the start and end of each experiment. Weight of the model for each experimental run exhibited by load cell was compared with its weight obtained from scalar and % error with respect to scalar was calculated that is shown in Table (5.2), which is very little and acceptable.

Table 5.2: Percent Error for Load Cell

Model Height (cm)	% Error (Load Cell and Scalar)
15	0.27
25	0.609
35	0.1935
45	0.267

6 Mathematical Modeling

Objective of this research is to determine the dispersion coefficient of butane gas in heavy oil. High viscosity oil was used to perform the experiments for determination of live oil viscosity, density and solubility of butane gas in heavy oil and bitumen for different model heights. The parameters achieved from experiments were used in the simulation study to achieve the objective. Dispersion coefficient D_0 was calculated by modeling the physical model and simulating the experimental results with calculated results by solving the developed model. In this chapter the details of the model development are presented. Solution of the model along with the equations is briefly discussed.

6.1 Development of mathematical model

Earlier estimates based on mass transfer model which comprises only the molecular diffusion could not explain the observed high recovery rates in porous media (Das, 1995; Dunn et al., 1981; Das and Butler, 1998). This directed the researchers attention to a secondary mechanism (like convective dispersion) to justify the high recovery rates in porous media.

Dispersion or effective diffusion is the mixing of the fluids due to combined effect of diffusion and convective motion. Dispersion specifically is directly relevant to the dynamic process like Vapex where gravity induces the convective motion in fluids. Described by Darcy's Law at the macroscopic scale in a porous medium, dispersion strongly influences the heavy oil and bitumen recovery from the typical porous reservoirs subjected to Vapex (Upreti et al., 2007). When fluids become mobile and start to move through porous media mass transport exceeds that due to diffusion alone. For effective

designs and optimal operations of commercial Vapex applications, the accurate prediction of heavy oil recovery with Vapex is very essential and dispersion of solvent gas is a key parameter.

Following is the development of a detailed mathematical model to determine the solvent dispersion in Vapex. The assumptions of the model developed are as follows:

Assumptions

Constant temperature and pressure

Experiments were carried out at constant temperature with a standard deviation of [0.01] ^{o}C, and at constant pressure with deviation of [0.003] psig.

Saturation mass fraction

The mass fraction of solvent gas at the exposed oil surface of porous medium is the saturation mass fraction under equilibrium.

Dispersion direction

The dispersion of the butane gas takes place along the radial direction only (transverse dispersion).

Live oil production dependency

The production of live oil along the radial direction is under influence of molecular diffusion, the effects of surface renewal, viscosity reduction, and capillary action.

Darcy Law

The flow of the live oil along the vertical direction inside the pores in the boundary layer is governed by the Darcy flow in porous medium.

Live Oil Density

Due to very low density of the solvent gas, it was assumed that density of the live oil remains constant throughout the recovery process.

Porosity & permeability

Porosity and permeability of the medium was constant during the extraction process.

Chemical Reactions

There are no chemical reactions during the extraction process.

The unsteady state mass balance for solvent gas in a cylindrical differential element is given by, Figure (6.1):

$$\begin{pmatrix}\text{Accumulation of solvent}\\ \text{mass over a finite time}\\ \text{interval } \Delta t\end{pmatrix} = \begin{pmatrix}\text{Rate of solvent}\\ \text{mass input along}\\ r \text{ and } z \text{ direction}\end{pmatrix} - \begin{pmatrix}\text{Rate of solvent}\\ \text{mass output along}\\ r \text{ and } z \text{ direction}\end{pmatrix} \qquad (6.1)$$

Since there is no generation.

Accumulation of Solvent Mass

Accumulation of the solvent gas across the finite element during a certain time can be written in the form as

$$\frac{\partial(\phi V \omega \rho)}{\partial t} \qquad (6.2)$$

Where V is volume of the differential element, ω is solvent mass fraction, ϕ is porosity of medium and ρ is the density of live oil. Volume of differential element is:

$$V = 2\pi r \, \mathrm{d}r \, \mathrm{d}z$$

Where $\mathrm{d}r$ and $\mathrm{d}z$ are the width and height of the differential element respectively. By putting the expression for V in Equation [6.2] the accumulation term becomes:

$$\frac{\partial(\phi \rho 2\pi r \, \mathrm{d}r \, \mathrm{d}z \, \omega)}{\partial t} \qquad (6.3)$$

Rate of Solvent Mass Input

Along r direction mass is transferred due to diffusion of the solvent gas in the stationary layer of bitumen, defined by Ficks Law of diffusion:

$$J_g = -\rho D \frac{\partial \omega}{\partial r} \tag{6.4}$$

Taking the cross sectional area ΔS transverse to r direction, rate of solvent mass input along r direction can be written as:

$$-D\rho \frac{\partial \omega}{\partial r} 2\pi r \, dz \Big|_{\text{input } r \text{ direction}} \tag{6.5}$$

Along z direction mass of the solvent is transferred in terms of present in live oil and is governed by Darcy flow, also diffusion of the solvent gas along z direction is negligible while the bulk is moving.

Taking the cross sectional area ΔA transverse to z direction, rate of mass input along z direction can be written as:

$$v\, 2\pi r \, dr \, \rho \, \omega \Big|_{\text{input } z \text{ direction}} \tag{6.6}$$

Where v in Equation [6.6] is velocity of the moving live oil.

Rate of Solvent Mass Output

Corresponding to Equations [6.5] and [6.6] rate of solvent mass output for (r) and (z) directions can be written as:

$$-D\rho \frac{\partial \omega}{\partial r} 2\pi r \, dz \Big|_{\text{output } r \text{ direction}} \tag{6.7}$$

and

$$v\, 2\pi r \, dr \, \rho \, \omega \Big|_{\text{output } z \text{ direction}} \tag{6.8}$$

Physical Model:

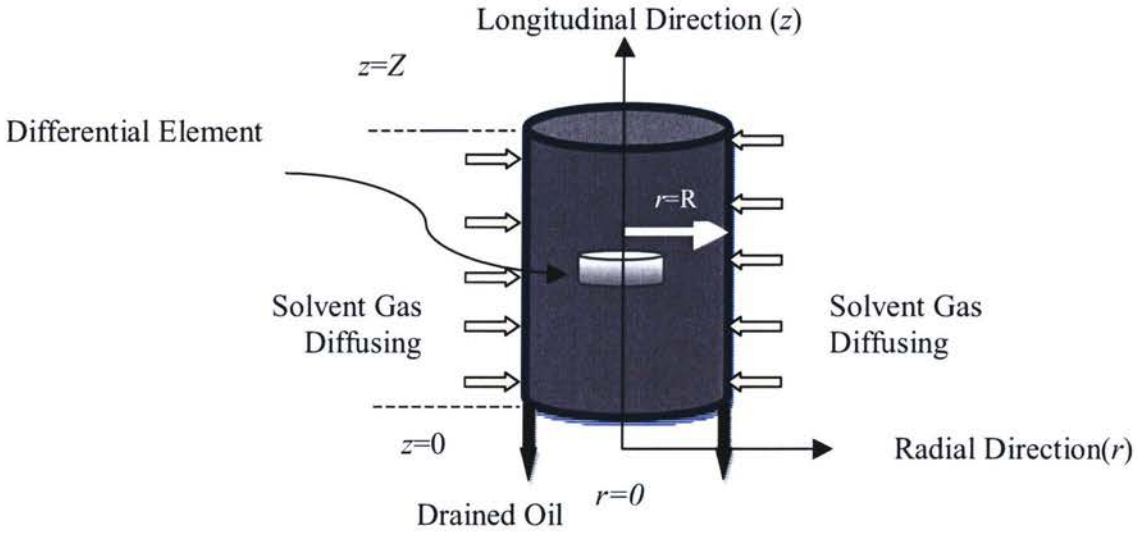

System:

Differential Element across the physical Model.

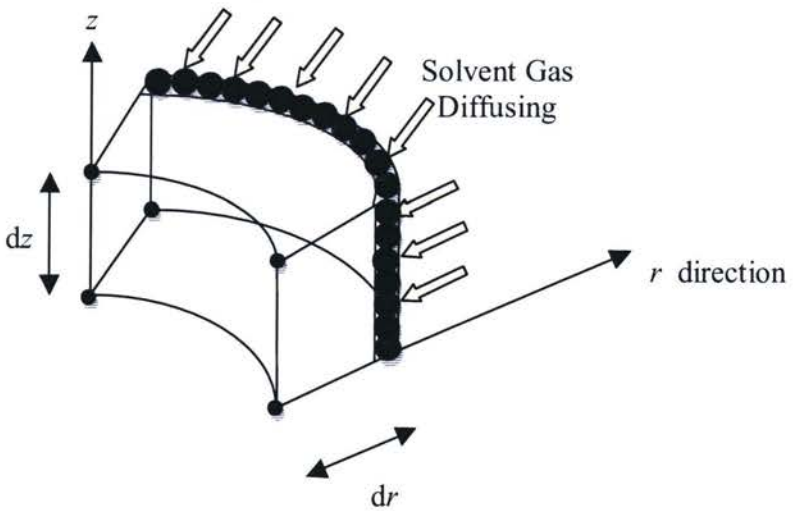

Figure 6.1: Mathematical Model

Combining Equations [6.3], [6.5], [6.6], [6.7], and [6.8], the mass balance equation for solvent gas over the finite element becomes:

$$\frac{\partial(\phi\rho 2\pi r\,dr\,dz\,\omega)}{\partial t} = -D\rho\frac{\partial\omega}{\partial r}2\pi r\,dz\Big|_{\text{input } r\text{ direction}} + D\rho\frac{\partial\omega}{\partial r}2\pi r\,dz\Big|_{\text{output } r\text{ direction}} + v\,2\pi r\,dr\,\rho\,\omega\Big|_{\text{input } z\text{ direction}} - v\,2\pi r\,dr\,\rho\,\omega\Big|_{\text{output } z\text{ direction}} \tag{6.9}$$

or

$$\frac{\partial(\phi\,\rho\,2\pi r\,dr\,dz\,\omega)}{\partial t} = -2\pi\,dz\,\rho\left[D\,r\frac{\partial\omega}{\partial r}\Big|_{r} - D\,r\frac{\partial\omega}{\partial r}\Big|_{r+dr}\right] + v\,2\pi r\,dr\left[\omega\big|_{z} - \omega\big|_{z+dz}\right] \tag{6.10}$$

or

$$\frac{\partial\omega}{\partial t} = \frac{1}{\phi}\frac{1}{r}\frac{\partial}{\partial r}\left[D\,r\frac{\partial\omega}{\partial r}\right] - \frac{1}{\phi}\frac{\partial(v\omega)}{\partial z} \tag{6.11}$$

or mass balance equation becomes

$$\frac{\partial\omega}{\partial t} = \frac{D}{\phi}\left[\frac{1}{r}\frac{\partial\omega}{\partial r} + \frac{\partial^2\omega}{\partial r^2}\right] + \frac{1}{\phi}\frac{\partial D}{\partial\omega}\left[\frac{\partial\omega}{\partial r}\right]^2 - \frac{1}{\phi}\left[v + \omega\frac{\partial v}{\partial\omega}\right]\frac{\partial\omega}{\partial z} \tag{6.12}$$

In above equation D is the dispersion of solvent gas along r direction, ω is the mass fraction of gas and v is the Darcy velocity of the live oil within porous media along z direction given by

$$v = \frac{K_r K\,\rho\,g\cos\theta}{\mu} \tag{6.13}$$

μ in the above expression is concentration dependent viscosity of live oil. K_r is the relative permeability, K is the medium permeability and g is the gravitational acceleration. Following correlation was used for μ (Oduntan et al., 2003; Kapadia et al., 2006; El-Haj, 2007)

$$\mu = \mu_0 \omega^{-2} \tag{6.14}$$

where μ_0 is live oil viscosity coefficient, calculated from experimentally obtained live oil viscosity and solvent gas solubility mass fraction. To determine the oil production from the model, dispersion of solvent in heavy oil was considered a linear function of solvent mass fraction, i.e

$$D = D_0 \omega \tag{6.15}$$

where D_0 is the coefficient of dispersion of solvent gas in heavy oil and bitumen.

Putting the above expressions from Equations [6.13–6.15] in Equation [6.12], the mass balance equation over finite element can be written as:

$$\frac{\partial \omega}{\partial t} = \frac{D_0 \omega}{\phi}\left[\frac{1}{r}\frac{\partial \omega}{\partial r} + \frac{\partial^2 \omega}{\partial r^2}\right] + \frac{D_0}{\phi}\left[\frac{\partial \omega}{\partial r}\right]^2 - \frac{K_r K \rho g \cos\theta}{\mu_0 \phi}\frac{\partial \omega}{\partial z} 3\omega^2 \tag{6.16}$$

Change in Height at Any Time

The change in the height of the bitumen in the physical sample (Z) with time at any location on the r-axis is given by the negative of Darcy velocity as:

$$\frac{\partial z(t)}{\partial t} = -v(r) \tag{6.17}$$

Where $v(r)$ is the averaged live oil velocity over the differential volume $2\pi r\mathrm{d}r\mathrm{d}z$ at the bottom of the packed medium where $z=0$, and changes in r direction.

Calculated Mass of Live Oil

The cumulative mass of produced live oil at any time was calculated from multiplying differential volume with live oil density and medium porosity. For a calculated change in height mass of live oil produced was obtained by integrating the multiple from 0 to R as:

$$m_{\mathrm{cal}} = 2\pi\rho\phi\int_0^{\mathrm{R}}(Z_0 - Z)r\,\mathrm{d}r \tag{6.18}$$

Initial and Boundary Conditions

Initially, there was no butane inside the medium so height of the bitumen was Z_0 that is the total height of the packed physical column. While the surface of the medium was considered at equilibrium concentration of butane at all times. The initial conditions at $t=0$ were:

$$\omega = \begin{cases} 0 & \forall\, 0 \le z \le Z_0,\ \forall\ 0 \le r < \mathrm{R} \\ \omega_{\mathrm{sat}} & \forall\, 0 \le z \le Z_0,\ r = \mathrm{R} \end{cases} \tag{6.19}$$

$$z = Z_0 \tag{6.20}$$

The boundary conditions at $t \ge 0$ were:

$$\omega = \omega_{\mathrm{sat}} \text{ at } r = \mathrm{R} \text{ and } 0 \le z \le Z(r,t);\ z = 0,\ Z(r,t) \text{ and } 0 \le r \le \mathrm{R} \tag{6.21}$$

where $Z(r,t)$ is the height of the bitumen in the porous medium at a given r and t.

Furthermore, because of symmetry, at all times

$$\frac{\partial \omega}{\partial r} = 0 \quad \forall\, 0 \le z \le Z \text{ and } r = 0 \tag{6.22}$$

In order to minimize computational time for higher model heights, normalization of sample height was performed by introducing dimensionless variable as:

$$\zeta = \frac{z}{Z_0} \tag{6.23}$$

where ζ is dimensionless height of the bitumen sample and is equal to 1 at $t = 0$. Equations [6.16 – 6.22] can be written as:

$$\frac{\partial \omega}{\partial t} = \frac{D_0 \omega}{\phi}\left[\frac{1}{r}\frac{\partial \omega}{\partial r} + \frac{\partial^2 \omega}{\partial r^2}\right] + \frac{D_0}{\phi}\left[\frac{\partial \omega}{\partial r}\right]^2 - \frac{K_r K \rho g \cos\theta}{\mu_0 \phi Z_0}\frac{\partial \omega}{\partial \zeta} 3\omega^2 \tag{6.24}$$

$$\frac{\partial \varsigma(t)}{\partial t} = -\frac{v(r)}{Z_0} \tag{6.25}$$

$$m_{cal} = 2\pi \rho \phi Z_0 \int_0^R (1 - \zeta)\, r\, dr \tag{6.26}$$

And

$$\omega = \begin{cases} 0 & \forall\, 0 \le \zeta \le 1, \quad \forall\, 0 \le r < \mathrm{R} \\ \omega_{sat} & \forall\, 0 \le \zeta \le 1, \quad \text{at } r = \mathrm{R} \end{cases} \tag{6.27}$$

$$\zeta = 1 \tag{6.28}$$

$$\omega = \omega_{sat} \text{ at } \zeta = 0, \varsigma(r,t) \text{ and } 0 \le r \le \mathrm{R}; \text{ and at } r = \mathrm{R} \text{ and } 0 \le \zeta \le 1 \tag{6.29}$$

$$\frac{\partial \omega}{\partial r} = 0 \quad \forall\, 0 \le \zeta \le 1 \text{ and } r = 0 \tag{6.30}$$

6.2 Mathematical Model Solution

The partial differential Equations [6.24] and [6.25] obtained from the mass balance across finite element were numerically solved by applying second order finite difference method to convert the above partial differential equations to ordinary differential equations. Geometry of the cylindrical model was divided into equispaced grid points in (r) and (ζ) direction denoted here as N_i and N_j respectively, with in the physical boundary of cylindrical model, (Figure 6.2).

Following are the set of ordinary differential equations obtained after applying Finite Difference methods with respect to cylindrical nodes:

For intermediate Grid points

For $0 < i < (N_I - 1)$ and $0 < j < (N_J - 1)$

$$\frac{d\omega_{i,j}}{dt} = \frac{D_0 \omega_{i,j}}{\phi}\left[\frac{1}{r_i}\frac{\omega_{i+1,j} - \omega_{i-1,j}}{2\Delta r} + \frac{\omega_{i+1,j} - 2\omega_{i,j} + \omega_{i-1,j}}{\Delta r^2}\right] + \frac{D_0}{\phi}\left[\frac{\omega_{i+1,j} - \omega_{i-1,j}}{2\Delta r}\right]^2 - \frac{K_r K \rho g \cos\theta}{Z_0 \mu_0 \phi} 3\omega_{i,j}^2 \left[\frac{\omega_{i,j+1} - \omega_{i,j-1}}{2\Delta \varsigma_i}\right] \tag{6.31}$$

For Axis Grid Points

When $i = 0$ for $0 < j < (N_J - 1)$

$$\frac{d\omega_{0,j}}{dt} = -\frac{K_r K \rho g \cos\theta}{Z_0 \mu_0 \phi} 3\omega_{0,j}^2 \left[\frac{\omega_{0,j+1} - \omega_{0,j-1}}{2\Delta\varsigma_i}\right] \tag{6.32}$$

When $i = 0$ and $j = 0$

$$\frac{d\omega_{0,0}}{dt} = -\frac{K_r K \rho g \cos\theta}{Z_0 \mu_0 \phi} 3\omega_{0,0}^2 \left[\frac{\omega_{0,1} - \omega_{sat}}{2\Delta\varsigma_0}\right] \tag{6.33}$$

When $i = 0$ and $j = (N_J - 1)$

$$\frac{d\omega_{0,N_J-1}}{dt} = -\frac{K_r K \rho g \cos\theta}{Z_0 \mu_0 \phi} 3\omega_{0,N_J-1}^2 \left[\frac{\omega_{sat} - \omega_{0,N_J-2}}{2\Delta\varsigma_0}\right] \tag{6.34}$$

For Right most Grid Points

When $i = (N_I - 1)$ and $j = 0$

$$\frac{d\omega_{N_I-1,0}}{dt} = \frac{D_0 \omega_{N_I-1,0}}{\phi}\left[\frac{1}{r_{N_I-1}}\frac{\omega_{sat} - \omega_{N_I-2,0}}{2\Delta r} + \frac{\omega_{sat} - 2\omega_{N_I-1,0} + \omega_{N_I-2,0}}{\Delta r^2}\right] + \frac{D_0}{\phi}\left[\frac{\omega_{sat} - \omega_{N_I-2,0}}{2\Delta r}\right]^2 - \frac{K_r K \rho g \cos\theta}{Z_0 \mu_0 \phi} 3\omega_{N_I-1,0}^2 \left[\frac{\omega_{N_I-1,1} - \omega_{sat}}{2\Delta\varsigma_{N_I-1}}\right] \tag{6.35}$$

When $i = (N_I - 1)$

$$\frac{d\omega_{N_I-1,j}}{dt} = \frac{D_0 \omega_{N_I-1,j}}{\phi}\left[\frac{1}{r_{N_I-1}}\frac{\omega_{sat} - \omega_{N_I-2,j}}{2\Delta r} + \frac{\omega_{sat} - 2\omega_{N_I-1,j} + \omega_{N_I-2,j}}{\Delta r^2}\right] + \frac{D_0}{\phi}\left[\frac{\omega_{sat} - \omega_{N_I-2,j}}{2\Delta r}\right]^2 - \frac{K_r K \rho g \cos\theta}{Z_0 \mu_0 \phi} 3\omega_{N_I-1,j}^2 \left[\frac{\omega_{N_I-1,j+1} - \omega_{N_I-1,j-1}}{2\Delta\varsigma_{N_I-1}}\right] \tag{6.36}$$

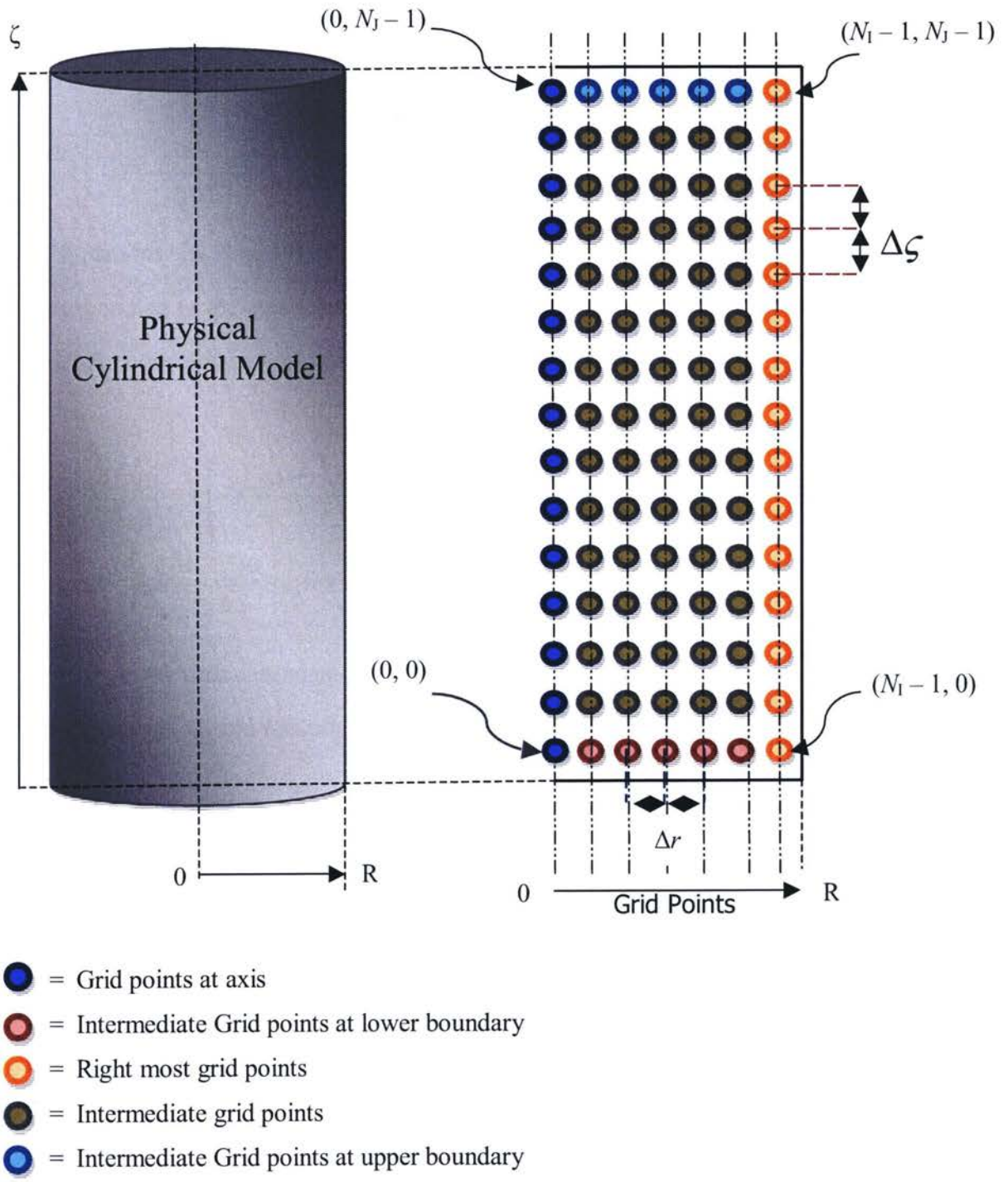

Figure 6.2: Cylindrical Model and Node Distribution

when $i = (N_I - 1)$ and $j = (N_J - 1)$

$$\frac{d\omega_{N_I-1,N_J-1}}{dt} = \frac{D_0\omega_{N_I-1,N_J-1}}{\phi}\left[\frac{1}{r_{N_I-1}}\frac{\omega_{sat}-\omega_{N_I-2,N_J-1}}{2\Delta r}+\frac{\omega_{sat}-2\omega_{N_I-1,N_J-1}+\omega_{N_I-2,N_J-1}}{\Delta r^2}\right]+$$
$$\frac{D_0}{\phi}\left[\frac{\omega_{sat}-\omega_{N_I-2,N_J-1}}{2\Delta r}\right]^2-\frac{K_r K\rho g\cos\theta}{Z_0\mu_0\phi}3\omega^2_{N_I-1,N_J-1}\left[\frac{\omega_{sat}-\omega_{N_I-1,N_J-2}}{2\Delta\varsigma_{N_I-1}}\right] \quad (6.37)$$

For Lower most Intermediate Grid Points

When $j = 0$

$$\frac{d\omega_{i,0}}{dt} = \frac{D_0\omega_{i,0}}{\phi}\left[\frac{1}{r_i}\frac{\omega_{i+1,0}-\omega_{i-1,0}}{2\Delta r}+\frac{\omega_{i+1,0}-2\omega_{i,0}+\omega_{i-1,0}}{\Delta r^2}\right]+$$
$$\frac{D_0}{\phi}\left[\frac{\omega_{i+1,0}-\omega_{i-1,0}}{2\Delta r}\right]^2-\frac{K_r K\rho g\cos\theta}{Z_0\mu_0\phi}3\omega^2_{i,0}\left[\frac{\omega_{i,1}-\omega_{sat}}{2\Delta\varsigma_{N_I-1}}\right] \quad (6.38)$$

For Upper most Intermediate Grid Points

When $j = (N_J - 1)$

$$\frac{d\omega_{i,N_J-1}}{dt} = \frac{D_0\omega_{i,N_J-1}}{\phi}\left[\frac{1}{r_i}\frac{\omega_{i+1,N_J-1}-\omega_{I-1,N_J-1}}{2\Delta r}+\frac{\omega_{i+1,N_J-1}-2\omega_{i,N_J-1}+\omega_{i-1,N_J-1}}{\Delta r^2}\right]+$$
$$\frac{D_0}{\phi}\left[\frac{\omega_{i+1,N_J-1}-\omega_{i-1,N_J-1}}{2\Delta r}\right]^2-\frac{K_r K\rho g\cos\theta}{Z_0\mu_0\phi}3\omega^2_{i,N_J-1}\left[\frac{\omega_{sat}-\omega_{i,N_J-2}}{2\Delta\varsigma_i}\right] \quad (6.39)$$

Change in Height of Physical Model

Change in height of the physical model at any time instance was calculated by averaging the mass fraction value for the exposed nodes to solvent gas at the bottom of the model. Second set of ordinary differential equations were written as:

$$\frac{d\varsigma_i}{dt} = -v_{i,0} = -3\frac{K_r K\rho g\cos\theta}{Z_0\mu_0}\left[\frac{\omega_{i,0}+\omega_{i+1,0}+2\omega_{sat}}{4}\right]^2 \quad \forall \quad 0\le i<(N_1-1) \tag{6.40}$$

$$\frac{d\varsigma_{N_1-1}}{dt} = -v_{N_1-1,0} = -3\frac{K_r K\rho g\cos\theta}{Z_0\mu_0}\left[\frac{\omega_{N_1-1,0}+3\omega_{sat}}{4}\right]^2 \tag{6.41}$$

In Equations [6.31–6.39] $\omega_{i,j}$ is the mass fraction of the gas at the mode (i,j) corresponding to the coordinate (r_i,ς_j). Δr is the constant inter grid distance along the radial direction and was calculated as:

$$\Delta r = \frac{R}{N_1} \tag{6.42}$$

where R = Radius of the cylindrical model.

Any $\Delta\varsigma_k$ is the time dependent intergrid distance along the axial direction at a given radial distance r_k, and was calculated as:

$$\Delta\varsigma_k = \frac{\varsigma_k}{N_J+1} \tag{6.43}$$

where ς_k is the bitumen height at r_k in the medium at any time.

The cumulative mass of live oil was calculated at the experimental time instants from

$$m_{cal} = 2\pi\rho Z_0\phi\sum_{i=0}^{N_{1-1}}(1-\zeta_i)r_{i+1}\Delta r \tag{6.44}$$

Equations [6.31–6.44] were numerically integrated using semi-implicit Bader-Deuflhard algorithm, and adaptive step size control (Press et al., 2001). Analytical Jacobians of

above equations were employed and the validity of the Jacobian equations was confirmed with the analytical solution to an error accuracy of 10^{-6}. The set of Jacobian equations written for corresponding grid points, employed to integrate ODEs are given in the Appendix F at the end of thesis.

Number of the grid points along the radial and vertical directions, N_I and N_J, were fixed after carrying out the integration with increased grid points until the change in calculated cumulative mass of the produced live oil became negligible. N_I and N_J were determined to be 25 and 10 respectively for normalized model height.

6.3 Dispersion Coefficient Determination

Dispersion coefficient of butane gas in porous media was determined using indirect method that includes finding live oil viscosity, density and solubility of solvent gas into heavy oil and generating live oil production data from experimental study. A detailed mathematical model was developed as shown above Equation [6.24]. For solution of the model developed, dependency of dispersion on concentration was employed by using a linear relationship equating by a coefficient known as dispersion coefficient and denoted as D_0. The model equation was solved for two unknowns D_0 and ω_{sat} (solvent mass fraction at oil interface) with set of input parameters shown in Table (6.1). The model solution was approximated by minimization of an objective function developed from root mean squared error between experimental and calculated live oil production. Live oil production was calculated from Equation [6.26] by solving Equations [6.24] and [6.25] simultaneously. The objective function is given as:

$$E = \sqrt{\frac{1}{N}\sum_{i=1}^{N-1}\left(m_{\text{cal},i} - m_{\text{exp},i}\right)^2} \tag{6.45}$$

where E is objective function, N is the number of experimental data points, and i shows the i-th experimental time instant.

The unknowns, D_0 and ω_{sat} in the model Equation [6.24] were determined by using an optimizer by supplying initial guess for both of them. Variable metric method in multi dimensions was used to improve D_0 and ω_{sat} for the next iteration based on minimization of the objective function. Dowel-Fletcher-Powell minimization algorithm (Press et al., 2001) was used to optimally determine the unknowns. The gradient of the objective function was supplied based on number of variables optimized. Tolerance on error for gradients was set to 10^{-6}. Following is the equation for gradient supplied for optimization algorithm:

$$\bar{G} = \begin{bmatrix} \left.\dfrac{\partial E}{\partial D_0}\right|_{\omega_{sat}} \\ \left.\dfrac{\partial E}{\partial \omega_{sat}}\right|_{D_0} \end{bmatrix}_k = \begin{bmatrix} \left.\dfrac{E_{k+1} - E_k}{D_{0,k+1} - D_{0,k}}\right|_{\omega_{sat}} \\ \left.\dfrac{E_{k+1} - E_k}{\omega_{sat,k+1} - \omega_{sat,k}}\right|_{D_0} \end{bmatrix} \tag{6.46}$$

where $k \geq 0$ is the iteration counter and for $k = 0$, E_1 was calculated using $D_{0,1} = D_{0,0}$ and $\omega_{sat,1} = \omega_{sat,0}$ where $D_{0,0}$ and $\omega_{sat,0}$ are the initial guess for dispersion coefficient and maximum solvent fraction at interface.

In the above equation $D_{0,k+1}$ and $\omega_{sat,k+1}$ are:

$$D_{0,k+1} = D_{0,k} \times (1 + 10^{-4}) \tag{6.47}$$

$$\omega_{sat,k+1} = \omega_{sat,k} \times (1 + 10^{-4}) \tag{6.48}$$

The above mentioned algorithm was programmed in a way to solve a set of models (different model heights) simultaneously to determine a single value of ω_{sat} for all models with individual D_0 to evaluate dispersion dependency towards drainage height. This was accomplished by setting three program blocks named as submodel, model and optimizer.

In the model block an overall objective function was determined by solving set of models through submodel with optimally set values of ω_{sat} and D_0 by optimizer block. The overall objective function was calculated as:

$$E_{overall} = \sum_{j=0}^{M} \sqrt{\frac{1}{N} \sum_{i=1}^{N-1} \left(m_{cal,i} - m_{exp,i}\right)^2} \tag{6.49}$$

where M is the number of models solved. The gradient of overall objective function was evaluated in the same block from Equation [6.46] by solving set of models through submodel with same value of ω_{sat} and different values of D_0 obtained from optimizer block. Sub Model was used to solve set of ODEs [Equations (6.31−6.44)] along with their Jacobian Equations [F1−F40] for each individual model by using integration and step size control algorithms by taking optimally set values of ω_{sat} and D_0 through Model block. While optimizer block was used to imply optimization algorithms.

The above algorithm was very computationally intensive because a large number of finite difference equations associated with Jacobian evaluations were needed to obtain accurate solutions. Implemented on 64-bit Itanium computer minimum time the algorithm took to converge for one model heights was 12 hours depending upon the initial guess for ω_{sat} with error values of convergence in the order of 10^{-1}.

Table 6.1: Parameters for Model Simulation

Codes	Parameters	Value	
Nr	Number of Nodes in r Direction	25	
Nz	Number of Nodes in Z Direction	10	
xi	Initial Limit for Integration	0	
hi	Initial Step Size	1×10^{-10}	
hmax	Maximum Step Size	10	
eps	Accuracy of Integration	1×10^{-6}	
Kr	Relative Permeability	1	
K	Permeability	1.0857e-6	(cm^2)
rho	Live Oil Density	0.81	(g/cm^3)
g	Gravity	3531600	(cm/min^2)
theta	Dip Angle	0	
phi	Porosity	0.38	
μ_0	Live oil Viscosity	0.7987543	(g/cm.min)
ω_{Sat}	Maximum Saturation Concentration	0.50–0.90	
D_0	Coefficient of Dispersion	1.1×10^{-4}	(cm^2/s)
nvar	Number of Optimization Variables	4	
STPMX	Maximum Step Length (Line search)	1	
TOLG	Tolerance on Gradient	1×10^{-6}	
R	Radius of Physical Model	3	(cm)
Z	Height of Physical Model	25,35,45	(cm)
t	Simulated Time	0–300	(min)

7 Results & Discussion

To evaluate the dispersion coefficient of butane with varying model heights the set of models or a single model was solved with same value of solvent mass fraction at the interface applicable to any model height. As fundamentally when temperature and pressure conditions are same for different model heights, solvent mass fraction at interface should be the same. Moreover models were solved with effective height by subtracting 5 cm from each model length. Only three model heights were considered during simulation study excluding 15 cm model. As from the experiments no much difference in production was observed between 15 to 25 cm models as well as the correlation for production rate to drainage height was developed base on data from 25, 35 and 45 cm models. Therefore the same models used for correlation during experimental study were used to investigate dispersion coefficient of butane.

It was observed, when solving a single model and evaluating D_0 and ω_{sat} independent of model height, the root mean square error between simulated and experimental live oil produced was minimized very efficiently by the optimization algorithm. As the search for less error is free to look for two different variables with a range of values. But when particularly three models with 25, 35 and 45 cm heights were solved simultaneously to determine solvent dispersion coefficient with same maximum solvent fraction, minimization of the root mean square error was found to be very critical for initial guess of solvent mass fraction and dispersion coefficient. If the initial guess for ω_{sat} and D_0 was not in a particular range, the algorithm could not minimize the objective function to the mark where discrepancy between experimental and simulated live oil production become acceptable. Figures (7.1–7.3) shows the comparison of simulated and experimental results obtained for 25, 35 and 45 cm model heights, when initial guess for

ω_{sat} and D_0 was not in a good range. The algorithm could not reduce overall objective function less than 49.0.

In order to provide a good initial guess to solve set of models with fundamental condition of same ω_{sat} for each model height, each model was solved separately with varying ω_{sat} from 0.5–0.9 and D_0 from 1×10^{-4} to 9×10^{-4} cm^2/s. The resultant objective functions were plotted against ω_{sat} and a zone was located where there is least discrepancy between ω_{sat} for all set of models with minimum objective function values as shown in Figure (7.4).

From Figure (7.4) initial guess range for solvent mass fraction was selected between 0.54–0.57, three model heights were solved together. Optimal D_0 for each model height along with single value of ω_{sat} was evaluated by minimizing the discrepancy between experimental and simulated live oil production. The optimum values obtained for ω_{sat} and D_0 are shown in Table (7.1) and corresponding comparison between simulated and experimental results are shown in Figures (7.5–7.7). It was observed that the predicted production follows experimental production very closely during the operation time of 300 minutes. The rate of production during this time stays practically constant as has been experimentally determined.

The overall objective function that is summation of objective function for each individual model height was found to be minimum at $\omega_{sat} = 0.55$ with optimal dispersion coefficients of $2.73\times10^{-4}\omega$, $33.1\times10^{-4}\omega$ and $212\times10^{-4}\omega$ cm^2/s for 25, 35 and 45 cm model heights respectively.

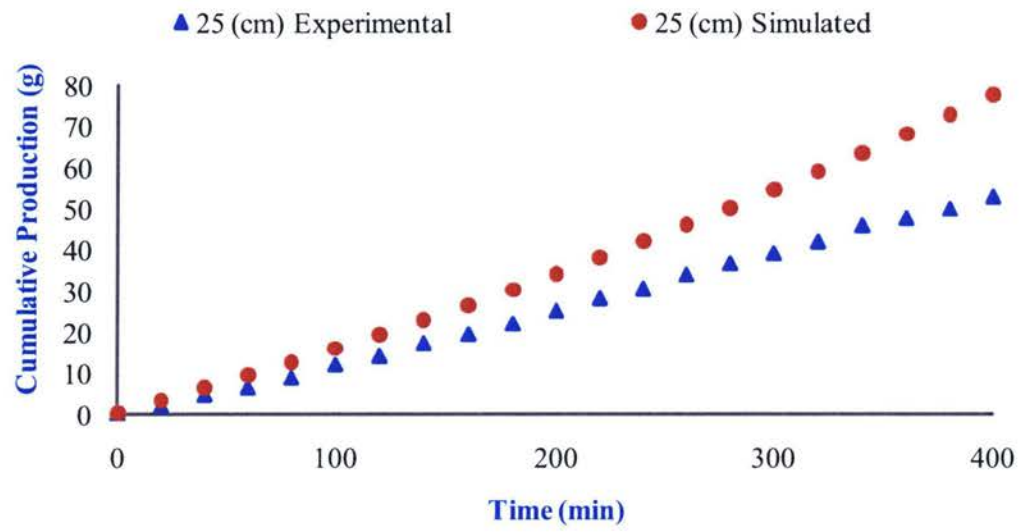

Figure 7.1: Experimental vs Simulated Live Oil Production (25 cm)
(Initial guess not in range)

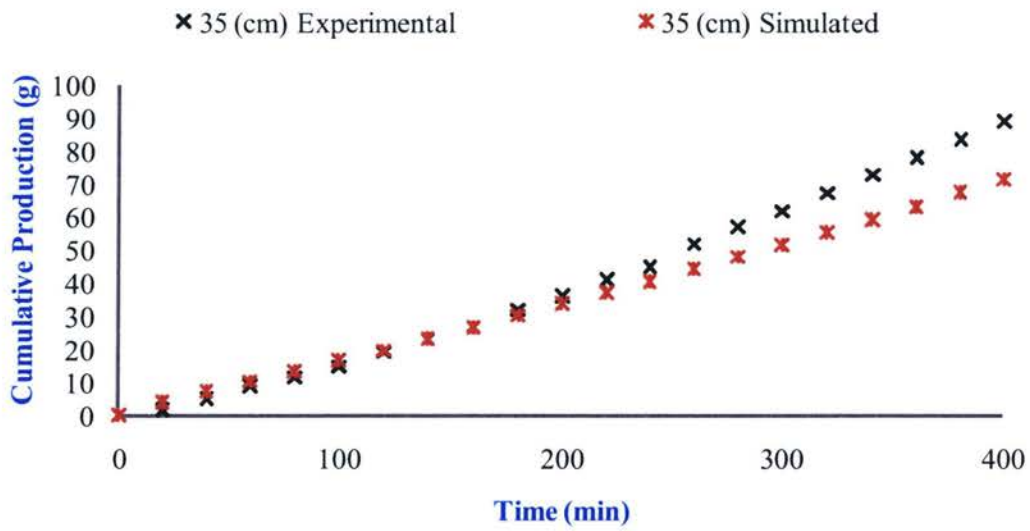

Figure 7.2: Experimental vs Simulated Live Oil Production (35 cm)
(Initial guess not in range)

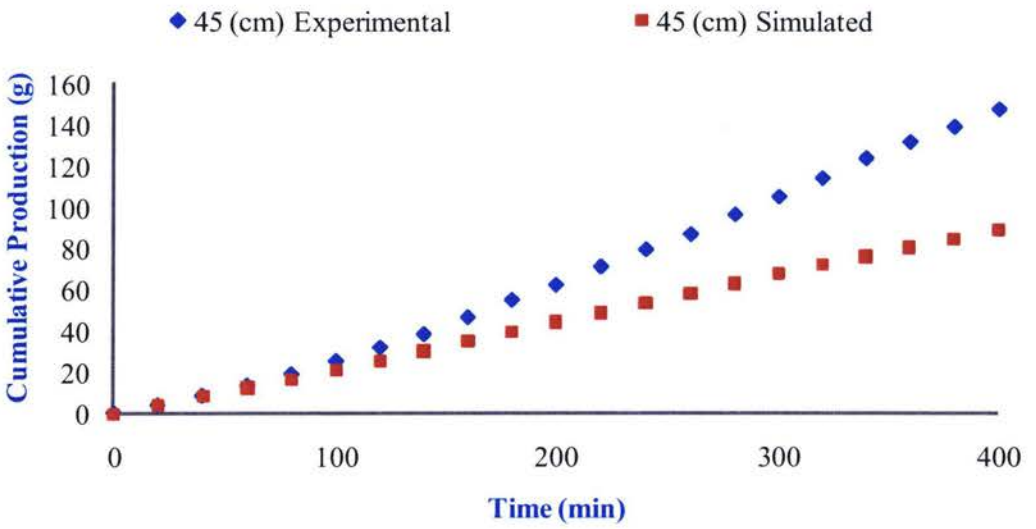

Figure 7.3: Experimental vs Simulated Live Oil Production (45 cm)
(Initial guess not in range)

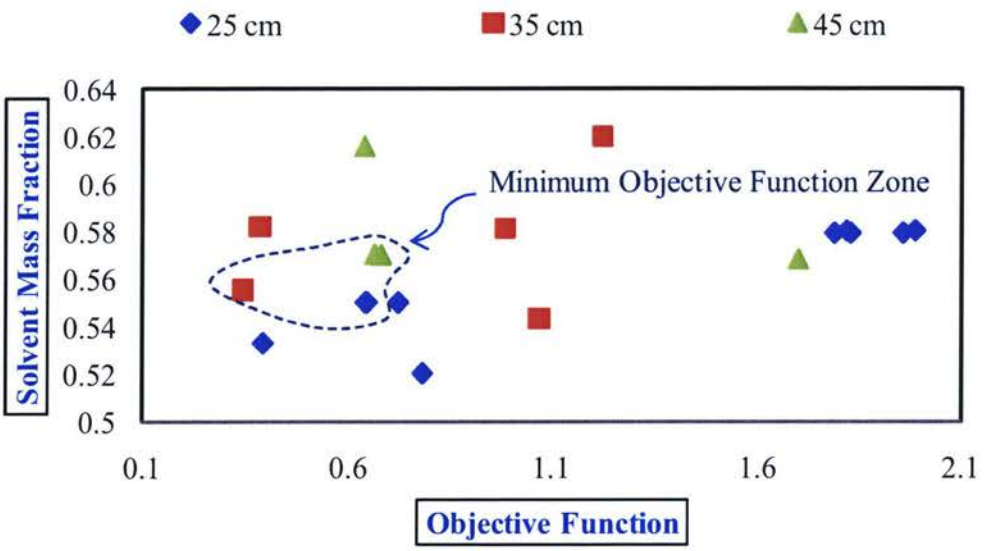

Figure 7.4: Solvent Mass Fraction vs Objective Function
(Different Model Heights)

Table 7.1: Optimal Values for Coefficient of Dispersion (Three Model Heights)

Drainage Height (cm)	Maximum Solvent Mass Fraction ω_{sat}	Coefficient of Dispersion D_0 (cm^2/s)	Objective Function E
25	0.55	2.73×10^{-4}	5.28×10^{-1}
35	0.55	33.1×10^{-4}	6.04×10^{-1}
45	0.55	212×10^{-4}	7.93×10^{-1}

Over all Objective Function: 1.925×10^{-0}

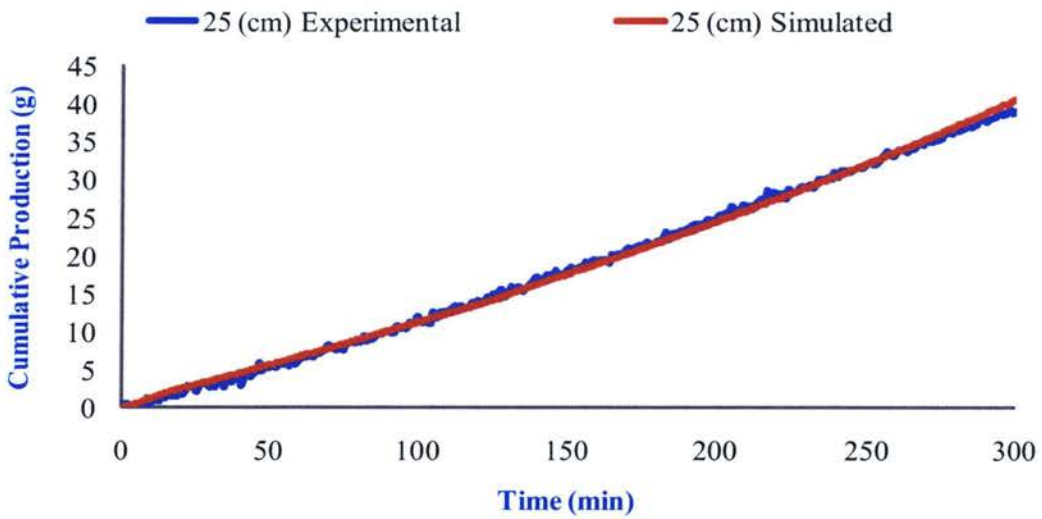

Figure 7.5: Experimental vs Simulative Live Oil Production (25 cm) (with ω_{sat} in a good initial guess range)

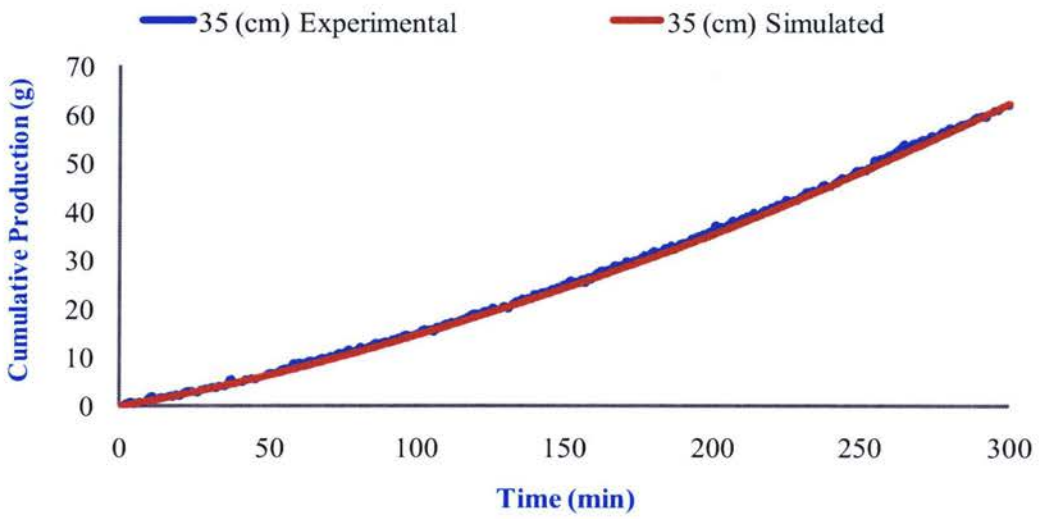

Figure 7.6: Experimental vs Simulative Live Oil Production (35 cm)
(with ω_{sat} in a good initial guess range)

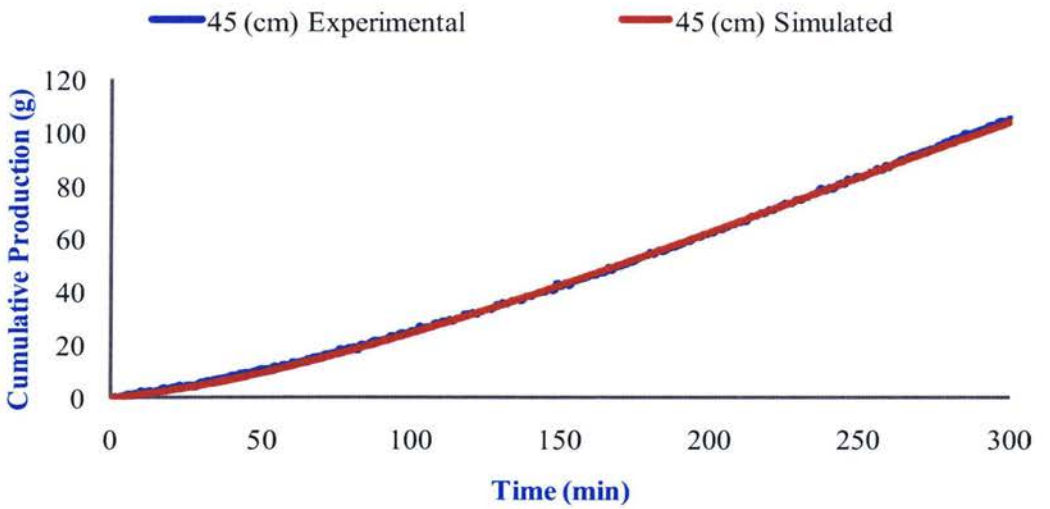

Figure 7.7: Experimental vs Simulative Live Oil Production (45 cm)
(with ω_{sat} in a good initial guess range)

It is observed that the dispersion coefficient is a strong function of the drainage height as from Table (7.1), if the drainage height is increased two times the corresponding dispersion coefficient may increase with much higher ratio subject to the condition of same solvent mass fraction. Although rate of surface renewal is much faster for longer model heights to shorter ones because of increased gravitational head, but as a matter of fact total surface area for solvent gas contact to the heavy oil is also higher as compared to the shorter ones. In order to compensate for higher surface area in case of larger model heights, mass calculated equations for 35 and 45 cm were modified as:

$$m_{cal} = 2\pi\rho Z_0\phi \times A \int_0^R (1-\varsigma) r\, dr \quad \text{(for 35 cm Model)} \tag{7.1}$$

$$m_{cal} = 2\pi\rho Z_0\phi \times B \int_0^R (1-\varsigma) r\, dr \quad \text{(for 45 cm Model)} \tag{7.2}$$

where A and B are the ratio of model height with respect to 25 cm model which are 1.5 and 2.0 respectively. The algorithm was run with an initial guess of 0.55 for ω_{sat} and 1.0×10^{-4} cm^2/sec for D_0, to solve three models together. The optimal values of dispersion coefficient obtained were $2.73\times10^{-4}\omega$, $4.51\times10^{-4}\omega$ and $11.6\times10^{-4}\omega$ cm^2/sec with $\omega_{sat} = 0.55$ and objective function values of 1.28×10^{-1}, 1.39×10^{0} and 9.0×10^{-1} for 25, 35 and 45 cm model heights respectively. The comparison between experimental and simulated values of live oil production obtained from Equations [7.1] and [7.2] for first 300 minutes of experimental time is shown in Figures (7.8–7.9), and optimal dispersion coefficient with objective function values are shown in Table (7.2).

From the above analysis it is observed that the coefficient of dispersion of butane increases with the drainage height. As in actual circumstances (physically) the larger models have larger area of contact for solvent to oil. Therefore incorporation of ratio factors in calculated mass equations for 35 and 45 cm can be justified. The optimal values of dispersion coefficient obtained from Equations [7.1 & 7.2] can be considered for dispersion dependency towards drainage height.

There is not much work to date has been reported in butane gas dispersion coefficients in heavy oil and bitumen, especially dispersion dependency towards the drainage height has not been evaluated before. The minimum optimal value of dispersion coefficient obtained from this work corresponding to the shortest model length (25 cm) used is almost four times lower than the dispersion coefficient of butane gas numerically determined by El-Haj (2007) with model height of 21 cm. The dispersion coefficient is a function of concentration and depends upon live oil viscosity and solubility limit of solvent under temperature and pressure conditions. The lower value of dispersion coefficient of butane obtained in this study is due to: 1) The viscosity of heavy oil used in this study was higher (350,000 mPa.s) than used by El-Haj (2007) (280,000 mPa.s). 2) Saturation mass fraction at liquid gas interface calculated from this work was determined as 0.55, which is lower by 0.16 as used by El-Haj (2007).

The difference in saturation mass fraction compared with El-Haj (2007) can be explained as, 1) The higher viscosity of heavy oil used for current study. 2) Change in velocity of the diluted oil through porous media was not considered for the model developed by Randa, as well as net volume of live oil from the differential block was ignored without multiplying the calculated mass expression with porosity of the medium.

The change in bitumen height in the porous medium with respect to radius at different times for 25, 35 and 45 cm models is shown in Figures (7.10–7.12). The curves represent reduction in bitumen height for every 30 minutes of the experimental time instances. The graphs exhibit the behaviour of diluted oil drainage. As the solvent gas diffuses through the exposed oil surface it drains by the action of gravity with the incorporation of dispersive action of solvent gas. Once it drains another heavy oil surface is exposed to solvent gas and the procedure of the surface renewal continues due to the bulk motion of the diluted oil. In case of 45 cm model the effect of higher value of dispersion coefficient for solvent gas is clear from Figure (7.12) that shows the interface renewal trend more curved in radial direction. This is because of the assumption for solvent dispersion in radial direction.

To express the dependency of dispersion on effective drainage height the results obtained from Table (7.2) were curve fitted. Maximum r^2 value was obtained for a second order polynomial and the following equation was obtained

$$D_0 = a\times\left(\frac{L}{D}\right)^2 - b\times\left(\frac{L}{D}\right) + c \quad (\text{cm}^2/\text{s}) \tag{7.3}$$

where a, b and c are coefficient of the equation and the values are 9.558×10^{-5}, 6.897×10^{-4} and 1.510×10^{-3} respectively. And $\frac{L}{D}$ is the drainage height to diameter ratio of the physical model.

Note: The above relationship is valid for drainage height greater than 25 cm.

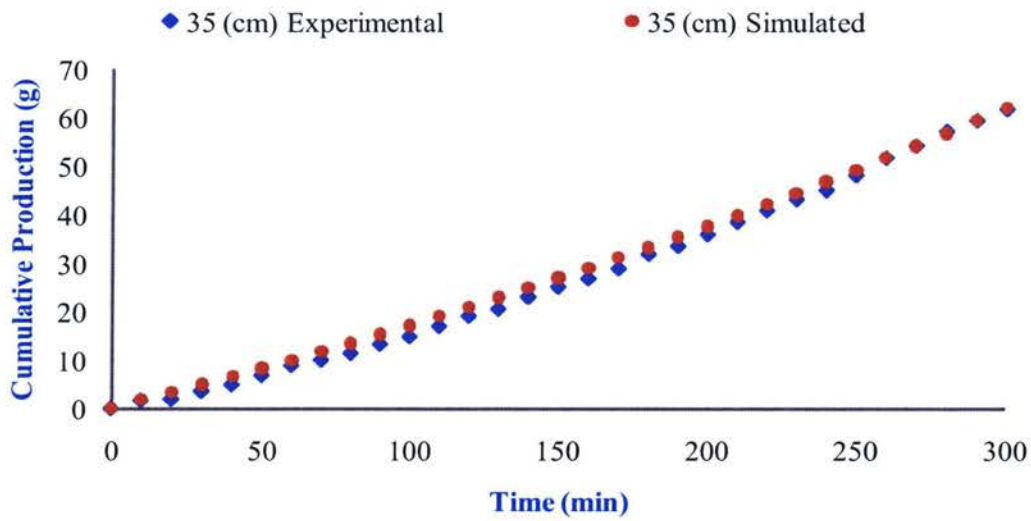

Figure 7.8: Experimental vs Simulative Live Oil Production (35 cm, with ratio)

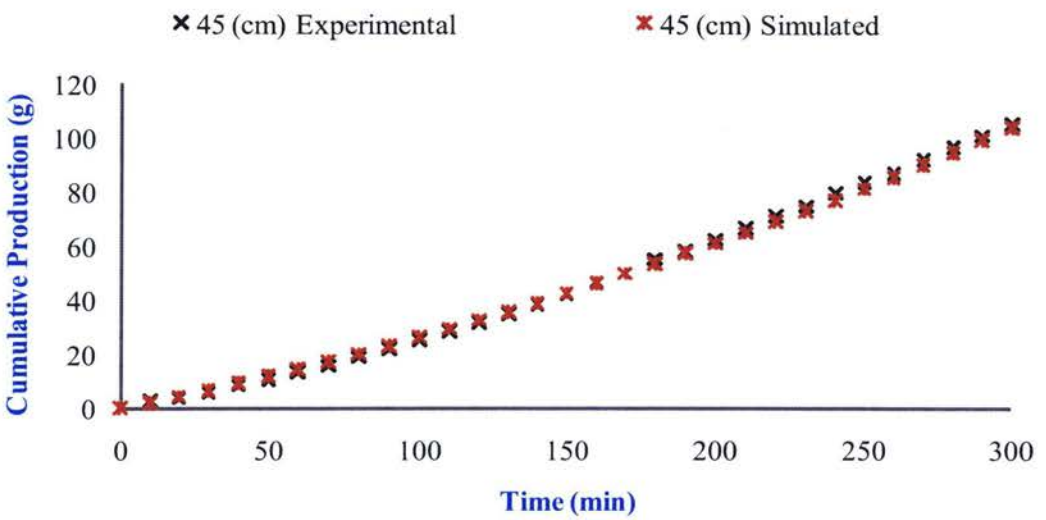

Figure 7.9: Experimental vs Simulative Live Oil Production (45 cm, with ratio)

Table 7.2: Optimal Values for Coefficient of Dispersion
(Three Model Heights, with Area Ratio)

Drainage Height (cm)	Maximum Solvent Mass Fraction ω_{sat}	Coefficient of Dispersion D_0 (cm^2/sec)	Objective Function E
25	0.55	2.73×10^{-4}	1.28×10^{-1}
35	0.55	4.51×10^{-4}	1.39×10^{0}
45	0.55	11.6×10^{-4}	9.0×10^{-1}

Over All Objective Function: 2.148×10^{-0}

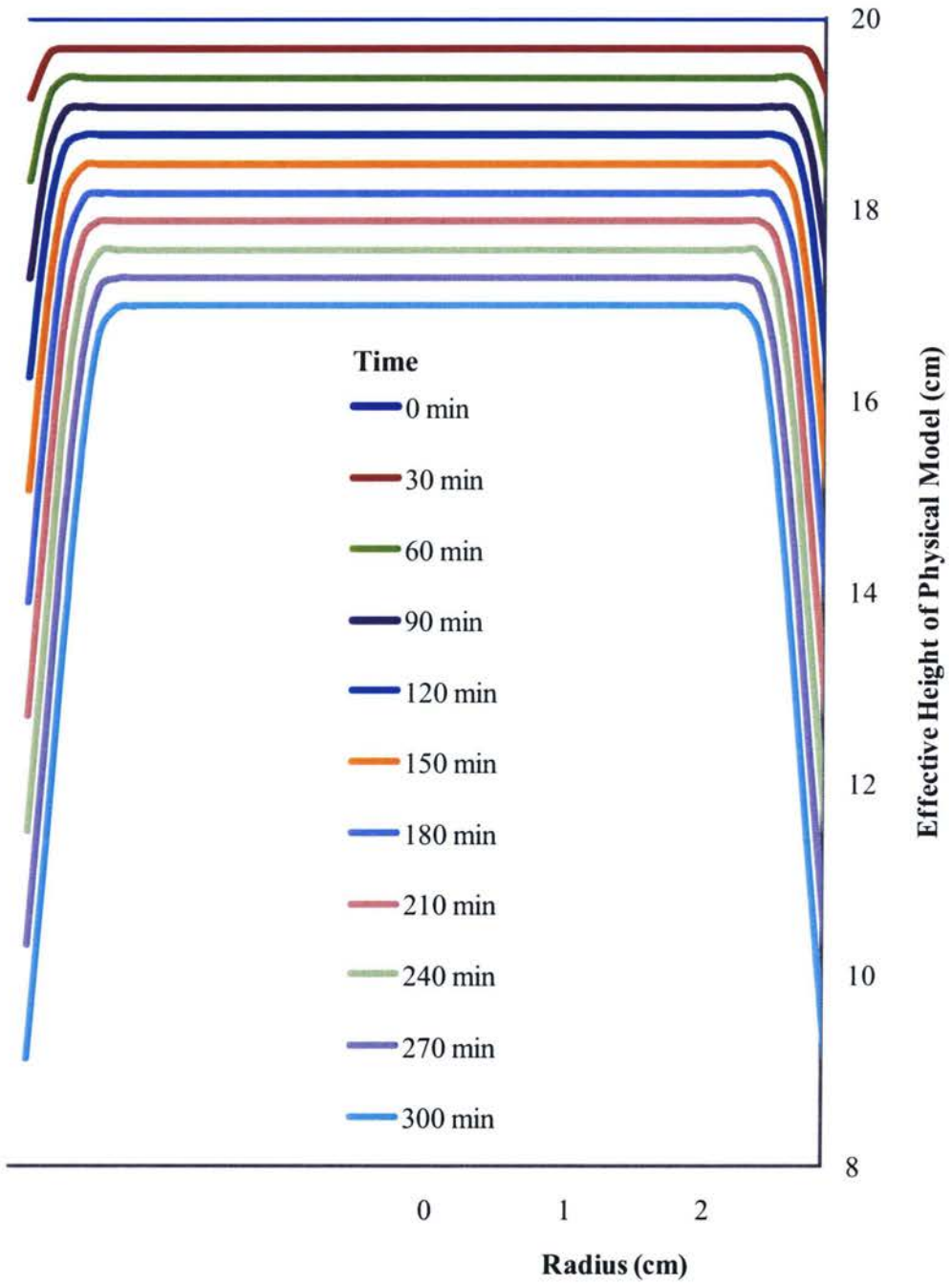

Figure 7.10: Change in Height with Time (Model 25 cm)

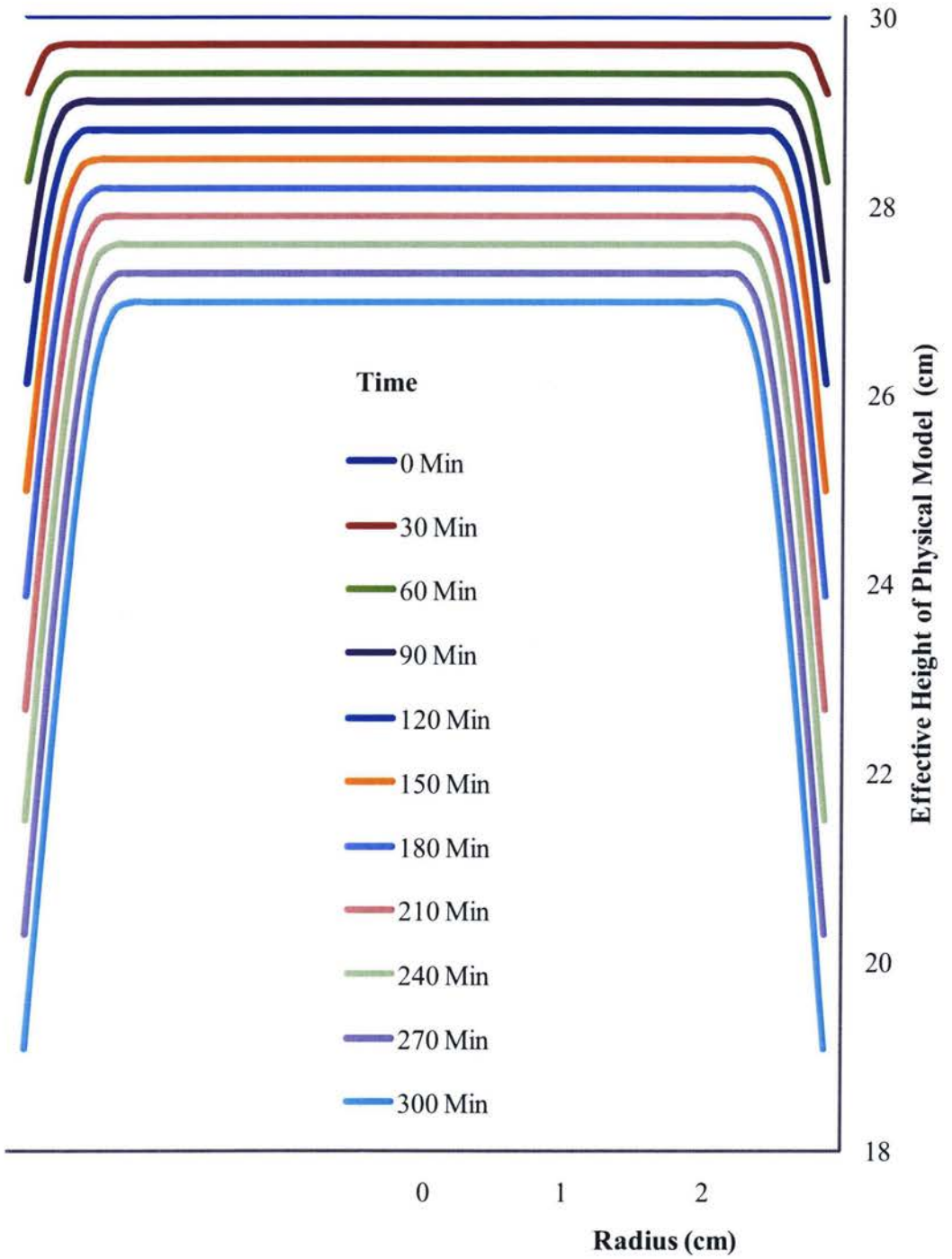

Figure 7.11: Change in Height with Time (Model 35 cm)

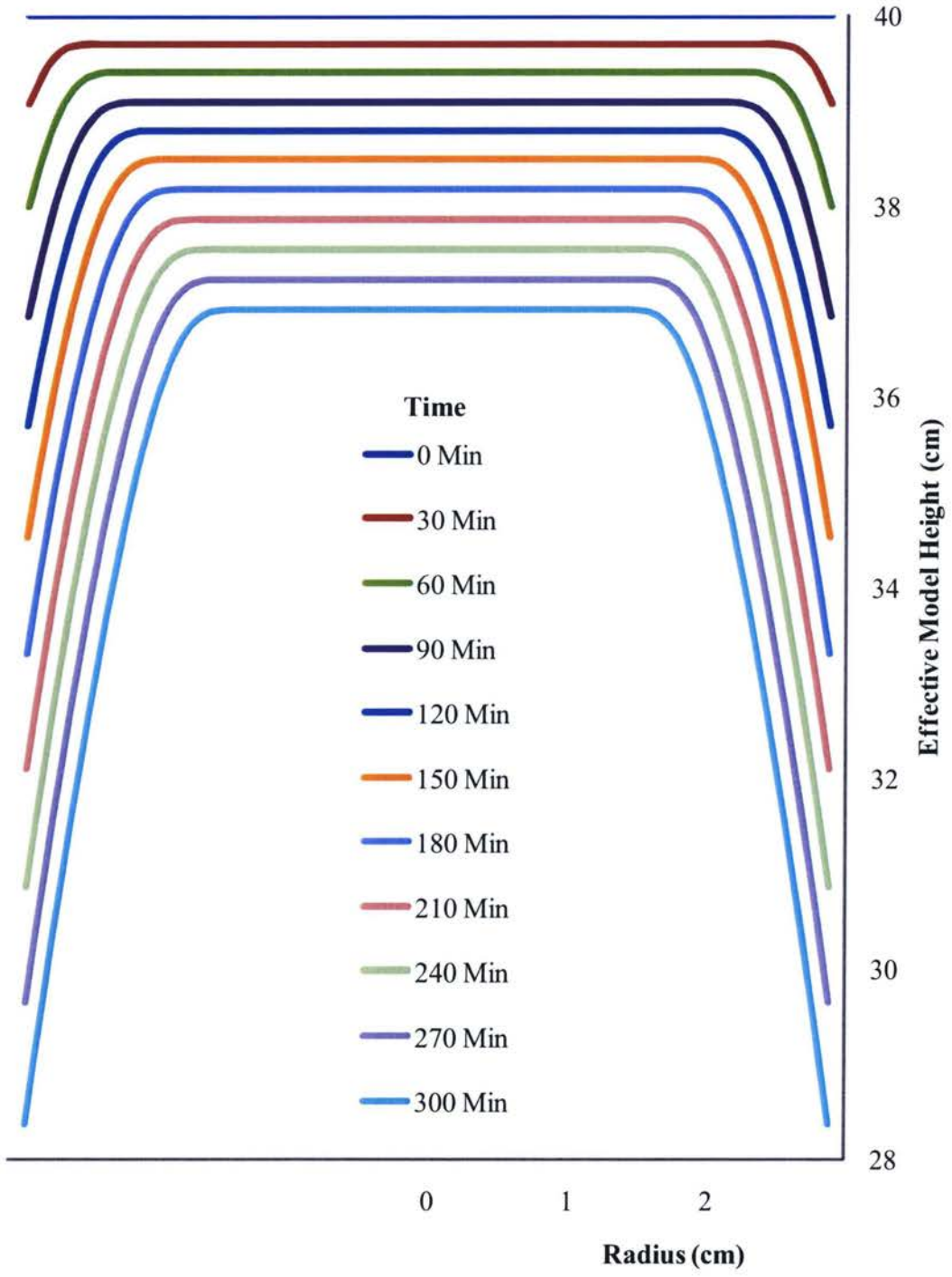

Figure 7.12: Change in Height with Time (45 cm Model Height)

8 Conclusions & Recommendations

In this thesis the dispersion coefficient of butane in vapor extraction of heavy oil and bitumen was determined as a linear function of its concentration in heavy oil and bitumen packing of different drainage heights. The experiments were performed at constant temperature and dew point pressure of solvent (butane). Cylindrical models with four different heights and same radius packed with uniform mixture of bitumen and glass beads expressing a constant permeability porous media were used. Sets of data for cumulative mass of live oil production were obtained. The live oil viscosity, density and butane mass fraction in heavy oil (viscosity of 350,000 mPa.s (at 22°C), specific gravity of 1.0014) was also determined. A power relationship between live oil production rate to the effective drainage height was established. It was found that live oil production rate in Vapex is proportional to the drainage height to the power of 1.495.

A mathematical model was developed based on solvent mass transfer through a differential element to simulate live oil production rates. An algorithm was developed utilizing multi direction and multivariable optimization technique to simultaneously solve a set of models (different heights). The solvent mass fraction at liquid gas interface and dispersion coefficient of butane in heavy oil was optimally determined by minimizing the root-mean-square error between experimental and simulated live oil production. The dispersion coefficients (in cm^2/s) were determined to be 2.73×10^{-4}, 4.51×10^{-4} and 11.6×10^{-4} times the butane mass fraction respectively for 25, 35 and 45 cm model heights. It was found that dispersion coefficient of butane for this particular heavy oil system increases with drainage height. A polynomial expression was established between solvent dispersion and drainage height.

8.1 Recommendations for Future Work

1. The dispersion coefficients of other gases such as propane, ethane, methane or their mixtures can be measured for different temperature and pressure conditions.

2. The solvent mass fraction at the interface can be experimentally determined using gas chromatography.

3. The linear dependency of dispersion on solvent concentration can be extended by incorporating an undetermined optimal control function.

4. The mathematical model can be expanded to investigate the effect of longitudinal dispersion.

Bibliography

AEUB., 2005. Alberta Energy and Utility board.

Akbarzadeh, K., Ayatollahi, S., Nasrifar, K., Yarranton, H. W., Moshfeghian, M., 2002. Equations Lead to Asphaltene Deposition Prediction. Oil & Gas Journal, 100 (44): 55–54.

Allen, J. C., 1973. Method for Recovering Viscous Oils by Solvent Extraction; Technical Report, Texaco Development. US. Application No. 391434, August 24, 1973.

Bird, B. R., Stewart, E. S., Lightfoot, N. E., 2002. Transport Phenomena, Second Edition, Chemical and Biological Engineering Department, University of Wisconsin-Madison, New York.

Boustani, A., Maini, B. B., 2001. The Role of Diffusion and Convective Dispersion in Vapour Extraction Process. Journal Canadian Petroleum Technology, 40 (4): 68–77.

Butler, R. M. and Mokrys, I. J., 1989. Solvent Analog Model of Steam Assisted Gravity Drainage. AOSTRA Journal of Research, 5(1989): 17–32.

Butler, R. M. and Mokrys, I. J., 1991. A new Process (Vapex) for Recovering Heavy Oils Using Hot Water and Hydrocarbon Vapor. The Journal of Canadian Petroleum Technology, 30: 97-106.

Butler, R. M. and Mokrys, I. J., 1993. Recovery of Heavy Oils using Vaporized Hydrocarbons. The Journal of Canadian Petroleum Technology, 32(6): 56–62.

Butler, R. M. and Mokrys, I. J., 1998. Closed Loop Extraction Methods for Recovery of Heavy Oil and Bitumen Underlain by Aquifers: The Vapex Process. Journal of Canadian Petroleum Technology, 37(4): 41–50.

Butler, R.M. and Jiang, Q., 2000. Improved Recovery of Heavy Oil by Vapex with Widely Spaced Horizontal Injectors and Producers. The Journal of Canadian Petroleum Technology, 39 (1): 48–56.

Butler, R.M., Mokrys, I. J., Das, S. K., 1995. The Solvent Requirement for Vapex Recovery. Pape # SPE 30293, In ternational Heavy Oil Symposium, Calgary, June 19–21.

CIM Directory Feature., 1993. Syncrude: Past Performance – Future Success, CIM Directory.

Das, S. K. and Butler, R. M., 1995. Extraction of Heavy Oil and Bitumen Using Solvent at Reservoir Pressure; Paper No 95-118, Sixth Petroleum Conference of the South Saskatchewan Section of Petroleum Society, Regina, SK, October 16-18.

Das, S. K. and Butler, R. M., 1996. Diffusion Coefficients of Propane and Butane in Piece River Bitumen. Canadian Journal of Chemical Engineering, 74: 985–992.

Das, S.K., 1995. In Situ Recovery of Heavy Oil and Bitumen Using Vaporized Hydrocarbon Solvents, Ph.D. thesis, Department of Chemical and Petroleum Engineering, University of Calgary, Calgary.

Das, S.K., 1998. Vapex: An Effective Process for the Recovery of Heavy Oil and Bitumen. SPE 50941, SPE Journal, 232-237.

Das, S.K. and Butler R.M., 1994. Effect of Asphalting Deposition on the Vapex Process: A Preliminary Investigation Using Hele-Shaw Cell. The Journal of Canadian Petroleum Technology, 33(6): 39–45.

Das, S.K. and Butler., R.M., 1998. Mechanism of the vapour extraction process for heavy oil and bitumen. J. Pet. Sci. Eng., 21(1): 43-59.

Dunn, S.G., Nenniger E. H., Rajan, V.S.V., 1989, A Study of Bitumen Recovery by Gravity Drainage Using Low Temperature Soluble Gas Injection. Canadian journal Chemical Engineering, 67: 978–991.

El-Haj, R., 2007. Experimental Determination of Solvent Gas Dispersion in Vapex Process. MASc Thesis, Ryerson University, Chemical Engineering Department, Toronto, Ontario.

ERCB., 1989. Energy Resources Conservation Board, Alberta's Reserves of Crude Oil, Oil Sands, Gas, Natural Gas Liquids and Sulphur, ST 95.

Fraueneld, T., Jossy, C., Rispler, K., Kissel, G., 2006. Evaluation of the Bottom Water Reservoir Vapex Process. The Journal of Canadian Petroleum Technology, 45(9): 29–35.

Friedrich, K., 2005. Effects of a Non Condensable Gas on the Vapex Process, MASc . thesis, Department of Chemical Engineering, University of Waterloo, Ontario.

Grogan, A. T. and Pinczewski, W. V., 1987. The Role of Molecular Diffusion Processes in Tertiary CO_2 Flooding. Journal of Petroleum Technology, 39(5): 591–602.

Gupta, S., Gittins, S, Picherack, P., 2003. Insight into Some Key Issues with Solvent Aided Process. The Journal of Canadian Petroleum Technology, 43(2): 54–61.

Hayduk, W. and Cheng, S. C., 1971. Review of Relation Between Diffusivity and Solvent Viscosity in Dilute Liquid Solutions. Chem. Eng. Sci, 26: 636–646.

Hayduk, W. and Minhas, B. S., 1982. Correlations for Prediction of Molecular Diffusivities in Liquids. Canadian Journal of Chemical Engineering, 60: 295–299.

Hiss, T. G. and Cussler, E. L., 1973. Diffsuion in High Viscosity Liquids. ALCHE Journal, 19: 698–703.

http://en.wikipedia.org/wiki/API

Imran, M., Upreti, S. R., Lohi, A., 2008. Optimal Oil Production from Vapex Potential Directions. Petroleum Science Research Progress, Nova Publishers, ISBN: 978-1-60456-012-1.

James, L. A., Chatzis, I., Loannidis, M. A., 2003. Determination of Diffusion Coefficient of Butane in Heavy Oil and the Mass Transfer Rate at the Pore Scale in Vapex. In Petroleum Society's Canadian International Petroleum Conference, Calgary.

Jiang, Q., 1997. Recovery of Heavy Oil and Bitumen Using Vapex Process from Homogeneous and Heterogeneous Reservoirs. Ph.D. thesis, Department of Chemical and Petroleum Engineering, University of Calgary, Alberta.

Jiang, Q. and Butler, R. M., 1996 a. Experimental Studies on Effect of Reservoir Heterogeneity on the Vapex Process. Journal of Canadian Petroleum Technology. 35 (10): 46–54.

Jiang, Q. and Butler, R. M., 1996 b. Selection of Well Configuration in Vapex. Paper # SPE 37145, SPE International Conference on Horizontal Well Technology, Canada, November 18–20.

Jiang, Q., Butler, R.M., and Yee, C.T., 2000. The Steam and Gas push (SAGP)-2: Mechanism Analysis and Physical Model Testing. Journal of Canadian Petroleum Technology. 39 (4): 52–61.

Jin, W., 1999. Heavy Oil Recovery Using the Vapex Process. MASC Thesis, University of Waterloo, Waterloo, Ontario.

Kapadia, R. A., Upreti, S. R., Lohi, A., Chatzis, I., 2006. Determination of Gas Diperssion in Vapor Extraction of Heavy Oil and Bitumen. Journal of Petroleum Science and Engineering, 51: 214–222.

Karmaker, K. and Maini, B. B., 2003. Experimental Investigation of Oil Drainage Rates in the Vapex Process for Heavy Oil and Bitumen Reservoirs, Paper SPE 84199 presented at the 2003 SPE Annual Technical Conference and Exhibition, Denver, October 5–8.

Lim, G. B., Kry, R. P., Harker, B.C., Jha, K. N., 1996. Three Dimensional Scaled Physical Modeling of Solvent Vapor Extraction of Cold Lake Bitumen. Journal of Canadian Petroleum Technology, 35(4): 32–40.

Luhning, R. W., Das, S. K., Fisher, L. J., Bakker, J., Grabowski, J., Engleman, J. R., Wong, S., Sullivan, L. A., Boyle, H. A., 2003. Full Scale Vapex Process Climate Change Advantage and Economic Consequences. The Journal of Canadian Petroleum Technology, 42: 29-33.

Mokrys, I.J. and Butler, R. M., 1993. In Situ Upgrading of Heavy Oils and Bitumen by Propane Deasphalting: The Vapex Process. Paper # SPE 25452, Production Operations Symposium, Oaklahoma City, OK, March 21–23.

Nghiem, L. X., Kohse, B. F., Sammon, P. H., 2001. Compositional Simulation of the VAPEX Process. Journal Canadian Petroleum Technology, 40 (8): 54–61.

Oduntan, A. R., Chatzis, I., Smith, J., Lohi, A., 2001. Heavy Oil Recovery Using the Vapex Process: Scale-Up Issues. Paper # 2001-127, Petroleum Society's Canadian International Petroleum Conference, June 12–14.

PCF., 2000. Petroleum Communication Foundation, Canada's Oil Sands and Heavy Oil, Calgary, Alberta.

Press, W. H., Teukolsky, S. A., Vetterling, T. W., Flannery, P. B., 2001. Numerical Recipes in C++, The Art of Scientific Computing, Second Edition., EXXON Research and Engineering Company, Cambridge University.

PTAC., 2006. Petroleum Technology Alliance Canada, Expanding Heavy Oil and Bitumen Resources while Mitigating GHG Emissions and Increasing Sustainability, May, 2006.

Singhal, A.K.; Das, S.K.; Leggitt, S. M.; 1997. Screening of Reservoirs for Exploitation by Application Steam Assitsed Gravity Drainage / Vapex Processes. The Journal of Canadian petroleum Technology., 1122–1124.

Spanos, T., Davidson, B., Dusseault, M., Shand, D., Samaroo, M., 2003. Pressure Pulsing at the Reservoir Scale. A New IOR Approach. The Journal of Canadian Petroleum Technology, 42(3): 16–28.

Speight, J.G., 1991. The Chemistry and Technology of Petroleum, 2nd Edition, Marcel Dekker.

Strausz, O.P., 1989. Bitumen and Heavy Oil Chemistry, Technical Hand Book on Oil Sands, Bitumen and Heavy Oil, Alberta Oil Sands Technology and Research Authority, Edmonton, Alberta.

Upreti, S.R. and Mehrotra, A. K., 2000. Experimental Measurement of Gas Diffusivity in Bitumen: Results for Carbon Dioxide. Industrial and Engineering Chemistry Research, 39 (4): 1080–1087.

Upreti, S.R. and Mehrotra, A. K., 2002. Diffusivity of CO_2, CH_4, C_2H_6 and N_2 in Athabasca Bitumen. Canadian Journal of Chemical Engineering, 80: 116–125.

Upreti, S.R., Lohi, A., Kapadia, R.A., and El-Haj, R., 2007. Vapor Extraction of Heavy Oil and Bitumen: A Review, Energy & Fuels., 21: 1562–1574.

Wilke, C. R. and Chang, P., 1955. Correlation of Diffusion Coefficients in Dilute Solutions. ALCHE Journal, 1(2): 262–270.

Xu, W., 2006. The Role of Interfacial Tension in Vapex. MASc Thesis, Faculty of Engineering, University of Regina, Saskatchewan, Canada.

Yang, C., 2005. A New Method for Measuring Solvent Diffusion Coefficients and Oil Swelling Factors of Heavy Oil Solvent Systems. PhD Thesis, University of Regina, Ontario.

Yazdani J. A. and Maini, B.B., 2004. Effect of Drainage Height and Grain Size on the Convective Dispersion in the Vapex Process: experimental study. Paper SPE 89409, SPE/DOE Symposium on Improved Oil Recovery, Tulsa, Oklahoma, April 17–21.

Yazdani J. A. and Maini, B.B., 2005. Effect of Drainage Height and Grain Size on Production Rates in the Vapex Process: Experimental Study. SPE Reservoir Simulation & Engineering, 206–213.

Appendix A

A. Potential Strategies to enhance oil production through Vapex (published paper)

Authors: Muhammad Imran, Simant R Upreti, Ali Lohi

Web Link: https://www.novapublishers.com/catalog/product_info.php?products_id=6239

INTRODUCTION

Vapex or vapor extraction is an innovative process, which was proposed by Butler and Mokrys (1991) to recover heavy oil from the highly viscous reserves of heavy oil deep inside the earth crust[1]. In this process, a light hydrocarbon solvent is injected via a horizontal well inside a reservoir. The absorption of solvent in the heavy oil reduces its viscosity, thereby causing it to drain into an underlying horizontal production well from where the oil is easily pumped to the surface.

The use of solvents in Vapex obviates the energy requirements and environmental impacts that plague thermal recovery processes. For example, Vapex uses about 3% of the energy consumed by Steam Assisted Gravity Drainage (SAGD), and reduces greenhouse gas emission by 80% (Upreti et al., 2007). Moreover, Vapex is very suitable for heavy oil reservoirs, which frequently have high water contents, thin pay zones, low thermal conductivities of rock formations, and underlying aquifers. Under these circumstances, the traditional recovery methods such as surface mining, cyclic steam stimulation, SAGD, and cold heavy oil production are not viable.

The oil production in Vapex is directly related to the transfer of solvent into the heavy oil. The viscosity of heavy oil reduces with the solvent concentration, which augments as the solvent penetrates and mixes with the heavy oil (Das and Butler, 1998). In this process, the primary mode of solvent transfer is molecular diffusion, which is slower than thermal diffusion in SAGD (Gupta et al., 2003). Therefore, the oil production in Vapex builds up slowly with low heavy oil recoveries in the beginning. Nonetheless, the

[1] Located mostly in Canada and Venezuela, these reserves have more than 700 billion m^3 of estimated original oil-in-place (OOIP). The Canadian reserves have more than 400 billion m^3 OOIP that is about twice that of the total conventional oil reserves of all Gulf nations (Janisch, 1981).

advantages of Vapex make it worthwhile to explore different ways to enhance and optimize its oil production. In this paper, we consider several possible strategies for the optimal oil production from Vapex.

SOLVENT SELECTION

Solvent selection for a Vapex implementation depends on a number of factors that ultimately influence oil production. In general, a low molecular weight, high diffusivity, and high solubility of a solvent in the heavy oil promote the solvent transfer rate in Vapex leading to an increased oil production. The dew point temperature of the solvent (corresponding to the reservoir pressure), and its density also play important roles. The reason is that maintaining the injected solvent in the vapor phase is crucial to effectively fill the reservoir space vacated by the produced oil, and to sustain oil production. Vapor condensation will not only demand excessively more solvent injection to fill the vacated reservoir, but also hinder the transfer of solvent as it would have to diffuse through an additional layer of solvent in the liquid phase. The above facts generally limit the set of adequate solvent to light gases such as ethane, propane, butane and carbon dioxide. Individual performances of these solvents vary. Experiments have shown that propane and butane are the most effective solvents for Vapex (Das and Butler, 1994). Oil production rates with propane have been found to be 50% more than those with ethane despite the fact that propane has a lower vapor pressure than that of ethane at a given temperature (Butler and Mokrys, 1993).

In high-pressure reservoirs, the condensation of a solvent is avoided by mixing it with another solvent or a non-condensable gas such as methane or carbon dioxide to reduce the solvent vapor pressure. Consider the temperature and pressure in the three Canadian reserves presented in Table 1.

For the recovery of Athabasca Oil Sands, butane is not the right choice of solvent since it will condense. The reason is that butane has a vapor pressure of about 141 kPa at 8°C. Propane on the other hand has a vapor pressure of about 611 kPa at the same temperature.

Thus, propane will be close to its dew point in that reservoir and is a good choice for a solvent. For higher reservoir pressures, propane may be injected with a little amount of ethane or a non-condensable gas.

Table 1 Temperature and Pressure in Three Canadian reservoirs (Luhning et al., 2003)

Property	Athabasca Oil Sands, Alberta	Cold Lake Oil Sands, Alberta	South East Alberta Heavy Oil
Temperature, °C	8	12	30
Pressure, KPa	500–600	3000	9500

However, neither propane nor butane is suitable for the recovery of Cold Lake Oil Sands and South East Alberta Heavy Oil, which have considerably high pressures. For these reservoirs, a solvent must be mixed with a non-condensable gas like methane or carbon dioxide to avoid any condensation. The amount of the non-condensable gas should be optimized to the lowest value just enough to avoid condensation, thereby allowing maximum possible solvent concentration in the heavy oil. The bottom line is that a solvent or a solvent mixture should be such that it does not condense at the reservoir temperature and pressure, and, under this constraint, enables the maximum reduction of heavy oil viscosity.

Besides solvent condensation, asphaltene precipitation is another important issue that production engineers need to be aware of while selecting a solvent for Vapex.

Asphaltene Precipitation

Asphaltenes are the high boiling point components, which constitute 15–20 wt % of a heavy oil (Mokyrs and Butler, 1993). These components have the tendency to precipitate with a change in pressure, temperature or composition (Akbarzadeh et al., 2002). In Vapex, the precipitation of asphaltenes takes place when the concentration of the solvent in heavy oil exceeds some threshold value, and occurs first near the solvent vapor–heavy

oil interface where the concentration of the solvent is highest (Butler and Jiang, 2000). The precipitation mostly occurs toward the end of production line if the solvent is injected very close to its dew point. Precipitated asphaltenes remain in the reservoir and the deasphalted oil drains. As soon as the interface moves, solvent vapors contact the fresh heavy oil for subsequent penetration and oil production (Das and Butler, 1994). Since asphaltenes are responsible for the high viscosity of a heavy oil, their precipitation further reduces the viscosity of the oil and eventually facilitates its production.

Based on the above facts, further work needs to be done to catalogue solvents and solvent mixtures of different compositions suitable for a Vapex implementation at varying reservoir temperature and pressure. A model should be developed to provide the estimates of oil production from a given reservoir using the catalogued solvents. The model should take into account the transport properties of the involved species, the likelihood of asphaltene precipitation, and solvent costs. It has to be noted that a great deal of experimental work is required to develop a database of solvent dispersion in heavy oil, and asphaltene precipitation envelopes for Vapex. Once the model is developed, production engineers would be able to utilize it to optimize oil production in Vapex implementations.

WELL CONFIGURATION

Well configuration in Vapex is another important aspect that has a bearing on oil production. The characteristic feature of Vapex is the use of horizontal solvent injection and oil production wells, which are dug parallel with a layer of heavy oil rich phase in between. Although this configuration provides a large area of contact between the solvent gas and heavy oil, the oil production could be further enhanced with an adequate choice of the injector location (Jiang and Butler, 1996ab; Butler and Jiang, 2000). To promote oil production, the space between the injector and producer in a reservoir with higher heavy oil viscosity should be less than that in a reservoir with lower heavy oil viscosity. Furthermore, the injection should not be continued for long durations because that might cause excessive asphaltene precipitation due to high solvent concentrations in the heavy oil. In low permeability reservoirs, such a situation may impede the solvent flow and in

turn reduce oil production. To prevent this situation, the location of the injector should be periodically changed. For example, the location could be moved to either the other end of the injection well or the end opposite to the producer on the underlying producer well.

In heavy oil reservoirs with different permeability layers, solvent injection from the top enhances oil production (Jiang and Butler, 1996). Note that with bottom injection, the oil cannot drain from an upper lower-permeability layer to the lower higher-permeability layer until the mass of the diluted oil is large enough to overcome the capillary forces. In the reservoirs with lower permeabilities, larger vapor chambers develop during Vapex, thereby requiring wider wells for better oil recovery. In the reservoirs with bottom water zones (common in Alberta and Saskatchewan), a wider well spacing provides very large solvent–heavy oil contact surface area (Butler and Jiang, 2000; Frauenfeld et al., 2006). Solvent injection in the bottom water zone helps to increase oil production by spreading and distributing the solvent vapor in the heavy oil rich formation above. An experimental study by Butler et al. (1995) shows that the Vapex using propane in such a reservoir could result in the same or even higher production rate than that in SAGD.

The above findings suggest that there is a significant scope to maximize oil production by selecting the injector location and moving it periodically on the basis of reservoir features such as fractures and underlying acquifers. To reap this benefit, computational fluid dynamics (CFD) studies need to be performed at the outset to examine the effect of injector location and its movement inside a reservoir. Experiments need to be carried out at laboratory and pilot-plant scales to enable the validation of the CFD studies. Once these studies are validated through experiments, it would become possible to evaluate different solvent injection and oil production configurations and switchings. The injection policies could then be optimized for direct application in Vapex implementations.

RATE OF SOLVENT INJECTION

The rate of heavy oil recovery from Vapex depends upon the rate of vapor chamber growth. A higher growth rate yields higher rate of oil production. This phenomenon is quantified in Table 2, which summarizes the results of an experimental study by Butler and Jiang (2000).

Table 2 The Effect of Solvent Injection Rate on Oil Production (Butler and Jiang, 2000)

Temperature (°C)	Pressure (psig)	Solvent	Solvent Injection Rate (ml/h)	Oil Production Rate (g/h)[#]
21	30	Butane	10	13.2
			20	24.1
27	185	propane and butane	20	37.8
			30	40.4
			40/20[*]	55.6
	300		40/20[*]	48.4

[*]Solvent injection rate of 40 ml/h for two hours, and then reduced to 20ml/h.
[#]Oil production rate in the first 10 hours.

The rate of growth of vapor chamber can also be augmented by periodically reducing the interfacial tension between the solvent and the heavy oil phases. A reduction in the interfacial tension enhances the relative permeability of both phases and reduces capillary forces. As a result, the vapor chamber begins to grow and the trapped heavy oil mobilizes again, thereby enhancing the otherwise obstructed oil production (Xu, 2006).

The above objective could be achieved by varying the rate of solvent injection to disturb the pressure field in order to reduce the interfacial tension periodically. A cyclical variation, or the pulsing of solvent injection rate could be used to facilitate solvent dispersion and boost oil production. CFD studies could be utilized to assess the effects of such pressure-field disturbances induced by the injection policies. A newly emerging field of seismic pulse generation in the reservoirs needs to be tested for enhancement in the Vapex oil production. A recent investigation by Spanos et al. (2003) has shown that higher oil production rates can be attained by applying the right kind of pulse energy. The determination of the optimal policies of pulsation as well as solvent injection rate is the next step in the endeavor to maximize oil recovery using Vapex.

CONCLUSION

Based on the state-of-art knowledge of Vapex, this paper identified a large scope for the enhancement of oil production. The important areas for the enhancement include solvent

selection, well configuration, and solvent injection rate. Mass transfer modeling and CFD studies need to be performed to assess various scenarios in order to optimize oil production in Vapex. Experimental studies are needed not only to generate the transport properties of various solvents but also to validate model simulations. These tools will enable production engineers to select optimal operation parameters for Vapex implementations.

ACKNOWLEDGEMENT

Natural Sciences and Engineering Research Council, Canada

Appendix B

B. Data for butane vapour pressure at different temperatures

Table B. 1: Butane Vapor Pressure at different Temperatures

Temp °C	Pressure (psig)
10	14.967
11	16.479
12	17.990
13	19.501
14	21.013
15	22.524
16	24.035
17	25.546
18	27.058
19	28.569
20	30.080
21	31.113
22	32.146
23	33.178
24	34.211
25	35.244
26	36.404
27	37.564
28	38.725
29	39.885
30	41.045

Appendix C

C. Sample of Live Oil Viscosity Calculations

The live oil viscosity was calculated by rearranging equation (4.3), and substituting for all of the parameters from Table (C.1) to equation (C.a).

$$\mu(\text{cp}) = \frac{\pi\, \text{d}^4\ \Delta p\ 68948 \times 100}{128\, Q\, L} \qquad \left[\frac{\text{cm}^4\ \text{psi}}{\text{cm}^3/\text{sec cm}}\right]\left[\frac{\text{dyne/cm}^2}{\text{psi}}\right]\left[\frac{\text{cp}}{\text{dyne/cm}^2\text{s}}\right] \qquad \text{(C.a)}$$

Table C. 1: Data for Live Oil Viscosity Calculations

Time (min)	Volumetric Flow Rate (cm^3/s)	Pressure Drop Across Capillary Tube (Δp)	Live Oil Viscosity (mPa.s)
150	0.113	3.12	9.88
220	0.124	3.4	9.82
290	0.124	3.44	9.97
370	0.107	2.87	9.48
440	0.139	3.91	10.8
500	0.116	3.24	10.04
570	0.136	3.91	10.31

Appendix D

D. Sample of butane solubility and live oil density calculations.

To calculate the butane solubility and live oil density, substitute in equation (4.5) and (4.6) for all the parameters from Table (D.1).

Table D. 1: Data for Butane Solubility and Live Oil Density Calculations

Dead Oil Mass (g)	Liberated Butane Mass (g)	Live Oil Volume (cm^3)	Live Oil Density (g/cm^3)	Dissolved Butane Fraction
9.35	5.38	18.055	0.8163	0.365
9.39	5.43	18.212	0.813	0.366
7.5	4.28	14.52	0.811	0.363
9.34	5.37	18.055	0.815	0.365
8.21	4.79	15.7	0.828	0.363
9.75	5.70	18.99	0.813	0.368
9.45	5.38	18.447	0.804	0.362

Appendix E

E. Sample Data for Cumulative Live Oil Production for 15,25,35 and 45 cm model heights.

The cumulative live oil production data was calculated from load cell readings every minute. This sample data represents an averaged for every 10 minutes Table (E.1)

Table E. 1: Cumulative Live Oil Production Data

Time (min)	Cumulative Mass of Live oil Weight (g)			
	Model Length (cm)			
	15	25	35	45
0	0	0	0	0
10	0.1468	0.5883	1.6893	2.5620
20	1.3946	1.9120	1.9096	3.8063
30	1.9084	2.7210	3.5254	5.7827
40	2.8625	4.5594	4.9209	8.4178
50	3.4497	5.2948	6.8305	10.7602
60	4.3305	6.2508	8.8870	13.3953
70	4.6975	8.2364	9.9886	15.5913
80	5.7251	8.7512	11.3841	18.7388
90	6.6059	10.0749	13.2937	21.5936
100	7.1197	11.9869	14.8361	25.2535
110	8.2940	12.6488	16.9660	28.3279

Time (min)	Cumulative Mass of Live oil Weight (g)			
	Model Length (cm)			
	15	25	35	45
130	10.1290	15.1491	20.5648	35.0621
140	11.8172	17.1346	23.0620	38.2097
150	12.4044	18.0171	25.1185	41.9428
160	13.5053	19.3408	26.8812	46.4811
170	14.0191	20.9587	28.9377	49.7750
180	15.7073	21.9147	31.8755	54.8989
190	16.6615	23.5326	33.5648	57.9001
200	18.2762	25.0033	35.9885	62.2188
210	19.3038	26.4741	38.5591	66.2447
220	20.3314	28.0920	40.9094	71.2222
230	22.0930	29.1215	43.1862	74.6626
240	22.6801	30.3717	45.0223	79.4937
250	23.9279	32.0631	48.1071	83.5928
260	25.6161	33.8281	51.7059	86.9599
270	26.4235	35.0782	54.2031	92.0838
280	27.8180	36.5490	57.2143	96.5489
290	28.8456	37.6521	59.4177	100.9409
300	30.1668	38.9758	61.7680	105.2596

310	31.0476	40.8878	64.4855	109.6515
Time (min)	**Cumulative Mass of Live oil Weight (g)**			
	Model Length (cm)			
	15	**25**	**35**	**45**
320	31.9284	41.8438	67.2764	114.3362
330	32.8091	43.2411	70.0674	119.1673
340	34.7175	45.8150	72.7849	124.0716
350	35.7451	45.9620	75.5024	127.5851
360	36.9929	47.5799	78.0730	132.0503
370	37.6535	49.1978	80.7991	137.6134
380	39.5618	49.8596	83.5309	139.5165
390	40.2224	51.6981	86.5581	143.6888
400	41.9106	52.8012	89.2162	147.9344

Appendix F

Following are the set of Jacobian equations employed to integrate the ODEs (Equations [(6.31−6.41)]:

For intermediate grid points

For $0 < i < (N_i - 1)$ and $0 < j < (N_j - 1)$

$$\varpi_{i,j} = \frac{D_0}{\phi}\left[\frac{1}{r_i}\frac{\omega_{i+1,j} - \omega_{i-1,j}}{2\Delta r} + \frac{\omega_{i+1,j} - 2\omega_{i,j} + \omega_{i-1,j}}{\Delta r^2} - \frac{2\omega_{i,j}}{\Delta r^2}\right] - \frac{K_r K\rho g\cos\theta}{Z_0\mu_0\phi}3\omega_{i,j}\left[\frac{\omega_{i,j+1} - \omega_{i,j-1}}{\Delta\varsigma_i}\right] \tag{F1}$$

$$\varpi_{i+1,j} = \frac{D_0\omega_{i,j}}{\phi}\left[\frac{1}{2r_i\Delta r} + \frac{1}{\Delta r^2}\right] + \frac{D_0}{\phi}\left[\frac{\omega_{i+1,j} - \omega_{i-1,j}}{\Delta r}\right]\frac{1}{2\Delta r} \tag{F2}$$

$$\varpi_{i-1,j} = \frac{D_0\omega_{i,j}}{\phi}\left[-\frac{1}{2r_i\Delta r} + \frac{1}{\Delta r^2}\right] - \frac{D_0}{\phi}\left[\frac{\omega_{i+1,j} - \omega_{i-1,j}}{\Delta r}\right]\frac{1}{2\Delta r} \tag{F3}$$

$$\varpi_{i,j+1} = -\frac{K_r K\rho g\cos\theta}{Z_0\mu_0\phi}3\omega_{i,j}^2\left[\frac{1}{2\Delta\varsigma_i}\right] \tag{F4}$$

$$\varpi_{i,j-1} = +\frac{K_r K\rho g\cos\theta}{Z_0\mu_0\phi}3\omega_{i,j}^2\left[\frac{1}{2\Delta\varsigma_i}\right] \tag{F5}$$

$$\varpi_{\varsigma} = \frac{K_r K\rho g\cos\theta}{Z_0\mu_0\phi}3\omega_{i,j}^2\left[\frac{\omega_{i,j+1} - \omega_{i,j-1}}{2\Delta\varsigma_i^2}\right] \tag{F6}$$

For Axis Grid Points

When i = 0 for $0 < j < (N_j - 1)$

$$\varpi_{o,j} = -\frac{K_r K \rho g \cos\theta}{Z_0 \mu_0 \phi} 3\omega_{0,j} \left[\frac{\omega_{0,j+1} - \omega_{0,j-1}}{\Delta\varsigma_i} \right] \tag{F7}$$

$$\varpi_{0,j+1} = -\frac{K_r K \rho g \cos\theta}{Z_0 \mu_0 \phi} 3\omega_{0,j}^2 \left[\frac{1}{2\Delta\varsigma_i} \right] \tag{F8}$$

$$\varpi_{0,j-1} = -\varpi_{0,j+1} \tag{F9}$$

$$\varpi_{\varsigma} = \frac{K_r K \rho g \cos\theta}{Z_0 \mu_0 \phi} 3\omega_{0,j}^2 \left[\frac{\omega_{0,j+1} - \omega_{0,j-1}}{2\Delta\varsigma_i^2} \right] \tag{F10}$$

When $i = 0$ and $j = 0$

$$\varpi_{0,0} = -\frac{K_r K \rho g \cos\theta}{Z_0 \mu_0 \phi} 3\omega_{0,0} \left[\frac{\omega_{0,1} - \omega_{sat}}{\Delta\varsigma_0} \right] \tag{F11}$$

$$\varpi_{0,1} = -\frac{K_r K \rho g \cos\theta}{Z_0 \mu_0 \phi} 3\omega_{0,0}^2 \left[\frac{1}{2\Delta\varsigma_0} \right] \tag{F12}$$

$$\varpi_{\varsigma} = \frac{K_r K \rho g \cos\theta}{Z_0 \mu_0 \phi} 3\omega_{0,0}^2 \left[\frac{\omega_{0,1} - \omega_{sat}}{2\Delta\varsigma_0^2} \right] \tag{F13}$$

When $i = 0$ and $j = (N_j - 1)$

$$\varpi_{0,N_j-1} = -\frac{K_r K \rho g \cos\theta}{Z_0 \mu_0 \phi} 3\omega_{0,N_{j-1}} \left[\frac{\omega_{sat} - \omega_{0,N_{j-2}}}{\Delta\varsigma_0} \right] \tag{F14}$$

$$\varpi_{0,N_j-2} = \frac{K_r K \rho g \cos\theta}{Z_0 \mu_0 \phi} 3\omega_{0,N_{j-1}}^2 \left[\frac{1}{2\Delta\varsigma_0} \right] \tag{F15}$$

$$\varpi_{\varsigma} = \frac{K_r K \rho g \cos\theta}{Z_0 \mu_0 \phi} 3\omega_{0,N_{j-1}}^2 \left[\frac{\omega_{sat} - \omega_{0,N_{j-2}}}{2\Delta\varsigma_0^2} \right] \tag{F16}$$

For Right Most Grid Points

When $i = (N_i - 1)$ and $j = 0$

$$\varpi_{N_i-1,0} = \frac{D_0}{\phi} \left[\frac{1}{r_{N_{i-1}}} \frac{\omega_{sat} - \omega_{N_{i-2},0}}{2\Delta r} + \frac{\omega_{sat} - 2\omega_{N_{i-1},0} + \omega_{N_{i-2},0}}{\Delta r^2} - \frac{2\omega_{N_i-1,0}}{\Delta r^2} \right]$$
$$- \frac{K_r K \rho g \cos\theta}{Z_0 \mu_0 \phi} 3\omega_{N_{i-1},0} \left[\frac{\omega_{N_{i-1},1} - \omega_{sat}}{\Delta\varsigma_{N_{i-1}}} \right] \tag{F17}$$

$$\varpi_{N_i-2,0} = \frac{D_0 \omega_{N_{i-1},0}}{\phi} \left[-\frac{1}{r_{N_{i-1}}} \frac{1}{2\Delta r} + \frac{1}{\Delta r^2} \right] - \frac{D_0}{\phi} \left[\frac{\omega_{sat} - \omega_{N_{i-2},0}}{\Delta r} \right] \frac{1}{2\Delta r} \tag{F18}$$

$$\varpi_{N_i-1,1} = -\frac{K_r K \rho g \cos\theta}{Z_0 \mu_0 \phi} 3\omega_{N_{i-1},0}^2 \left[\frac{1}{2\Delta\varsigma_{N_{i-1}}} \right] \tag{F19}$$

When $i = (N_i - 1)$

$$\varpi_{N_i-1,j} = \frac{D_0}{\phi}\left[\frac{1}{r_{N_{i-1}}}\frac{\omega_{sat} - \omega_{N_{i-2},j}}{2\Delta r} + \frac{\omega_{sat} - 2\omega_{N_{i-1},j} + \omega_{N_{i-2},j}}{\Delta r^2} - \frac{2\omega_{N_i-1,j}}{\Delta r^2}\right] + \\ -\frac{K_r K\rho g\cos\theta}{Z_0\mu_0\phi} 3\omega_{N_{i-1},j}\left[\frac{\omega_{N_{i-1},j+1} - \omega_{N_{i-1},j-1}}{\Delta\varsigma_{N_{i-1}}}\right] \tag{F20}$$

$$\varpi_{N_i-2,j} = \frac{D_0\omega_{N_{i-1},j}}{\phi}\left[-\frac{1}{r_{N_{i-1}}}\frac{1}{2\Delta r} + \frac{1}{\Delta r^2}\right] - \frac{D_0}{\phi}\left[\frac{\omega_{sat} - \omega_{N_{i-2},j}}{\Delta r}\right]\frac{1}{2\Delta r} \tag{F21}$$

$$\varpi_{N_i-1,j+1} = -\frac{K_r K\rho g\cos\theta}{Z_0\mu_0\phi} 3\omega^2_{N_{i-1},j}\left[\frac{1}{2\Delta\varsigma_{N_{i-1}}}\right] \tag{F22}$$

$$\varpi_{N_i-1,j-1} = -\varpi_{N_i-1,j+1} \tag{F23}$$

$$\varpi_{\varsigma} = \frac{K_r K\rho g\cos\theta}{Z_0\mu_0\phi} 3\omega^2_{N_{i-1},j}\left[\frac{\omega_{N_{i-1},j+1} - \omega_{N_{i-1},j-1}}{2\Delta\varsigma^2_{N_i-1}}\right] \tag{F24}$$

when $i = (N_i - 1)$ and $j = (N_j - 1)$

$$\varpi_{N_i-1,N_j-1} = \frac{D_0}{\phi}\left[\frac{1}{r_{N_{i-1}}}\frac{\omega_{sat} - \omega_{N_{i-2},N_{j-1}}}{2\Delta r} + \frac{\omega_{sat} - 2\omega_{N_{i-1},N_{j-1}} + \omega_{N_{i-2},N_{j-1}}}{\Delta r^2} - \frac{2\omega_{N_i-1,N_j-1}}{\Delta r^2}\right] \\ -\frac{K_r K\rho g\cos\theta}{Z_0\mu_0\phi} 3\omega_{N_{i-1},N_{j-1}}\left[\frac{\omega_{sat} - \omega_{N_{i-1},N_{j-2}}}{\Delta\varsigma_{N_{i-1}}}\right] \tag{F25}$$

$$\varpi_{N_i-2,N_j-1} = \frac{D_0\omega_{N_{i-1},N_{j-1}}}{\phi}\left[-\frac{1}{r_{N_{i-1}}}\frac{1}{2\Delta r} + \frac{1}{\Delta r^2}\right] - \frac{D_0}{\phi}\left[\frac{\omega_{sat} - \omega_{N_{i-2},N_{j-1}}}{\Delta r}\right]\frac{1}{2\Delta r} \tag{F26}$$

$$\varpi_{N_i-1,N_j-2} = \frac{K_r K \rho g \cos\theta}{Z_0 \mu_0 \phi} 3\omega^2_{N_{i-1},N_{j-1}} \left[\frac{1}{2\Delta\varsigma_{N_{i-1}}} \right] \tag{F27}$$

$$\varpi_{\varsigma} = \frac{K_r K \rho g \cos\theta}{Z_0 \mu_0 \phi} 3\omega^2_{N_{i-1},N_{j-1}} \left[\frac{\omega_{\text{sat}} - \omega_{N_{i-1},N_{j-2}}}{2\Delta\varsigma^2_{N_i-1}} \right] \tag{F28}$$

For Lower most Intermediate Grid Points

When $j = 0$

$$\varpi_{i,0} = \frac{D_0}{\phi}\left[\frac{1}{r_i} \frac{\omega_{i+1,0} - \omega_{i-1,0}}{2\Delta r} + \frac{\omega_{i+1,0} - 2\omega_{i,0} + \omega_{i-1,0}}{\Delta r^2} - \frac{2\omega_{i,0}}{\Delta r^2} \right] + - \frac{K_r K \rho g \cos\theta}{Z_0 \mu_0 \phi} 3\omega_{i,0} \left[\frac{\omega_{i,1} - \omega_{\text{sat}}}{\Delta\varsigma_{N_{i-1}}} \right] \tag{F29}$$

$$\varpi_{i+1,0} = \frac{D_0 \omega_{i,0}}{\phi}\left[\frac{1}{r_i} \frac{1}{2\Delta r} + \frac{1}{\Delta r^2} \right] + \frac{D_0}{\phi}\left[\frac{\omega_{i+1,0} - \omega_{i-1,0}}{\Delta r} \right] \frac{1}{2\Delta r} \tag{F30}$$

$$\varpi_{i-1,0} = \frac{D_0 \omega_{i,0}}{\phi}\left[-\frac{1}{r_i} \frac{1}{2\Delta r} + \frac{1}{\Delta r^2} \right] - \frac{D_0}{\phi}\left[\frac{\omega_{i+1,0} - \omega_{i-1,0}}{\Delta r} \right] \frac{1}{2\Delta r} \tag{F31}$$

$$\varpi_{i,1} = -\frac{K_r K \rho g \cos\theta}{Z_0 \mu_0 \phi} 3\omega^2_{i,0} \left[\frac{1}{2\Delta\varsigma_{N_{i-1}}} \right] \tag{F32}$$

$$\varpi_{\varsigma} = \frac{K_r K \rho g \cos\theta}{Z_0 \mu_0 \phi} 3\omega^2_{i,0} \left[\frac{\omega_{i,1} - \omega_{\text{sat}}}{2\Delta\varsigma^2_{N_i-1}} \right] \tag{F33}$$

For the upper most intermediate grid points

$j = (N_j - 1)$

$$\varpi_{i,N_j-1} = \frac{D_0}{\phi}\left[\frac{1}{r_i}\frac{\omega_{i+1,N_j-1} - \omega_{i-1,N_j-1}}{2\Delta r} + \frac{\omega_{i+1,N_j-1} - 2\omega_{i,N_j-1} + \omega_{i-1,N_j-1}}{\Delta r^2} - \frac{2\omega_{i,N_j-1}}{\Delta r^2}\right] - \frac{K_r K\rho g\cos\theta}{Z_0\mu_0\phi} 3\omega_{i,N_j-1}\left[\frac{\omega_{\text{sat}} - \omega_{i,N_j-2}}{\Delta\varsigma_i}\right] \quad \text{(F34)}$$

$$\varpi_{i+1,N_j-1} = \frac{D_0\omega_{i,N_j-1}}{\phi}\left[\frac{1}{r_i}\frac{1}{2\Delta r} + \frac{1}{\Delta r^2}\right] + \frac{D_0}{\phi}\left[\frac{\omega_{i+1,N_j-1} - \omega_{i-1,N_j-1}}{\Delta r}\right]\frac{1}{2\Delta r} \quad \text{(F35)}$$

$$\varpi_{i-1,N_j-1} = \frac{D_0\omega_{i,N_j-1}}{\phi}\left[-\frac{1}{r_i}\frac{1}{2\Delta r} + \frac{1}{\Delta r^2}\right] - \frac{D_0}{\phi}\left[\frac{\omega_{i+1,N_j-1} - \omega_{i-1,N_j-1}}{\Delta r}\right]\frac{1}{2\Delta r} \quad \text{(F36)}$$

$$\varpi_{\varsigma} = \frac{K_r K\rho g\cos\theta}{Z_0\mu_0\phi} 3\omega_{i,N_j-1}^2\left[\frac{\omega_{\text{sat}} - \omega_{i,N_j-2}}{2\Delta\varsigma_i^2}\right] \quad \text{(F37)}$$

Change in Height of Physical Model

$$\varsigma_{i,0} = -\frac{K_r K\rho g\cos\theta}{Z_0\mu_0}\left[\frac{\omega_{i,0} + \omega_{i+1,0} + 2\omega_{\text{sat}}}{8}\right] \quad \text{(F38)}$$

$$\varsigma_{i+1,0} = \varsigma_{i,0} \quad \text{(F39)}$$

$$\varsigma_{N_i-1,0} = -\frac{K_r K\rho g\cos\theta}{Z_0\mu_0}\left[\frac{\omega_{N_i-1,0} + 3\omega_{\text{sat}}}{8}\right] \quad \text{(F40)}$$

Where ϖ and ζ shows the Jacobian expression for corresponding node for solvent concentration and model height respectively.